Planetary materials: A record of early Solar System events to planetary processes

Audrey Bouvier, Katherine Bermingham, Evelyn Füri

Planetary materials:
A record of early Solar System events to planetary processes

Audrey Bouvier[a], Katherine Bermingham[b], Evelyn Füri[c]

[a] Bayerisches Geoinstitut, Universität Bayreuth, Universitätsstrasse 30, Bayreuth, Germany
[b] Department of Earth and Planetary Sciences, Rutgers University, Piscataway, NJ, United States
[c] Université de Lorraine, CRPG, CNRS, Vandoeuvre-lès-Nancy, France

Post−peer review, pre−copyedit version submitted to Treatise on Geochemistry, Third Edition

Abstract
Planetary materials provide fundamental insights into the composition and formation of the Solar System. Meteorites and their components preserve a record of the physicochemical conditions in the protoplanetary disk as well as of the evolution of planetary surfaces and interiors. Beyond the Moon, spacecraft missions have returned samples of the Solar wind (Genesis) and an S-type silcaceous asteroid (Hayabusa), as well as two C-type carbonaceous asteroids (Hayabusa2 and OSIRIS-REx) and the coma of a comet (Stardust) which sampled the outer Solar System. This chapter describes the chemical diversity of meteorites and mission returned samples and how their compositions have led to major advancements in understanding Solar System formation, planet accretion, and the building blocks of the only known life-bearing planet, Earth.

Keywords
Chronology; Isotopic anomalies; Meteorites; Planetesimals; Planet formation; Protoplanetary disk; Returned samples; Solar nebula

Key points
This chapter reviews an up-to-date meteorite classification, the utility of chondrites (and their components), achondrites, and iron meteorites as tracers of protoplanetary disk processes, the chronology of Solar System events, and the elemental and isotopic compositions that record the physical and chemical evolution of the disk and the formation of planets.

Nomenclature

σ	standard deviation
δ	deviation in parts per thousand
ε	deviation in parts per ten thousand
μ	deviation in parts per million
β^-	beta decay is a type of radioactive decay in which an atomic nucleus emits a beta (b^-) particle (fast energetic electron or positron), transforming into an isobar with a mass number that is identical to the parent isotope and an atomic number that is increased by one
α (^{4}He emission)	alpha decay or a-decay is a type of radioactive decay in which an atomic nucleus emits an alpha particle (helium nucleus) and decays into a different atomic nucleus, with a mass number that is reduced by four and an atomic number that is reduced by two
λ	decay constant in $year^{-1}$
ALMA	Atacama large millimeter/submillimeter array
au	astronomical unit which is 149,597,870,700 m (1 au is approximately the average distance between Earth and the Sun)
CC and NC	so-called carbonaceous chondrite and non-carbonaceous meteorites
CNSA	China National Space Administration
E.C.	electron capture is a type of radioactive decay in which a proton-rich nucleus absorbs an inner atomic electron thereby changing a nuclear proton to a neutron, transforming into an isobar with a mass number that is identical to the parent isotope and an atomic number that is decreased by one
ESA	European Space Agency
Ga	billion years old (or ago)
Gyr	billion years
ICP-MS	inductively coupled plasma mass spectrometry
in situ analysis	in situ analysis corresponds to high-spatial resolution mass-spectrometric analysis
JAXA	Japan Aerospace Exploration Agency
LLR	long-lived radionuclide
$M_\odot$	Solar mass
Ma	million years old (or ago)
Ma and Ga	Ma and Ga are adopted for geohistorical dates in 10^6 and 10^9 years before present, and express geohistorical time in years duration as Myr and Gyr, respectively (using International System of Units prefixes)
MC-ICP-MS	multicollector inductively coupled plasma mass spectrometry
Myr	million years
(nano) SIMS	(nano) secondary ion mass spectrometry
NASA	National Aeronautics Space Administration, United States of America
ppm	the parts per million notation is a unit used to describe small values of miscellaneous dimensionless quantities (e.g., 1 mg/1 g)
Roscosmos	Russian Federal Space Agency
SLR	short-lived radionuclide
t_0	time zero, the cosmochemical age of the Solar System defined by CAI ages
$t_{1/2}$	half-life or a radioactive isotope in yr
T_c	closure temperature
TIMS	thermal ionization mass spectrometry
yr	year

1. INTRODUCTION

1.1. Significance of planetary materials in cosmochemistry

Planetary materials include rock, fluid, and gas samples from Earth as well as dust particles, meteorites, and samples returned to Earth via missions to the Sun, Moon, asteroids, and comets. Laboratory measurements of these diverse materials yield unique insights into the processes and timescales that shaped the Solar System and planets in their infancy 4.57 billion years ago. Their mineral, elemental, and isotopic compositions are required to ground-truth the interpretations of planet formation that are based on numerical models, spacecraft data, and astronomical observations of neighboring systems and exoplanets (Lammer et al., 2020). Meteorites are solid stony or metal-rich objects that originate from a planetary body and survive impact on the surface of a different planet, such as Earth. They provide a random sampling of asteroids, the Moon, and Mars. The mineral, elemental, and isotopic compositions of meteorites document the formation conditions of the first solids and planetesimals in the Solar System as well as the surface and interior evolution of larger planetary bodies. These compositions have been detailed by scientists over the last 60 years of meteoritics. The rate of meteorite discovery and their accompanying datasets, however, have increased sharply over the past twenty years, thereby greatly expanding the database of planetary material compositions. Primarily, this expansion is a result of an increase in the number and scale of meteorite recovery programs, not only in Antarctica but also in the Sahara, Arabia and Atacama deserts. In addition, meteor radar and digital imagery networks that are operational in several countries, capture fall events and narrow the triangulation of landing areas for the quick recovery of material (e.g., The Global Fireball Observatory). These monitoring systems contribute to the increasing number of observed meteorite falls, with 8–12 specimens recovered each year (Gattacceca et al., 2021). With up to 3000 meteorites approved annually by the Nomenclature Committee of the Meteoritical Society (e.g., Gattacceca et al., 2023), there are over 75,000 officially named meteorites in 2024 in the Meteoritical Bulletin Database.

Typically, meteorite data are not accompanied by information about the launch sites. Sample-return missions are needed to link meteorite compositions to parent bodies. This is done by retrieving samples from targeted bodies (e.g., planets, moons, asteroids, and comets) and by collecting information about the sampling site, parent body size, orbital dynamics, and surface composition. Following a 30-year hiatus after the last Apollo and Luna missions in the early 1970s, space missions have successfully returned samples from a comet, the Solar wind, asteroids, and the Moon. In conjunction with the increase in the availability of planetary materials, significant analytical developments over the past fifteen years have pushed the measurement limits of detection, precision, accuracy, and spatial resolution. These advancements have enabled the detection of previously unidentified short-lived radionuclides that were present in the early Solar System, as well as small isotopic anomalies (so-called nucleosynthetic isotope anomalies) in many elements which are related to the uneven distribution of presolar grains in the protoplanetary disk. The new era of space missions, coupled with the augmentation of the number, diversity, and quality of meteorite data, have generated unprecedented insights into the formation and evolution of the Solar System.

This chapter reviews the major discoveries of the past decade about the composition and evolution of the Solar System that were driven by the study of meteorites. Results from the relevant space mission-returned samples are included. In Section “Introduction,” an overview of Solar System formation from a cosmochemical perspective is presented. In Section “Planetary materials,” an up-to-date summary of meteorite classification is provided which is accompanied by brief descriptions of sample mineralogy, petrography, and isotopic compositions. In Section “Constraints from meteorites on the physicochemical conditions of the early Solar System,” the physicochemical conditions of the early Solar System as recorded by various planetary materials are described. Meteoritic evidence of the process of condensation of solids in the early Solar System to planetary formation processes is discussed in Section “Disk composition and evolution: Insights from meteorite chronology and isotopic variations.” The chronological records of these

events and how they are used to constrain the initial distribution of short-lived radionuclides in the disk and the thermal evolution of planetesimals are also reviewed. In Section "Sample-based constraints on Solar System formation" the focus shifts to the timescales of planetary formation, the distribution of short-lived isotopes, and the nucleosynthetic isotope anomalies that underpin the discovery of two fundamental disk reservoirs—the so-called carbonaceous chondrite (CC) and non-carbonaceous (NC) domains. This chapter ends with a synthesis of the current state of knowledge and open questions regarding the primary processes of nebular and terrestrial planet formation that are recorded by meteoritic materials.

1.2. The formation of the Solar System

The Solar System formed at 4.57 Ga from the collapse of part of a large and cold molecular cloud that was estimated to be between 65 and 200 light-years in size and between 10 and 50 K in temperature (Fig. 1). The molecular cloud was located within the minor spiral Orion-Cygnus arm of the Milky Way galaxy. As observed today, the local interstellar medium (ISM) is dominated by the large cavity known as the Local Bubble, a region of very low density that contains interstellar clouds (e.g., the Local Interstellar Cloud, the G-Cloud, the Hyades) that are observed within 300 light-years of the Sun. These regions are evidence of the pivotal role played by massive stars through their stellar winds and clustered supernovae in shaping the ISM (Frisch et al., 2011).

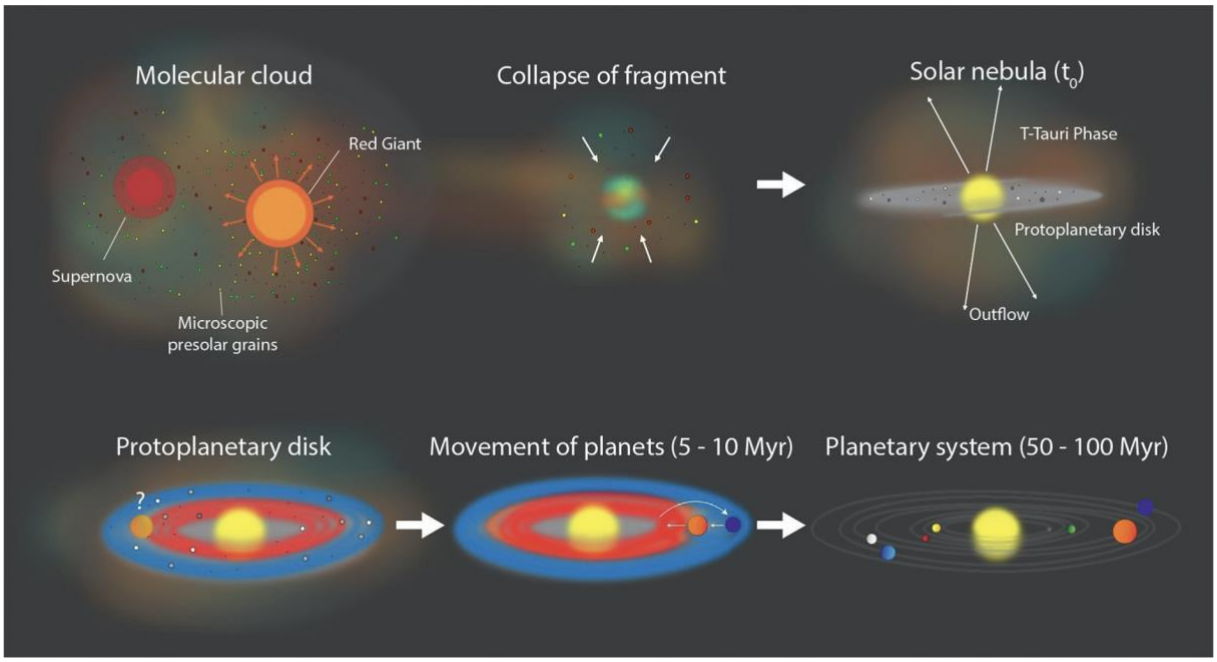

Figure 1: A pictorial representation of the formation of the Solar System. A fragment of a molecular cloud composed of gas (~99%) and dust (~1%, interstellar grains, and circumstellar grains from prior events such as Red Giants and supernovae) formed the basis of the Solar System. The fragment collapsed, and more than 98% of its mass accreted to form the proto-Sun. The material that did not accrete to the Sun inherited the angular momentum of the system and flattened out to form a rotation accretion disk, which is called the protoplanetary disk. During these early phases, jets of material were emitted from the star to the outer regions of the developing protoplanetary disk, as observed in very active T-Tauri stars. The cosmochemical start of the Solar System (t_0) is anchored in this phase. Within the following few million years, the NC (red) and CC (blue) compositional divide in the disk developed, possibly influenced by the formation of Jupiter. These reservoirs persisted until between 5 and 10 Myr when the movement of the giant planets scattered material between the inner and outer Solar System, after which the nebular gas dissipated. During the subsequent 50–100 Myr, accretion of the terrestrial planets and the gas and ice giants continued until the formation of the eight-planet system that is observed today.

Molecular clouds have a relatively higher density than the surrounding ISM. They contain 99% gas (predominantly H and He in a 3:1 ratio, with trace amounts of a few gaseous elements and molecules) and 1% solid phases (i.e., ices and dust). The dust includes circumstellar condensates and interstellar grains, otherwise known as presolar grains. Many of the elements heavier than H and He were inherited by the Solar System from presolar grains that formed in previous generation stars (e.g., Red Giant stars) and supernovae (Fig. 1). Such stellar events created the elements via nuclear reactions through which fresh atomic nuclei were synthesized from pre-existing nuclei or nucleons. The dominant stellar processes that are preserved in the isotopic composition of the elements present in the Solar System include isotopes that are produced during explosive burning (i.e., supernova), the slow and rapid (s- and r-processes) neutron capture processes, and the p-process which produces isotopes predominantly by disintegration (Burbidge et al., 1957).

The gravitational collapse of the molecular cloud fragment that went on to form the Solar System may have been triggered by a shock wave associated with a supernova or an ambipolar diffusion event (Cameron and Truran, 1977; Boss, 1995). As the fragment collapsed, material from the surrounding nebula (the luminescent part of the ISM) accreted onto the protostar (proto-Sun) thereby increasing its mass (Fig. 1). This first stage of infalling matter is estimated to have lasted about 0.1–0.3 Myr (Yang and Ciesla, 2012). During this time, a small fraction of the nebula that had not yet accreted onto the proto-Sun inherited the angular momentum of the system and flattened out to form a rotation accretion disk of dust and nebular gas which is termed the protoplanetary disk. The Sun and protoplanetary disk are collectively referred to as the Solar nebula. During this early period, jets of material were emitted from the star to the outer regions of the evolving disk, as observed in active T-Tauri stars, which are newly-formed (<10 Ma) low to intermediate mass stars (<3 Solar masses, $M_{\odot}$) with central temperatures that are too low for nuclear fusion to have begun. If jets were active in the Solar System, the outflow during the T-Tauri phase may have ejected early-formed solids from the inner disk toward the outer regions of the disk (Shu et al., 2001). Concurrently, as matter concentrated towards the young Sun, angular momentum was transferred outward through a viscous spiraling of the disk with the remaining reservoir of gas and dust forming planets (Greaves, 2005).

Within 1 Myr of t_0, the NC and CC compositional divide developed in the disk, a process that was possibly influenced by the early formation of Jupiter (Warren, 2011; Kruijer et al., 2017). These reservoirs persisted until the giant planets scattered material between the inner and outer Solar System. After this, the nebular gas dissipated, which slowed the transfer rate of matter toward the center of the disk. The Solar nebula (including the nebular gas) has been estimated to have dispersed after ~4 Myr based on meteorite paleomagnetism studies (Wang et al., 2017). Numerical models of disk evolution, however, state that the disk (including nebular gas) persisted for 5–10 Myr (Walsh et al., 2011). Mars accreted most of its mass within the first 5–10 Myr (Dauphas and Pourmand, 2011; Brasser, 2013), while the other terrestrial planets continued to accrete throughout the subsequent 50–100 Myr marked by giant collisions such as the Moon-forming impact. Subsequent late accretion represents the last 0.5% mass addition to planets continuing until today.

Understanding the processes that led to the rapid accretion of dust and the formation of planetesimals in the Solar System requires chemical data and numerical models to be integrated with astronomical observations of the first stages of accretion. Planetary accretion is a process that describes the gravitational accumulation of dust particles to form larger objects until eventually planetary-sized bodies exist (Fig. 2). The formation of the terrestrial and gas giant planets has been described by two principal models. The classical model proposes that the coalescence of local dust into larger objects occurred by way of *runaway growth* until collisions due to gravitational forces dominated and resulted in a few planets growing quickly via *oligarchic growth* (Levison et al., 2015). This model does not account for the inefficiency associated with the growth of particles by collisional sticking beyond the cm-size to form

planetesimals (i.e., during the circumstellar disk buildup process; e.g., Blum and Wurm, 2008). The radial drift timescales for m-sized boulders are also too short to permit planetesimals to form within 1 Myr (e.g., Adachi et al., 1976). A long-standing issue associated with most numerical simulations of planetary accretion is that they generally have a very low probability to reproduce the formation of Mars, a small planetary embryo that rapidly stopped its growth as mentioned above (Fischer and Ciesla, 2014; Woo et al., 2018).

As an alternative accretion model, a highly efficient mechanism for rapid planetary growth via mm-sized *pebble accretion* was proposed (Lambrechts and Johansen, 2012). Planets grow by accreting pebbles (mm-sized objects formed of dust and ice grain aggregates), planetesimals and gas. Pebble accretion leads to the formation of fewer but substantially more massive embryos within the first 10 Myr (Fig. 2) (Voelkel et al., 2021). Once bodies reached the km-scale (1–10 km), their movements were controlled by gravity and collisions. A major limitation of the pebble accretion model is to transfer sufficient mass from the outer to the inner parts of the disk during the lifetime of the gas to form planetesimals and the terrestrial planets (Raymond and Morbidelli, 2022). Additionally, isotopic anomalies indicate a minor contribution of CC materials to the terrestrial planets (e.g., Dauphas et al., 2024) and isotopic heterogeneities between NC objects need to be preserved during accretion (e.g., Mah et al., 2021).

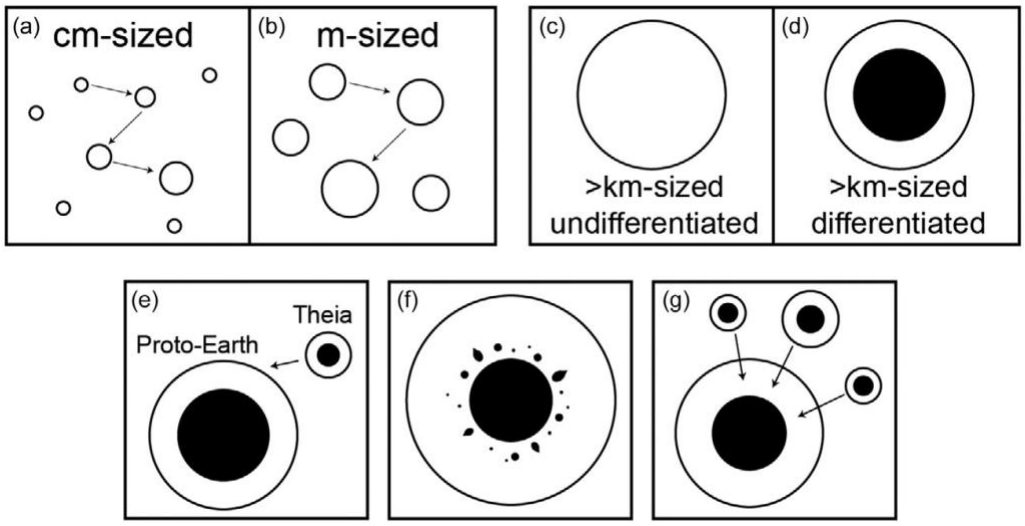

Figure 2: A schematic depicting the process of planetary accretion. (a,b) Growth of cm-sized pebbles into m-sized objects occurred, possibly via pebble accretion and streaming instability. (c,d) Once 1–10 km-sized rocky planetesimals accreted, those that were large enough and formed early enough (when ^{26}Al was abundant) went through a magma ocean stage and ultimately differentiated to form a metal-rich core and silicate-rich mantle and crust. Those that were not large enough or formed when ^{26}Al was in low abundance (after 2 Myr) remained undifferentiated. (e) Earth's late-stage accretion began when a Mars-sized planetary embryo (*Theia*) hit the proto-Earth in a glancing blow. This event resulted in the formation of the Earth-Moon system. (f) Following this, final core formation occurred in the Earth, resulting in its core, mantle, and crust structure. After core formation ceased, Earth developed a primordial crust after the solidification of the magma ocean resulting from the Moon forming giant impact. (g) After final core formation, ~0.5 to 2 wt% of Earth's mass was added to the silicate portion during the final major addition of mass, during what is referred to as Late Accretion or the Late Veneer.

For both models, mechanisms such as streaming instability facilitating the concentration and clumping of solid particles within the gas have been proposed to overcome the barriers of dust growth (i.e., bouncing and fragmentation) and radial drift leading to planetesimal formation. The roles of dust traps and the *snow line* (i.e., the water ice evaporation/condensation front) have also been evoked to explain efficient sticking of dust grains (Lichtenberg et al., 2021). Once 1–10 km-sized rocky planetesimals accreted, those

that were large enough and formed when the short-lived radionuclide ^{26}Al was abundant underwent wholescale melting (i.e., a magma ocean stage) and ultimately differentiated to form a metal-rich core and silicate-rich mantle and crust (Fig. 2). Those rocky planetesimals that were not large enough or formed when ^{26}Al was in low abundance (after ~2 Myr) did not undergo wholescale melting and remained undifferentiated. Additionally, collisional evolution could have led to significant heating of large planetesimals and icy bodies (Golabek and Jutzi, 2021). Large bodies, such as Mars and Earth, were assembled over a longer period than planetesimals. Consequently, there was not enough ^{26}Al inherited by these bodies to cause wholescale melting. Instead, heat sources for melting and differentiation came from accretionary impacts and gravitational segregation of metallic iron into the center of the planet.

Towards the end of Earth's accretion phase, a planetary embryo (*Theia*) hit the proto-Earth in a glancing blow and resulted in the formation of the Moon in an event known as the *Giant Impact* (Fig. 2). Giant impacts are common in numerical simulations of rocky planet formation and they likely caused widespread melting of the proto-planet (Schaefer and Elkins-Tanton, 2018). After final core formation ceased, between 0.5 and 2 wt% of Earth's mass was added to the silicate portion during a period called Late Accretion or the *Late Veneer*. This final major addition of mass may also have occurred on some planetesimals, the Moon, and Mars.

2. PLANETARY MATERIALS

2.1. Meteorites

A meteorite is a stony or metal-rich object that originated from a planetary body orbiting the Sun (Rubin and Grossman, 2010) and survived impact on the surface of a planet or moon. A *parent body* refers to the planetary object (asteroid, moon, planet, or possibly comet) from which a meteorite originated. Meteorites are ejected by natural means from their parent body, typically in the form of meteoroids ≤ 1 m in size (Rubin and Grossman, 2010). Ejection occurs as a result of fragmentation over time or some kind of planetary impact event. Meteoroids are transported to a region that is outside the dominant gravitational influence of the parent body. Following this, the meteoroid collides with a natural or artificial body larger than itself. A meteoroid becomes a *meteor* when it enters the atmosphere of the body on which it is landing, such as the shooting stars observed in Earth's atmosphere. A meteoroid becomes a meteorite when it lands on the ground of that body.

Meteorites are identified as *falls* (such as the Allende meteorite shown in Fig. 3) if they are recovered following an observed fall event (either by humans or their devices such as cameras or radar), or as *finds* if they are not associated with an observed fall. Meteorites are named based on the location where they were recovered. If many meteorites are found in the same general region, they are named and numbered (e.g., meteorites recovered from cold and hot deserts such as Antarctica and North Africa, respectively). Meteorites that are fragments of the same fall are said to be *paired*.

The first documented meteorite fall is Ensisheim, which fell in 1492 in France. From the estimated 127 kg total initial mass recovered, 53.8 kg remains on display in the village of Ensisheim. It was only in 1794 that Ernst Chladni (1756–1827), a German physicist and musician, proposed the concept that meteorites came from space. Chemical analyses of the stones of L'Aigle (1803), which was a meteor shower of over 3000 stones, by the chemist Louis-Jacques Thénard (1777–1857) confirmed the stones' compositional similarity to earlier analyses of fallen stones, which provided the final proof of the extraterrestrial origin of meteorites.

Most (~99%) recovered meteorites originate from asteroids, whereas the rest are identified as impact ejecta from the Moon's and Mars' surfaces. Meteorites sample at least 110 asteroidal parent bodies that have been identified using triple O isotopic composi- tions (Greenwood et al., 2017). Asteroidal sources

of meteorites found on Earth are >1-m-sized to 400 km diameter-sized (e.g., 1 Ceres, 4 Vesta) rocky, icy, and/or metallic parent bodies that currently reside in the asteroid belt between Mars and Jupiter. Given the diversity of chemical compositions that asteroids record, they likely accreted in different regions of the protoplanetary disk before being mixed into the asteroid belt during planetary migration (e.g., Walsh et al., 2011). Comets have not yet been sampled as meteorites, but materials of possible cometary origin have been observed within meteorites (Nittler et al., 2019).

Figure 3: Polished section (~6.5 × 4.5 cm) of the Allende CV3.6 carbonaceous chondrite meteorite, which fell on February 8th, 1969 in Mexico. The total known recovered mass is ~2 tons. Allende comprises a fine-grained (<100 mm) matrix of dark primary and secondary silicates, oxides, and opaque minerals, and lithic clasts such as chondrules (rounded vitreous objects), abundant refractory inclusions found as calcium-aluminum-rich inclusions (CAIs, white objects with various shapes) or ameboid olivine aggregates (AOAs), and dark inclusions. The matrix also contains abundant organic matter and circumstellar condensates (not visible at this scale). Credit: Laurence Garvie (ASU).

2.2. Meteorite classification

A great deal of research is devoted to identifying the chemical relations between meteorites to constrain the number and type of parent bodies that accreted from the disk, the timing of their formation, and their accretion location in the disk. Given the diversity of meteorites in the global collection, a detailed classification scheme had to be developed. The most widely used classification scheme used by meteoriticists and cosmochemists is based on the bulk compositional (i.e., a composition that includes all components of a sample) and petrological (mineralogical and textural) characteristics of meteorites. The goal of this classification scheme is to provide a descriptive label for meteorites with similar origins and formation histories that suggest they could originate from the same parent body. The classification scheme is data-driven, thus it can evolve as new data are collected and interpreted.

Following the recognition of an almost omnipresent bimodality in the nucleosynthetic isotope composition of bulk meteorites (Section “Nucleosynthetic isotope anomalies”), Warren (2011) proposed that the highest taxonomic division in meteorite and planetary classification should be between the *carbonaceous chondrite* (CC) and *non-carbonaceous* (NC) materials, shown in Fig. 4 as blue (CC) or red (NC). The NC-CC division was originally limited to the selection of meteorites considered by Warren (2011) (i.e., carbonaceous chondrites, ordinary chondrites, howardites, eucrites, diogenites, ureilites, angrites, martian samples, lunar samples, mesosiderites, and pallasites including the Eagle Station pallasite). The NC-CC division has since been extended to almost all meteorite groups, including many ungrouped meteorites. Presently, the iron meteorite Nedagolla is the only meteorite that has a published isotopic composition which does not fall within either the NC or CC group (Spitzer et al., 2021b).

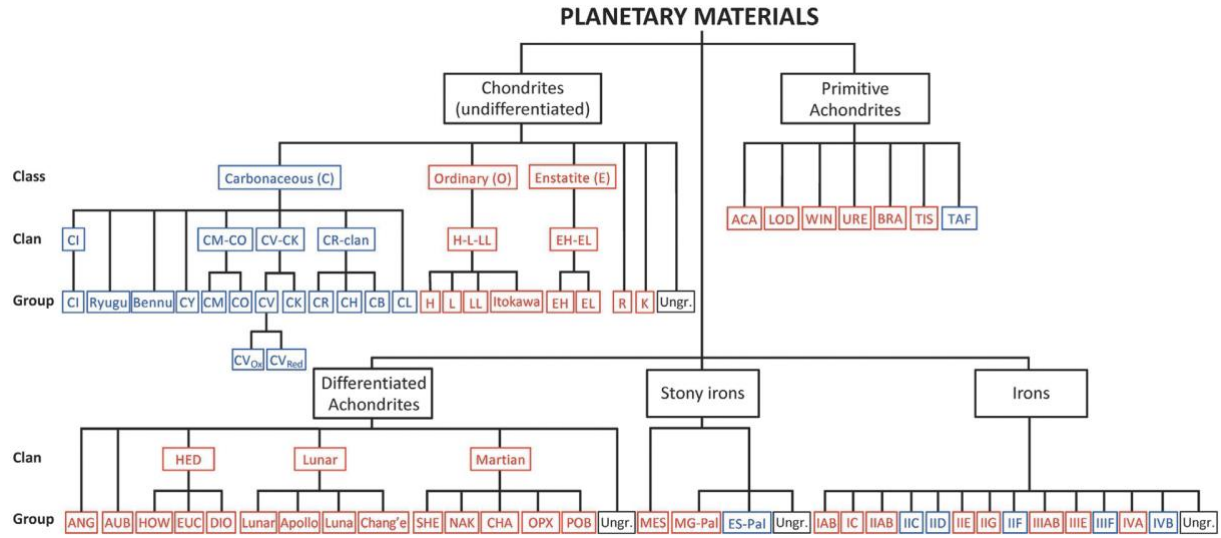

Figure 4: Classification of planetary materials (meteorites and returned samples) and their genetic relationships. Carbonaceous chondrite (CC) materials are shown in blue, and non-carbonaceous chondrite (NC) materials are shown in red. Ungrouped (Ungr.) are shown in black. See text for further details on group names and nomenclature. Figure based on Krot AN, Keil K, Scott ERD, Goodrich CA, Weisberg MK (2014) Classification of meteorites and their genetic relationships, In: Davis AM (Ed.) Treatise on Geochemistry (2nd edn.), Vol. 1. Elsevier, Amsterdam, pp. 1–63.

After the NC-CC division, a meteorite is classified as a chondrite (undifferentiated) or achondrite (primitive or differentiated) based on its bulk composition and texture. Further subdivision is based on a sample's mineralogy, petrography, and, if possible, O isotopic composition and the proportions of chondritic components (Fig. 4). Following Weisberg et al. (2006) and Krot et al. (2014), the hierarchy of terms for classification used here is *class*, *clan*, *group*, and *subgroup*. If the composition of a sample does not fall into an existing category, it is referred to as *ungrouped*.

A chondrite *class* consists of two or more groups sharing primary whole-rock chemical and O isotopic compositions (e.g., carbonaceous chondrites, ordinary chondrites, enstatite chondrites) (Hutchison, 2004; Weisberg et al., 2006). Designation of a primitive achondrite or differentiated achondrite into a class is not typically practiced.

Originally, a *clan* was defined as chondrites that share similar chemical, mineralogical, and isotopic compositions such that they can be interpreted as having formed at approximately the same time, in the same small region of the disk, in a narrow range of heliocentric distances (e.g., CI clan, CM-CO clan, CV-CK clan, CR clan, H-L-LL clan, EH-EL clan) (Kallemeyn and Wasson, 1981; Weisberg et al., 1995, 2006; Kallemeyn et al., 1996). Clan-status has also been assigned to meteorites from melted parent bodies such as achondrites or primitive achondrites (ACA-LOD clan, HED clan, SNC clan) (Weisberg et al., 2006). Nowadays, the clan status of a meteorite is less commonly used for classification than its class and group status because the significance of the clan-status is not well constrained.

The *group* status of a meteorite is its most commonly used taxonomy. A group is defined as a minimum of five unpaired meteorites of closely similar petrology, whole-rock chemical and O isotopic characteristics (Wasson, 1985; Weisberg et al., 2006). For chondrites, the group status indicates that samples are from the same or similar asteroid. This terminology is also used for achondrites, however, there are some groups that include samples that may have formed on several different parent bodies (e.g., IAB irons, pallasites, brachinites, aubrites, and eucrite-like meteorites).

Systematic petrological differences between members of the same group permit the designation of a sample into *subgroups* (e.g., reduced CV_{Red}). If there are less than five members, a *grouplet* status is given.

2.3. Chondrites

Chondrites originate from parent bodies that have not undergone wholescale melting. As such, chondrites preserve comparatively unmodified precursor material from which their parent bodies were constructed and provide the opportunity to study the earliest-formed solids in the Solar System.

Chondrites are stony meteorites that are composed of a fine-grained matrix of pristine primary (from condensation) and secondary (newly formed by reaction) silicates, oxides, and opaque minerals. Embedded in the matrix are macroscopic lithic clasts (also referred to as chondrite components) such as *chondrules*, refractory inclusions found as *calcium-aluminum-rich inclusions* (CAIs) or *ameboid olivine aggregates* (AOAs), and dark inclusions (Fig. 3). The matrix also contains microscopic soluble and insoluble organics and presolar grains. A microxenolithic inclusion of comet-related material enriched in organic matter and presolar grains was identified in a CR chondrite (Nittler et al., 2019).

Chondrites are classified into three classes (carbonaceous, ordinary, and enstatite) and 17 groups based on their mineralogical and elemental compositions (Fig. 4). The most commonly studied chondrite groups are enstatite chondrites (high-iron (EH) and low-iron (EL)), ordinary chondrites (high-iron (H), low-iron (L), and low-iron, low-metal (LL)), and carbonaceous chondrites (CI, CM, CO, CV, CK, CR, CH, CB, CL, CY). Other chondrite groups are the Rumuruti (R) and Kakangari (K) chondrites. The different compositions of chondrite groups likely reflect different physicochemical conditions during the formation of their parent bodies within the protoplanetary disk. The CB and CH carbonaceous chondrite groups are unusually metal-rich, and may have been formed via a giant planetary impact (Krot et al., 2005a). Three CV subgroups (CV_{OxA}, CV_{OxB}, CV_{Red}) for oxidized and reduced types had been proposed based on the abundance of metallic Fe-Ni phases and Ni contents of sulfides (McSween, 1977). These subgroups, however, can be further related to two distinct parent bodies. Thus, they have been classified into two individual subgroups CV_{Ox} and CV_{Red} (Gattacceca et al., 2020). In addition, there are almost a hundred ungrouped chondrites that are reported in the Meteoritical Bulletin Database and do not fit the petrographic descriptions of established groups. Several chondrites sometimes classified as anomalous within a group or as ungrouped chondrites may be members of the recently proposed CL and CY carbonaceous chondrite groups (Metzler et al., 2021; Suttle et al., 2021; King et al., 2019), or may eventually constitute new groups or grouplets.

2.3.1. Petrologic types of chondrites

Although chondrite parent bodies did not undergo wholescale melting, they underwent varying degrees of secondary processing after accretion, such as thermal metamorphism, aqueous alteration, impact shock, and space weathering. Chondrites were also further modified by terrestrial atmosphere entry and weathering.

The extent of parent body alteration is classified by petrologic type, which is a two-dimensional classification grid based on the chemical and petrologic subdivisions of the chondritic meteorites (Fig. 5) (Van Schmus and Wood, 1967). Petrologic types 1 and 2 indicate relatively low-temperature alteration processes due to the presence of water. The preservation of pristine minerals such as olivine and pyroxene and observation of chondrules distinguishes type 2 from type 1 chondrites. Type 3 chondrites (with possible sub-types 3.00–3.9) are the most pristine and least modified by secondary processes. Types 4, 5, and 6 indicate equilibration due to thermal metamorphic effects and recrystallization processes. Heating effects can be discerned up to type 7 if chondrites have been metamorphosed to just below the point of melting (metal-troilite assemblages and partial melting of silicates) and contain practically no observable chondrules (Tait et al., 2014; Tomkins et al., 2020). Although not in use in the current nomenclature, a possible type 8 has been proposed to denote significant extraction of silicate melt (corresponding to at least

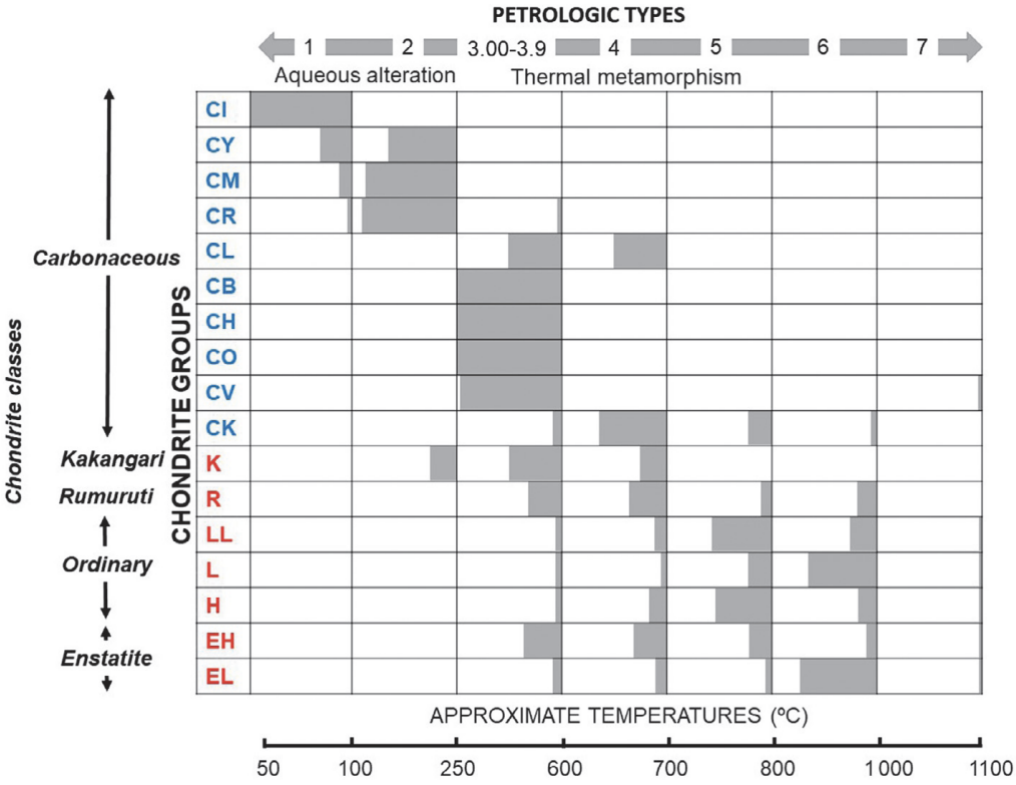

Figure 5: The chondrite classification system. The existing classes, groups, and petrologic types are shown for all chondrites. The chondrite groups are divided into three main classes, shown by the vertical two-headed arrows. Approximate temperatures of metamorphism (thermal or aqueous) are shown on the lower x-axis. Petrologic type is indicated on the upper x-axis. Types 3 (with sub-types 3.00 to 3.9) to 7 are unequilibrated to thermally altered chondrites, with type 7 designating chondrites that have been thermally metamorphosed nearing the point of melting. Types 1 and 2 are aqueously altered chondrites (Tomkins et al., 2020; McSween and Huss, 2022). Shaded areas illustrate the approximate relative proportions of each petrologic type reported in the Meteoritical Bulletin Database, except type7 chondrites that are rare. CR6 and CR7 meteorites are reported in the Meteoritical Bulletin Database, but they have been instead proposed to be primitive achondrites that are not related to CR chondrites (Ma et al., 2022). CY data are from Suttle et al. (2021). Figure based on Van Schmus WRV, Wood JA (1967) A chemical-petrologic classification for the chondritic meteorites. *Geochimica et Cosmochimica Acta* 31: 747–765 and McSween Jr, H, Huss G (2022) *Cosmochemistry*, 2nd ed., Cambridge University Press.

5 vol% of plagioclase) which would correspond to the transition between lodranite and acapulcoite primitive achondrites (Jacquet, 2022). Note, this petrological scheme is not applied to any meteorites that have undergone aqueous alteration followed by thermal metamorphism (e.g., some CI and CM meteorites).

The aqueously altered chondrites are identified by the presence of secondary minerals such as phyllosilicates (e.g., clays), chlorites, or magnetite, which formed by the reaction of melted water ice (due to heating from ^{26}Al decay and/or collisions) with anhydrous phases such as metallic Fe-Ni, Fe-sulfide, olivine, and glass (Rubin, 2023). Some secondary minerals may be difficult to identify due to their small sizes.

The thermal metamorphic types 3–6 are denoted using the 100 × Fe/(Fe + Mg) ratio of the main mafic mineral phases olivine and pyroxene which corresponds to fayalite and ferrosilite contents, respectively, and their degree of equilibration (Dodd et al., 1967). For type 3 chondrites, sub-types from 3.00 to 3.2 are established based on the Cr_2O_3 content of ferroan olivine in chondrules (Grossman and Brearley, 2005) or Fe-Ni metal texture and chemistry (Kimura et al., 2008). Types 3.4–3.9 can be further distinguished by thermoluminescence sensitivity. Petrographic observations such as the structural state and

disappearance of low-Ca pyroxene (Van Schmus and Wood, 1967), feldspar growth, and sharpness of chondrule boundaries are used to distinguish between types 4, 5, and 6. Other analytical methods have been proposed to quantify the thermal metamorphic peak of type 3 CV chondrites based on Raman spectroscopy of organic matter present in the matrix (Bonal et al., 2006).

In general, enstatite and ordinary chondrites have been most affected by thermal metamorphism with petrologic types ranging from 3 to 6 or 7. Carbonaceous chondrites can either be aqueously altered with petrologic types from 1 (CI) to 2 (CM, CY) to 3 (CR), or be primitive (3) to thermally metamorphosed with types 3.0 to 3.8 (CO), types 3.9 to 4 (CL), to highly metamorphosed from 3 to 6 (CK), or even 7 (CV) (without any classified CV types 4, 5 or 6) (Fig. 5). Five meteorites have been classified as CR6 or CR7 based on their triple oxygen isotopic compositions, Fe-rich silicate compositions, metal abundance, and equilibrated textures (e.g., CR7 NWA 7531; Ruzicka et al., 2015). These meteorites (along with some ungrouped chondrites) are actually primitive achondrites with the proposed group name of Tafassites, and they originate from a different parent planetesimal compared to CR chondrites (Ma et al., 2022).

2.3.2. Shock effects and brecciation

Shock effects due to impact processes are caused by the compression and disruption of colliding planetary bodies. The consequence of shock on the composition of the primary minerals (olivine, orthopyroxene, plagioclase) and texture of enstatite and ordinary chondrites has been described in detail (Stöffler et al., 1991; Rubin et al., 1997). These meteorite groups show the most pronounced effects of impact processes among the chondrite groups. The shock effects preserved in carbonaceous chondrites suggest less intense impact events, possibly due to sampling bias or their higher porosity, when compared to enstatite and ordinary chondrites (Scott et al., 1992).

Shock levels are distinguished using a scale ranging from S1 to S6 that is based on the optical microscope observation of olivine and plagioclase in polished thin sections. A shock level of S7 may be used when partial to complete melting is observed. Many high-pressure polymorphs of major minerals (stishovite for SiO_2, bridgmanite for $(Mg,Fe)SiO_3$) suspected to exist within Earth's interior were first or uniquely observed in natural settings within shocked meteorites (e.g., El Goresy et al., 2004; Tschauner et al., 2014).

Breccias are formed by impacts of asteroids and comets with planetesimals or planets. They are composed of fragments of rocks from a common (*monomict*) or different (*polymict*) origin. Breccias may contain xenolithic clasts of materials, which may not have been sampled yet as individual meteorites (Bischoff et al., 2006). Impact breccias provide a record of regolith formation, mixing of planetesimals, and major impact periods related to planet migration in the Solar System. An atypical polymict breccia meteorite is Almahatta Sitta. This meteorite was recovered in Sudan after the fall event of the asteroid 2008 TC3, which is the first asteroid detected and observed in space directly prior to impacting Earth. The breccia contains mostly ureilite fragments mixed with a variety of chondritic and achondritic materials (Bischoff et al., 2022).

2.3.3. Terrestrial weathering

Most (~98%) of the classified meteorites are found in cold or hot deserts such as Antarctica and Northwest Africa, respectively. Changes to the mineralogy and chemical composition of meteorites take place over time due to exposure to Earth's oxidizing environment. Terrestrial weathering begins from the entry of the sample through the Earth's atmosphere and continues while the meteorite sits on the surface. The longest duration of terrestrial weathering has been documented to be more than two million years for meteorites found in the Atacama Desert (Drouard et al., 2019). Mineralogical and textural changes can also

occur during curation, after the meteorite has been collected. Many museums and collectors go to great lengths to prepare and preserve planetary materials under dry, and, where possible, oxygen-poor conditions (e.g., in nitrogen-filled glove boxes or storage cabinets).

The changes caused by terrestrial weathering must be taken into consideration during the study of a meteorite. Minerals can react with Earth's atmosphere, water, and other environmental factors such as microbial activity, which leads to alterations in their appearance, structural integrity, and elemental and isotopic composition (Bland et al., 2006; Stephant et al., 2018). Oxidation and heating can create the characteristic reddish-brown internal appearance of a meteorite, but it can also produce cracks and fragmentation as well as obliteration of the original fusion crust into a patina.

Weathering scales from A to C for Antarctic meteorites and from W1 to W6 for other finds have been defined for ordinary chondrites. These scales are based on mineralogical changes (e.g., oxidation of metals and sulfides into secondary oxides and sulfates, alteration of silicates, and formation of secondary carbonates or caliche) and structural observations (e.g., cracks) (Wlotzka, 1993). For metal-poor chondrites, such as CK and R, a weathering index wi-1 to wi-6 was defined based on the staining of silicates, alteration and oxidation of sulfides, and silicate replacement by phyllosilicates (Rubin and Huber, 2005).

2.3.4. Chondrite Components

2.2.4.1. Chondrules

Chondrules are a major component of many chondrites (except in CI) and represent 15–80 vol%, with many carbonaceous chondrites being composed of approximately equal amounts of chondrules and fine-grained matrix. Chondrules are rounded inclusions, which vary in sizes from hundreds of micrometers to millimeters in diameter, and occasionally they are found with diameters of several millimeters (Fig. 3). Chondrules can contain olivine, pyroxene, oxides, mesostasis, sulfides, and metal. Chondrule petrology indicates that they formed as molten or partially molten droplets in space before being accreted to their parent body.

There is a complementary relation between the elemental composition of the matrix and chondrules in carbonaceous chondrites which is known as *matrix-chondrule complementarity*. Chondrules have low Si/Mg and Fe/Mg ratios, when compared to bulk carbonaceous chondrites with Solar abundance ratios. The matrix has the opposite signature, high Si/Mg and Fe/Mg ratios. In some carbonaceous chondrites, chondrules have low Al/Ti ratios, whereas the matrix has the opposite signature and the bulk is chondritic. It has been proposed that the reservoir sources of chondrules and matrix were unrelated and the apparent comple- mentarity was established by chemical exchange during secondary parent body processes (e.g., Zanda et al., 2018). Alternatively, chondrite-matrix complementarity was established in the nebula and may reflect formation and evolution from a single, CI-like reservoir rather than parent body processes on carbonaceous chondrite asteroid(s) (Palme et al., 2015). As the bulk compositions of carbonaceous chondrites have CI chondritic Mg/Si ratios, their respective chondrules and matrices must be chemically connected. With a Mg-rich component used as the precursor for chondrules, the remaining Mg-depleted material would form the matrix, preserving the complementarity at the bulk scale (Hezel and Palme, 2010).

The processes responsible for chondrule formation are still a matter of debate. Chondrules may have resulted from melting of nebular precursors (Marrocchi et al., 2018) induced by transient heating events in the Solar nebula, such as those associated with shock waves and planetesimal bow shocks (Rubin, 2000; Desch and Connolly, 2002; Morris et al., 2012). Alternatively, some chondrules may have a planetary origin, being formed via impacts (for CB/CH; Krot et al., 2005a,b) or possible remelting of planetary crust (Villeneuve et al., 2011).

2.3.4.2. Calcium-aluminum-rich inclusions

Calcium-aluminum-rich inclusions (CAIs) are submillimeter- to centimeter-sized clasts in chondrites. They have a refractory chemical composition and mineralogy that set them apart from other chondrite components. The elemental and isotopic composition of CAIs indicates they formed in the high-temperature regions of the Solar nebula (i.e., close to the nascent Sun) (Grossman, 1972). They are, however, found in carbonaceous chondrites that contain hydrous minerals which indicates that their parent bodies accreted near or beyond the snow line. Abundances of CAIs vary from 15 to 4 vol% in CO, CV, CK, CM, <1 vol% in CR, CY, CH, and CB, and they are rarely found in K, R, ordinary or enstatite chondrites. Calcium-aluminum-rich inclusions are very rarely found in CIs, but this is likely because CIs are extensively altered and thus do not retain textural evidence of their original componentry. As CAIs are most abundant and largest in size in anhydrous CV3, the most studied meteorites for CAIs are Allende ($CV3_{ox}$) (Fig. 3) and Efremovka ($CV3_{red}$). Recently, large inclusions found in desert finds (e.g., NWA 2364, NWA 3118, NWA 6991) were also studied for their chemical and isotopic compositions (Bouvier and Boyet, 2016; Ivanova, 2023).

Calcium-aluminum-rich inclusions are considered to be the first solids that condensed from the nebular gas of Solar compo- sition under a total pressure of $<10^{-3}$ bar and temperature of 1600–2000 K (Grossman, 1972). They are primarily composed of minerals such as hibonite, corundum, anorthite, spinel, perovskite, and melilite, as well as some alteration products (e.g., sodalite) (see Ivanova, 2023 for a review). The classification of CAIs is based on their texture (fine-grained Type A or coarse-grained Type B or C), mineralogy (melilite, fassaite, and a third component consisting of all other phases), and chemical compositions (rare earth element, REE, patterns) (see Brearley and Jones (1998) for detailed chemical characteristics of CAIs). Hibonite-rich CAIs called PLACs (PLAty hibonite Crystals) and FUN (Fractionated and Unidentified Nuclear isotopic effects) inclusions have anomalous O isotopic compositions and low ^{26}Al abundance compared to normal CAIs (Wasserburg et al., 1977; Ireland 1990; Kööp et al., 2016). Amoeboid olivine aggregate inclusions (AOAs) are another type of fine-grained inclusions, which are typically composed of virtually Fe-free olivine associated with Al-diopside, anorthite, and spinel. They exhibit a wide variety of textures and compositions, indicating complex formation histories.

Calcium-aluminum-rich inclusions can display distinctive textures and shapes (amoeboid, spherical, disk shape, crucible shape, deformed), which are a result of their formation and plastic deformation in a high-temperature environment followed by rapid cooling and, possibly, melting (Ivanova, 2023). A *Wark-Lovering rim* (WLR) can be found around certain CAIs. A WLR consists of minerals identical to the main portion of the CAI (e.g., melilite, spinel, and pyroxene) but crystallized after the core of the inclusion had been formed (Wark and Lovering, 1977). The origin of WLRs is still not well established, but data suggest a late formation, 2–3 Myr after the formation of the core of the host CAIs, most likely during brief heating episodes as a result of thermal processing in the Solar nebula (Mane et al., 2015). If this occurred, it implies that CAIs remained as free-floating objects in the Solar nebula for 2–3 Myr until their accretion with chondrules and matrix to form chondrite parent bodies.

Calcium-aluminum-rich inclusions are key chondrite components for constraining high-temperature processes and transfer of material that occurred during the early stages of Solar System formation. Their elemental compositions and mineralogy provide information about the thermal history, gas compositions, and redox changes of the Solar nebula and can be used to infer the timing of chondrite parent body accretion. For further reading on CAIs and AOAs, refer to a recent review on the petrological and chemical compositions of refractory inclusions by Ivanova (2023).

2.3.4.3. Matrix

The matrix in chondrite meteorites is a fine-grained (i.e., grains are often less than a micrometer in size, down to 50 nm) material that surrounds and embeds larger components such as chondrules, refractory inclusions, and metal grains, mixed with presolar grains. It is a major component of chondrites, particularly in carbonaceous chondrites with up to 50 vol% of matrix. Common minerals in the matrix include silicates such as olivine and pyroxene, amorphous Fe-Mg silicates, and oxides such as magnetite in carbonaceous chondrites, as well as Fe-Ni metal and sulfides (troilite). The exact mineralogy depends on the type of chondrite and its thermal and aqueous alteration history. The near-solar (i.e., CI-like) composition of the matrix implies that the amorphous silicates have similar origins and that gas and dust were not separated during condensation (Scott and Krot, 2005). The matrix (mineralogy, composition) of chondrite meteorites provides important information about the chemical and physical conditions in the Solar nebula as well as parent body processes (McSween and Huss, 2022). As mentioned above, one of the most important open questions is whether the matrix and chondrules may have formed in the same or in different locations of the Solar nebula (e.g., Hezel and Palme, 2010 for further discussion). The matrix is generally porous (up to 30% for types 1–3 chondrites), which can influence the overall density and mechanical properties of the meteorites and their parent bodies (e.g. Corrigan et al., 1997).

2.3.4.4. Presolar grains

Presolar grains are predominantly found in chondrites. They are small (nanometer- to micrometer-sized) dust particles which fall into two general types, *interstellar grains* and *circumstellar condensates*. Interstellar grains have no direct association with a specific stellar event. They formed in dense molecular clouds either from atoms that did not condense into grains after ejection from stars, or from atoms that were vaporized in the ISM by supernova shocks or radiation (McSween and Huss, 2022). Circumstellar condensates (or *stardust*) are grains that condensed from hot gas ejected in the immediate vicinity of parent stars that were in the final stages of their life. In practice, circumstellar condensates are often referred to as presolar grains even though this term also refers to interstellar grains.

Different types of presolar grains have been identified, such as silicon carbide (SiC), oxide, silicate, graphite, diamond, and Al-rich refractory grains, and rarely silicon nitride grains (Davis, 2011). These grains vary in concentration and distribution between meteorite groups, but they are generally best preserved in primitive carbonaceous chondrites, interplanetary dust particles, micrometeorites, cometary matter, as well as in Ryugu's carbon-rich exogenous clasts (Fig. 6) (Leitner et al., 2020; Nguyen et al., 2023 and refs. therein). The location in a sample, size, and elemental and isotopic composition of individual presolar grains of a meteorite can be determined by nano-SIMS. Alternatively, a mass spectrometer using resonance ionization to eliminate isobaric interferences of elements can be used as it was developed for the isotopic analysis of presolar grains (called CHILI for Chicago Instrument for Laser Ionization probe) (Stephan et al., 2016).

Because presolar grains are formed in stellar environments, their isotopic compositions are very different (or anomalous) from those measured in Solar System-derived materials. The highly anomalous isotopic compositions of presolar grains reflect the integration of the final nucleosynthetic process as well as nucleosynthetic events in precursor stars (i.e., a single stellar event may not necessarily define an isotopic composition of a presolar grain, although the final event may dominate). Presolar grains have been linked to asymptotic giant branch stars, supergiants, supernovae, and novae (e.g., Zinner, 1998; Nittler, 2003; Hoppe et al., 2022). Extreme enrichments (i.e., tens to hundreds of percent) for isotopes of some elements have been documented in presolar grains (e.g., O, C, N, Si, Mg, Cr, Ti, Ru, Mo, Xe, Ba, Nd, Sm) (Zinner, 1998; Nittler, 2003). Thus, even small concentrations (tens to hundreds of parts per million, ppm) of

presolar grains can dominate the budget for certain isotopes in meteorites and their components (Sections "Disk composition and evolution: Insights from meteorite chronology and isotopic variations" and "Sample-based constraints on Solar System formation").

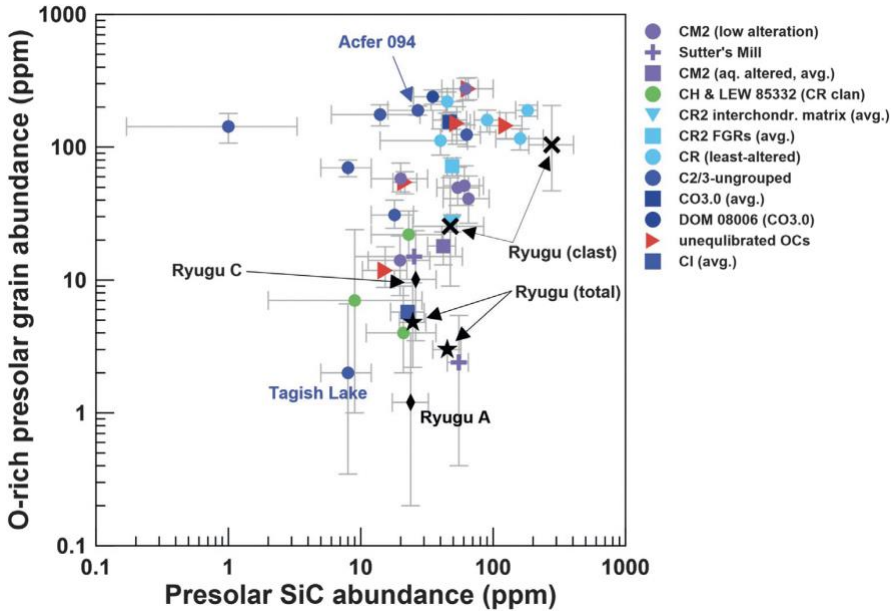

Figure 6: Abundances (on a log scale) of presolar O-rich and SiC grains in primitive to aqueously altered chondrites (Leitner et al., 2020 and refs. therein). Also included are Ryugu samples collected at the surface (A), within an artificial crater (C), C-rich clasts (black crosses), and total for bulk (black stars) (Nguyen et al., 2023). All estimated error bars are 1s based on grain distributions. Credit: Jan Leitner (Universität Heidelberg).

2.4. Primitive and differentiated achondrites

Achondrites are divided into two broad categories—*primitive achondrites* and *(igneously) differentiated achondrites*, the latter are commonly referred to as achondrites (Fig. 4). Based on their mineralogy, textures, and elemental compositions, primitive and differentiated achondrites are interpreted to have originated from initially chondritic parent bodies that have undergone variable degrees of melting. Thus, their original chondritic textures and components (e.g., chondrules, CAIs, AOAs, presolar grains, matrix) are often not preserved. Achondrites and primitive achondrites provide the opportunity to study early melting events and their products.

Goodrich and Delaney (2000) proposed that primitive achondrites can be distinguished from differentiated achondrites based on their Fe-Mg-Mn systematics. Primitive achondrites have chondritic Mn/Mg ratios because they are the residues of partial melting, whereas differentiated achondrites have super-chondritic Mn/Mg and near constant Fe/Mn ratios because they are melts or cumulate products of melts from wholescale melting of their parent bodies (Fig. 7). Accordingly, the non-chondritic meteorites that can be classified as primitive achondrites are the acapulcoites, lodranites, winonaites, ureilites, and brachinites, whereas the differentiated achondrites include the lunar basalts, Martian meteorites, HEDs (howardite-eucrite-diogenites), angrites, and aubrites (Goodrich and Delaney, 2000; Weisberg et al., 2006) (Fig. 4). Nevertheless, disagreement persists about which category certain meteorites should be assigned to. For example, owing to the high degree of melting inferred for ureilites and brachinites, both meteorite groups are sometimes classified as differentiated achondrites (Mittlefehldt, 2014).

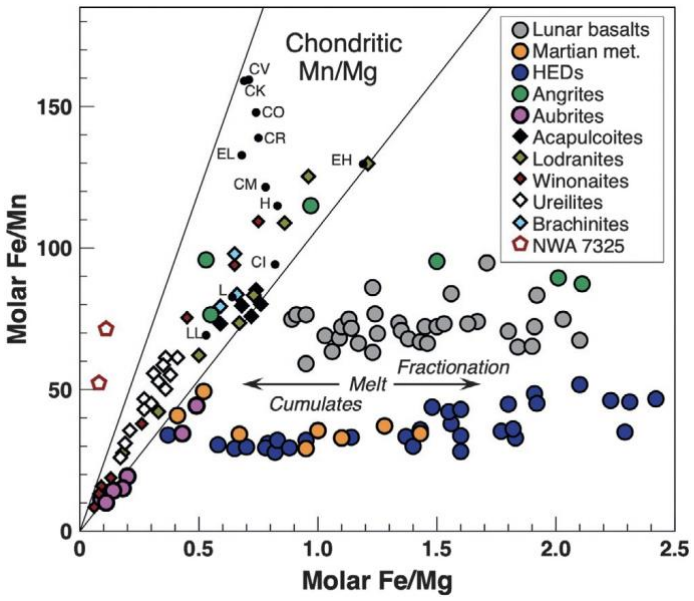

Figure 7: Molar Fe/Mn vs Fe/Mg for chondrites (small black spheres) and achondrites. The black lines graphically delineate Fe/Mn-Fe/Mg variations in chondritic meteorites. A melt produced by equilibrium partial melting from chondritic material will have a high Fe/Mg ratio; fractional crystallization of such melts moves them horizontally to even higher Fe/Mg, whereas the produced cumulates move horizontally to lower Fe/Mg. Differentiated achondrites (lunar basalts, Martian meteorites, HEDs, angrites, aubrites) have super-chondritic Mn/Mg and near constant Fe/Mn ratios because they are melts or cumulate products of melts. Primitive achondrites have chondritic Mn/Mg. The ungrouped achondrite NWA 7325 has a unique sub-chondritic Mn/Mg molar ratio (Yang et al., 2020). Modified from Goodrich CA, Delaney JS (2000) Fe/Mg-Fe/Mn relations of meteorites and primary heterogeneity of primitive achondrite parent bodies. Geochimica et Cosmochimica Acta 64(1): 149–160 and Yang J, Lin Y, Changela H, Xie L, Chen B, Yang J (2020) Early sulfur-rich magmatism on the ungrouped achondrite Northwest Africa 7325 differentiated parent body. Meteoritics & Planetary Science 55: 1951–1978 with data sources therein.

The increasing number of primitive achondrites discovered over the past two decades, particularly in Northwest Africa, has revealed that some mineralogical and geochemical criteria used to distinguish the different groups are outdated or inadequate. Eight primitive achondrites have recently been reclassified into a new, common group—the so-called Tissemouminites—based on their similar mineralogical characteristics (olivine fayalite content and FeO/MnO ratios, plagioclase K content), O isotopic signatures, and the presence of relict chondrules (Stephant et al., 2023). Textural, mineralogical, and isotopic criteria have also linked Tafassasset and 12 other meteorites as a first group of carbonaceous primitive achondrites (Ma et al., 2022). There are also nearly 150 *ungrouped achondrites* reported in the Meteoritical Bulletin Database which originate from various planetesimals formed throughout the Solar System. Among these, rare evolved andesitic (e.g., Erg Chech (EC) 002) and reduced achondrites (e.g., NWA 7325) may sample early planetary crusts formed by igneous differentiation (Barrat et al., 2021) or re-processing due to impact melting (Frossard et al., 2019), respectively.

2.4.1. Primitive achondrite mineralogy and texture

Primitive achondrites have near-chondritic bulk compositions (e.g., Mn/Mg ratios; Fig. 7) and mineral assemblages, but their textures have been modified by metamorphism or igneous processing at higher temperatures than those experienced by the most highly metamorphosed chondrites (Mittlefehldt, 2014). Temperatures within their parent bodies were sufficiently high (≥950 ˚C) for partial melting of metal and silicates to occur, but remained too low for complete melting and differentiation. Since primitive achondrites can be considered to be transitional between chondrites and *bona fide* achondrites, they are

important samples for tracing the earliest stages of melting and melt segregation on planetesimals and the thermal history of their parent bodies.

Primarily based on O isotopic compositions, links have been postulated between acapulcoites and lodranites and between winonaites and silicate inclusions in some IAB irons (Clayton and Mayeda, 1996). In addition, acapulcoites and lodranites have similar mineralogies, mineral compositions, and cosmic-ray exposure ages (Section "Mass-independent isotope variations"), suggesting that they may originate from a common parent body that was compositionally similar to, but more reduced than, H group ordinary chondrites (Keil and McCoy, 2018; McCoy et al., 1997).

The fine-grained acapulcoites presumably formed from very low degrees of partial melting (~1 to 4 vol%) just above the Fe,Ni-FeS cotectic (~1120 K), whereas the coarser grained lodranites were heated to higher temperatures (1370–1520 K) and are the residues of higher degrees of Fe,Ni-FeS cotectic and silicate partial melting (~5 to ≥10 vol%) (McCoy et al., 1997). Melting was likely triggered by the decay of short-lived ^{26}Al (Keil and McCoy, 2018), although shock events have also been considered as a potential heat source (Rubin, 2007).

The winonaite-IAB parent body presumably had a more complex formation history; incomplete differentiation was followed by localized impacts or catastrophic impact break-up and re-assembly (Benedix et al., 2000). Extensive heating to peak temperatures of ~1470 K caused metamorphism and partial melting of both Fe,Ni-FeS and silicates, as indicated by the presence of veins of Fe,Nimetal and troilite as well as trapped basaltic partial melts (Benedix et al., 1998, 2000). The bulk elemental composition, mineralogy, O isotopic composition of winonaites and silicate inclusions in IAB irons, together with nucleosynthetic Mo isotopic compositions of IABs and winonaites, indicate that their parent body formed from precursor material that was distinct from any known chondrites (Benedix et al., 1998; Clayton and Mayeda, 1996; Worsham et al., 2017), at redox conditions that were intermediate between those recorded by enstatites chondrites and acapulcoites (Kimura et al., 1992).

Ureilites, coarse-grained ultramafic achondrites that contain an unusually high abundance of carbon (averaging ~3 wt%), are considered to be mantle-derived samples from a C-rich body (Barrat et al., 2016). In contrast to the other primitive achondrites, their O isotopic compositions are highly variable and do not follow a mass-dependent fractionation trend (Clayton and Mayeda, 1996), indicating that their parent body did not experience large-scale melting. Similarly, the heterogeneous O isotopic composi- tions of brachinites (Clayton and Mayeda, 1996), which are medium- to coarse-grained olivine-rich achondrites, may indicate incomplete isotopic homogenization during melting and igneous processing or an origin from several distinct parent bodies (Keil, 2014; Krot et al., 2014). Nonetheless, the parent bodies of both ureilites and brachinites likely experienced more extensive degrees of partial melting (~20 to 30 vol%) than those recorded by other primitive achondrites (Mittlefehldt, 2014; Mittlefehldt et al., 1998).

2.4.2. Differentiated achondrite mineralogy and textures

Differentiated achondrites are igneous rocks (melts or cumulates) or breccias of igneous rock fragments from the silicate-dominated crust/mantle of large asteroids (e.g., 4 Vesta) or planetary bodies (Mars and Moon) that experienced wholescale melting and differentiation to form a core, mantle, and crust. Their elemental abundances (e.g., Mn/Mg and Fe/Mg; Fig. 7) are highly fractionated compared to chondritic materials (Mittlefehldt, 2014).

Angrites, a small group of mafic volcanic-plutonic rocks (Keil, 2012), originate from an unidentified parent body (the angrite parent body, APB) that may have been disrupted (Touboul et al., 2015) or consumed during the formation of the terrestrial planets (Tissot et al., 2022). The howardite, eucrite, diogenite (HED) group consists of basaltic, gabbroic, and ultramafic cumulate igneous rocks (McKeegan et al., 2011), most of which are brecciated (Mittlefehldt, 2015). They have been spectroscopically linked to

the asteroid 4 Vesta (McCord et al., 1970; Binzel and Xu, 1993), notably by NASA's Dawn mission that orbited the asteroid for more than a year (McSween et al., 2011). Vesta appears to be the only intact, surviving differentiated planetesimal. The peculiar O isotopic compositions of a few eucrite-like meteorites, however, suggest that they may originate from other parent bodies (Mittlefehldt, 2005). Aubrites, whose mineralogy, oxygen isotopic signature, and highly reduced nature show a close affinity with enstatite chondrites (EH and EL) (Keil, 2010), are currently considered to be the best available analogues of Mercury's surface (Cartier and Wood, 2019).

Lunar meteorites sample a variety of basaltic and anorthositic terrains on the Moon, and their total mass (>1100 kg; Meteoritical Bulletin Database) greatly exceeds that of samples returned by the Apollo, Luna, and Chang'e missions. Martian meteorites (shergottites, nakhlites, chassignites, ALH (Allan Hills) 84001 orthopyroxenite, NWA (Northwest Africa) 7034 polymict breccias, and NWA 8159 augite basalt) are of particular value given they are the only recognized samples of Mars currently available to study in laboratories on Earth (McSween, 1994; Udry et al., 2020). These differentiated achondrites are of particular importance for our understanding of the timescales of planetary accretion, large-scale melting (i.e., magma ocean stage), and differentiation.

2.5. Iron meteorites

Most iron meteorites are dominated by a continuous metal Fe-Ni matrix with between 5 and 60 wt% Ni (the majority falls within 5–10 wt% Ni range and >90 wt% Fe). Interspersed throughout the Fe-Ni matrix are minor amounts of Co (0.4–0.6 wt%), P (0.1–0.5 wt%), S (~0.1–1 wt%), and trace amounts of other elements that are predominantly siderophile (iron-loving) or chalcophile (S-loving) (percentages are determined without including the silicate-rich iron meteorites).

Some of these trace elements combine to form mineral inclusions such as troilite (FeS) and schreibersite ($(Fe,Ni)_3P$) (e.g., Goldstein et al., 2009; Krot et al., 2014; Mittlefehldt, 2014). Other minor phases can include graphite (C), chromite ($FeCr_2O_4$), daubréelite ($FeCr_2S_4$), carlsbergite (CrN), and several others. Readers are directed to comprehensive reviews of iron meteorite mineralogy, bulk chemistry, cooling rate determination, fractional crystallization modeling, isotopic compo- sitions, chronology, and formation processes (Buchwald, 1975; Benedix et al., 2014; Haack and McCoy, 2003; Krot et al., 2014, 2005a,b, Mittlefehldt, 2014; Mittlefehldt and McCoy, 2014; Weisberg et al., 2006).

Iron meteorites constitute 4–5% of all meteorite falls (Buchwald, 1975; Krot et al., 2014). The elemental compositions of metal phases indicate that most iron meteorites can be divided into 13 *chemical groups* (IAB, IC, IIAB, IIC, IID, IIE, IIF, IIG, IIIAB, IIIE, IIIF, IVA, IVB; Fig. 4). Those meteorites that do not fall into one of these groups are termed *ungrouped* (they were originally called *chemically anomalous*; Buchwald, 1975). Those data clusters that contain between two or four samples are termed *grouplets* (Scott, 1979). With a few exceptions, iron meteorites are not paired with chondrite groups or achondrites. The exceptions typically refer to silicate inclusions that have been found in ~6% of iron meteorites (Buchwald, 1975).

2.5.1. Iron meteorite structural and chemical groups

Originally, iron meteorites were classified into *structural groups* based on their macroscopic textures. Structural groupings are based on the *Widmanstätten texture* that develops in the Fe-Ni phase as the parent body cools (Buchwald, 1975). The Widmanstätten texture is typically cross-hatched as it reflects an oriented intergrowth of body-centered cubic a-Fe with ~5 wt% Ni (*kamacite*), high-Ni regions such as *taenite* (face-centered cubic g-Fe with ~20 to 50 wt% Ni), or ordered Fe-Ni with ~50 wt% Ni which is termed *tetrataenite* (Krot et al., 2014). The Widmanstätten texture formed as kamacite lamellae exsolved

from taenite on cooling, where the width of these lamellae is dependent on the cooling rate of the melt, the bulk Ni concentration, and the nucleation mechanism (Yang and Goldstein, 2005). Within a meteorite, kamacite lamellae widths are relatively constant. Between meteorites, however, kamacite lamellae widths are highly variable. Because kamacite lamellae align along octahedral planes, iron meteorites with this structure are termed *octahedrites*. *Ataxites* contain >10 wt% Ni and have microscopic kamacite lamellae. *Hexahedrites* contain 5–6 wt% Ni and are composed of large (up to 25 cm or more) kamacite crystals and lack taenite. Fine intergrowths of kamacite and taenite between the major kamacite lamellae in octahedrites are called *plessite* (Goldstein and Michael, 2006; Scott, 2020).

The iron meteorite *chemical group* classification scheme is based on the systematic element relations between samples. These chemical data are supplemented by mineralogy, mineral structures, cooling rates, and isotopic data, which, when integrated, indicate that each iron meteorite group likely represents one parent body core (Scott and Wasson, 1975). This interpretation has been bolstered by the NC or CC designation of a meteorite. If iron meteorites share the same stable mass-independent isotope composition, they may originate from a common parent body (Bermingham et al., 2018a; Fischer-Gödde et al., 2015; Kruijer et al., 2017; Worsham et al., 2017).

The first bulk chemical analyses of iron meteorites indicated that the concentrations of Ga and Ge clustered into three groups (*Class I–III*), and then later four groups (i.e., *Ga-Ge* groups) (Goldberg et al., 1951; Lovering et al., 1957). The four groups were designated *Groups I–IV*, with decreasing Ga and Ge concentrations (Lovering et al., 1957). As new data accumulated, letters were added to distinguish between additional groups (e.g., IVA and IVB). Analogous to chondrites, Ga and Ge have a narrow range in concentration within an iron meteorite group, however, these concentrations are more variable between groups (Wasson and Wai, 1976; Wai and Wasson, 1979). Gallium and Ge are the most volatile siderophile elements, thus the bulk chemical differences between iron meteorite chemical groups reflect chemical fractionation events that occurred during parent body accretion and core formation (Scott, 1972).

Over 12 papers, Wasson and colleagues published bulk sample chemical data for 13 elements on more than 750 iron meteorites using instrumental and radiochemical neutron activation analysis (instrumental neutron activation analysis, INAA; and radio- chemical neutron activation analysis, RNAA) (Kracher et al., 1980; Malvin et al., 1984; Schaudy et al., 1972; Scott et al., 1973; Scott and Wasson, 1976; Wasson, 1967, 1969, 1970; Wasson et al., 1989, 1998; Wasson and Kimbeblin, 1967; Wasson and Schaudy, 1971). On plots of Ni (wt%) vs log(E ppm; where E denotes a trace element such as Ga, Ge, Ir, Co, Au), ~85% of all iron meteorites fall unevenly into 1 of 13 clusters (e.g., IAB, IC, IIAB, IIC, IID, IIE, IIF, IIG, IIIAB, IIIE, IIIF, IVA, IVB; Fig. 8). On a Ni (wt%) vs log(Ir ppm) plot, most groups fall within restricted fields that form narrow elongated fields spanning a wide range in Ir concentrations. On a Ni (wt%) vs log(Ga ppm) plot, the same groups are present, but they fall within more restricted clusters. The remaining ~15% are ungrouped iron meteorites that have compositions that do not fall consistently into one of the 13 clusters and sample more than 50 different parent bodies (e.g., Scott, 1979). This is evident on a Ni (wt%) vs log(Ir or Ga ppm) plot where ungrouped iron meteorites fall in a scattered pattern.

As more samples were analyzed, the trace element data indicated that some of the original chemical groups were in fact related, thus a contraction of the nomenclature was required. This led to the current iron meteorite group terminology, where some groups have a combination of two letters after the roman numeral (e.g., IIIA and IIIB became IIIAB).

2.5.2. The magmatic iron meteorites

The chemical fractionations within 11 of the 13 groups (e.g., IC, IIAB, IIC, IID, IIF, IIG, IIIAB, IIIE, IIIF, IVA, and IVB) are generally consistent with the predicted chemical trends that occur during fractional crystallization of a large volume of molten metal (Scott, 1972; Willis and Wasson, 1978a,b). The

consistency between chemical composition and the predicted compositions for fractional crystallization of a molten metal, and the general absence of silicate inclusions, provided strong evidence that these iron meteorites are samples of asteroidal cores (Chabot and Haack, 2006; Wasson, 1985). Consequently, these groups are commonly referred to as the *magmatic iron meteorite groups*. The only known magmatic irons that contain abundant silicate are two IVA irons (Steinbach and São João Nepomuceno). The chemical composition and texture of the metal phases in these two samples, and their metallographic cooling rates, however, closely match the group IVA trends, and, thus, they remain part of the IVA group (Haack et al., 1996).

2.5.3. The non-magmatic iron meteorites

The IAB and IIE groups comprise the remaining two iron meteorite groups. Generally, meteorites in these groups display more limited and weaker trace element trends and contain silicate, graphite, and carbides (Goldstein et al., 2009; Scott and Wasson, 1975; Wasson, 2017; Wasson and Kallemeyn, 2002; Worsham et al., 2016). Wasson and Kallemeyn (2002) reclassified the IAB and IIICD groups as the *group IAB complex* based on the trace element compositions of the metal phase (e.g., Ni-Au plots). They denoted the *IAB main group* (>70 different iron meteorites), several different subgroups, and numerous grouplets. Most of the silicates in the IAB group, and some in the IIE group, occur in clasts in roughly chondritic proportions (roughly equal proportions of olivine and pyroxene with smaller abundances of feldspar), and some relict chondrules have been identified in silicate clasts in meteorites from the IAB and IIE groups (e.g., Campo del Cielo, IAB; Netschaëvo and Mont Dieu, IIE) (Olsen and Jarosewich, 1971; Schrader et al., 2017; Scott, 2020; Van Roosbroek et al., 2015).

The interelement trends with the IAB and IIE groups are not consistent with the predicted chemical trends that occur during fractional crystallization of an asteroid core. These iron meteorites are interpreted to have formed from impact-generated silicate and metal melts during early planetesimal collisions (e.g., Benedix et al., 2005; Benedix et al., 2000; Ruzicka, 2014; Wasson, 2017; Wasson and Kallemeyn, 2002; Worsham et al., 2017). As such, the IAB and IIE iron meteorites are collectively referred to as the *non-magmatic iron meteorite groups*. The formation processes of the IABs and IIEs, however, remain an active area of research (e.g., Hilton et al., 2020a,b; Hilton and Walker, 2020; Hunt et al., 2018; Kruijer and Kleine, 2019; Wasson, 2017; Worsham et al., 2016, 2017). Recent work combining petrographic observations, bulk sample chemical data, nucleosynthetic isotope data, and Hf-W metal-silicate segregation ages of IAB and IIE iron meteorites has generated new constraints on the composition of the bodies involved in the impacts, the number of impactors, the timing of collision, and the crystallization process that followed (e.g., Scott, 2020 for a review).

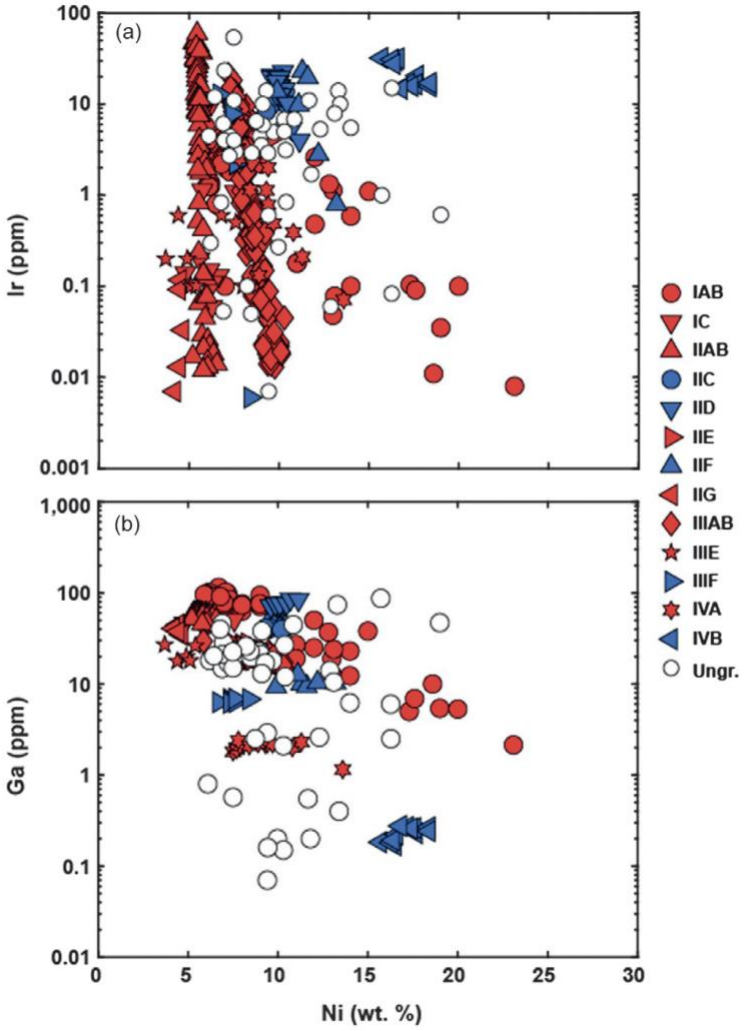

Figure 8: (a) log(Ir ppm) vs (Ni (wt%), (b) log(Ga ppm) vs Ni (wt%) for iron meteorites. The 13 colored symbols of different shapes denote the chemical groups that are collectively referred to as iron meteorite groups: IAB, IC, IIAB, IIC, IID, IIE, IIF, IIG, IIIAB, IIIE, IIIF, IVA, and IVB. These chemical groups are not equally populated. The NC- and CC-type irons are shown in red and blue, respectively. Ungr. = ungrouped are shown as the white symbols.

2.6. Stony irons

Mesosiderites are the most abundant type of stony-iron meteorites (365 specimens). They are characterized by an almost equal mix of silicate minerals and metallic Fe-Ni. The silicate part contains olivine, pyroxenes, and Ca-rich feldspar and is similar in composition to eucrites and diogenites (Rubin, 1997). They exhibit a brecciated texture, indicating a history of significant impact and fragmentation. The current theory for their formation suggests that mesosiderites originate from the violent collision of a differentiated asteroid, resulting in mixing of its metallic core and silicate mantle (e.g., Haba et al., 2019; Scott et al., 2001). Based on similar O isotopic composition and Ti-Cr isotopic anomalies and silicate compositions (Fe/Mn ratios in pyroxene and olivine), mesosiderites have been linked to the HED meteorites, which are believed to originate from the asteroid 4 Vesta (e.g., Rüfenacht et al., 2023) (Section "Differentiated achondrite mineralogy and textures"). Mesosiderites would have formed after a large impact on Vesta or a similar body. No mass-independent isotopic variations were however detected between mesosiderite clasts and minerals and with eucrites, arguing against a major contribution from an impactor with a different nucleosynthetic signature. The U-Pb chronology of zircons found in mesosiderites reveals

two distinct age populations at 4558.5 ±2.1 Ma (similar to zircon ages of basaltic eucrites) and 4525.39 ± 0.85 Ma (Haba et al., 2019). The two distinct ages therefore coincide with the timing of the crust formation and a large-scale reheating event (corresponding to the metal-silicate mixing) on the HED meteorite parent body. As 4 Vesta remains largely intact, the formation of mesosiderites is attributed to a hit-and-run collision with a smaller planetesimal (mass ratio 0.1) (Haba et al., 2019). This collision would have disrupted Vesta's northern hemisphere, leading to the accretion of ejected crust, mantle, and molten core debris onto the southern hemisphere. Mesosiderites then formed in the lower crustal region. The Rheasilvia impact crater at Vesta's south pole could be a likely source of these meteorites (Haba et al., 2019).

Pallasites are a second type of stony-iron meteorites. There are ~175 known pallasites and they constitute <1% of all meteorite falls. Pallasites are composed of roughly equal proportions of silicate (mainly olivine) and metal (with minor troilite). Based on mineral and metal compositions and O isotopic compositions, pallasites are divided into the main-group pallasites (MG-Pal), the Eagle Station group (ES-Pal) of which there are five members (Buseck, 1977; Scott, 1977a; Hilton et al., 2020a,b), and the ungrouped pallasites, which include the pyroxene pallasites grouplet of which there are now four members (Boesenberg et al., 2000; Yanai and Kojima, 1995).

The main-group pallasites are made up of angular or rounded olivine crystals that have minor amounts of low-calcium pyroxene, chromite, phosphates, troilite, and schreibersite (Buseck, 1977). The metal phase is Fe-Ni-rich and similar in composition to that of the IIIAB iron meteorite group (Scott, 1977a; Wasson and Choi, 2003). High precision O isotopic analyses of the main-group pallasites indicate they have compositions that overlap with the IIIAB irons but are otherwise distinct from other bodies (Greenwood, 2006). The nucleosynthetic isotope compositions of the main-group pallasites are similar to the IIIAB irons, which is an NC meteorite group (Warren, 2011).

The Eagle Station pallasite group includes Eagle Station, Cold Bay, Itzawisis, Karavannoe, and Oued Bourdim 001. Like the main-group pallasites, these meteorites are composed of Fe-Ni metal and olivine. The olivine, however, is more ferroan than that found in the main-group pallasites, and lower abundances of pyroxene, chromite, and schreibersite are observed (Buseck, 1977; Davis and Olsen, 1991). The Fe-Ni phases are similar in composition to the IIF irons and have a higher Ni and Ir concentration than the range observed in the main-group pallasites (Kracher et al., 1980). Olivines of Eagle Station pallasites are ^{16}O-rich (Greenwood et al., 2017), and their nucleosynthetic isotope compositions are similar to CV chondrites, which is a CC meteorite group (Warren, 2011).

Vermillion, Yamato 8451, NWA 1911, and Zinder are the members of the pyroxene pallasites. These pallasites are mixtures of metal and silicate phases, however, the presence of millimeter-sized pyroxenes is unique to this grouplet. Vermillion and Yamato 8451 contain ~14 to 63 vol% olivine, 30–43 vol% metal, 0.7–3 vol% pyroxene, up to 1 vol% troilite, and minor whitlockite (Boesenberg et al., 2000; Krot et al., 2014). The metal phases in these meteorites also differ from the main-group and Eagle Station pallasites. Yamato 8451 is composed of metal phases that have similar Ni and Ir abundances as the Eagle Station pallasites, however, their Au abundances are more similar to the main-group pallasites (Krot et al., 2014; Wasson et al., 1998). The metal phases in Vermillion have Ni, Ir, and Au abundances that are similar to low Ni, high Ir main-group pallasites, but these phases have unique moderately volatile elements abundances (e.g., Ga and Ge) unlike those of any other group of pallasites (Mittlefehldt et al., 1998). The O isotopic compositions of pyroxene pallasites are also distinct from those of main-group pallasites (Clayton and Mayeda, 1978; Greenwood, 2006; Greenwood et al., 2015).

Although it is generally agreed that pallasites are mixtures of mantle- and core-derived material, their formation mechanism is undecided. Originally, pallasites were considered to come from the core-mantle boundary of a differentiated parent body, possibly as late-stage liquids of the IIIAB core (Scott, 1977b; Wasson and Choi, 2003). If this were their formation mechanism, the metallographic cooling rates

of the main-group pallasites are predicted to be uniform. The range of cooling rates (2.5–18 K Myr^{-1}) of main-group pallasites and the overall slower cooling rates than the IIIAB irons, however, do not support this interpretation (Yang et al., 2010). This range of cooling rates could have developed if these pallasites were cooled at variable depths on the parent body. Alternative formation mechanisms include that the main-group pallasites are impact-generated mixtures of core and mantle material (Scott, 1977b; Tarduno et al., 2012; Yang et al., 2010; Walte et al., 2020). Combining high-precision ^{182}Hf-^{182}W isotopic data with nucleosynthetic Mo isotope compositions, Kruijer et al. (2022) found that most main-group pallasites exhibit uniform ^{182}W and nucleosynthetic Mo isotopic compositions that bear a similarity to the IIIAB irons. The chronological and isotopic genetic link supports the interpretation that main-group pallasite metal originated in the IIIAB parent body core. Combining these data with published Pd-Ag chronometric evidence of an early collisional disruption of the IIIAB parent body, led these authors to conclude that main-group pallasites formed by impact-induced mixing of metal and silicates rather than by an internal process on the IIIAB parent body. Isotopic anomalies in O and Cr in chromite and olivine (Windmill et al., 2022) and non-equilibrium Fe isotopic compositions between olivine and metal also support an impactor origin for the main group pallasites (Bennett et al., 2022). Future research that combines high precision chronological data with genetic data and petrologic observations will provide valuable insights into the formation mechanisms of these enigmatic stony irons.

2.7. Sample return missions

Sample return missions provide a complementary means of determining the composition of non-terrestrial bodies in the Solar System. Past space missions have successfully returned a variety of samples from the Sun (*Apollo*, *Genesis*), Moon (*Luna*, *Apollo*, *Chang'e*), Comet 81P/Wild 2 (*Stardust*), the asteroids 25143 Itokawa and 162173 Ryugu (*Hayabusa*), and, most recently, from 101955 Bennu (*OSIRIS-REx*). These samples, when preserved in pristine conditions and protected from terrestrial contamination, serve as an invaluable scientific resource that will remain available for future analyses as both the scientific understanding and analytical methods continue to improve.

The Sun contains more than 99% of all Solar System matter, and, thus, its composition is a key proxy of the average composition of the molecular cloud from which the Solar System formed. Solar matter can be sampled through the *Solar wind*, a continuous flow of charged particles emitted from the Sun's corona. The NASA Apollo Solar Wind Composition (SWC) experiment, deployed during the first five Apollo lunar landing missions, collected Solar wind particles for 77 min (Apollo 11) to ~45 h (Apollo 16). The exposed foils were returned to Earth for mass spectrometric analyses of elemental and isotopic abundances of light noble gases (Geiss et al., 1970, 2004). NASA's Genesis Discovery mission was the first deep-space robotic mission to return to Earth. During the mission, the spacecraft exposed several ultrapure target materials to the Solar wind at the Lagrange point L1 for 27 months (December 2001 to April 2004) (Burnett, 2011). Despite the crash of the sample return capsule in September 2008, laboratory analyses of the captured Solar wind provided unprecedented and fundamental insights on the isotopic compositions of Solar O (McKeegan et al., 2011), N (Marty et al., 2011), noble gases (He, Ne, Ar, Kr, Xe; Grimberg et al., 2006; Heber et al., 2009; Meshik et al., 2007; Wiens et al., 2007), and Mg (Jurewicz et al., 2020). Results from the Genesis mission established the average isotopic composition of the Sun which is used as a baseline for comparison with the compositions of meteorites and their parent bodies, planets and their atmospheres, and comets.

The Moon, Earth's only natural satellite, represents the *Rosetta Stone* for understanding the formation and evolution of planetary bodies in the inner Solar System. Six crewed NASA Apollo missions (1969–72), three automated Roscosmos Luna missions (1970–76), and the automated CNSA Chang'e-5 mission (2020) returned a total of ~382 kg of rocks and regolith from the nearside of the Moon. The returned

lunar rocks confirmed the origin of lunar meteorites. Over the past five decades, analyses of highland rocks (ferroan anorthosites and magnesian-suite rocks), mare basalts (basaltic rocks and pyroclastic glasses), breccias, impact melts, and the lunar regolith have led to major discoveries about the history of the Moon. The observation that the Moon is depleted in volatile elements but isotopically similar to the *bulk silicate Earth* (BSE, which is the Earth's composition without the contribution from the core) for non-volatile elements led to the currently accepted paradigm that the Moon formed via the Giant Impact, a collision between a planetary embryo (Theia) with the proto-Earth (Fig. 2) (Halliday and Canup, 2022; Hartmann and Davis, 1975). The nature and variety of returned rocks led to the formulation of the magma ocean concept that the Moon, the terrestrial planets, and large asteroids experienced large-scale melting and differentiation (Warren, 1985). Since the Moon is geologically inactive, its surface preserves a record of the bombardment history of the inner Solar System. Comparison of the density of impact craters on surfaces whose radiometric or cosmic ray exposure (CRE) ages were independently determined by laboratory analyses of returned rocks, has permitted calibration of the lunar cratering rate through time (Hiesinger et al., 2012; Neukum et al., 2001) as well as derivation of cratering chronologies and model ages of other planetary and asteroidal surfaces. The lunar *regolith* (i.e., unconsolidated, heterogeneous rock material covering the bedrock of a planetary body) has been found to contain large amounts of Solar wind-derived volatiles, implanted into the uppermost surface of rocks, mineral fragments, and glass (He et al., 2023), with potential implications for future in situ resource utilization (Curran et al., 2020). Importantly, the Moon continues to be the focus of active research, and upcoming missions (e.g., Artemis, Chang'e-6) are expected to return lunar samples from hitherto unvisited regions such as the South Pole-Aitken basin on the farside of the Moon.

Comets are ice-rich bodies that represent the best-preserved materials from the cold, outer regions of the protoplanetary disk. They likely formed over a wide range of distances and were subsequently stored in two distant reservoirs, the Kuiper Belt at ~50 au and the Oort cloud extending beyond 50,000 au (Brownlee, 2004). NASA's Stardust spacecraft collected interstellar dust and thousands of small particles from the coma of the Jupiter-family comet 81P/Wild 2 during a flyby on 2 January 2004 and returned them to Earth in January 2006 (Brownlee et al., 2003; Sandford et al., 2021). Since the coma particles were collected at high velocity (6.1 km/s) in silica aerogel, they were all modified to some extent by capture, and volatile and organic compounds were lost. Nevertheless, laboratory studies revealed that comet 81P/Wild 2 consists of a variety of materials of both Solar and presolar origins. The unexpected discovery of high-temperature materials, such as forsterite and enstatite as well as chondrule and CAI fragments that likely formed in the inner regions of the protoplanetary disk, revealed that micron- to millimeter-sized grains were transported outward to the comet-forming region where they accreted along with ices and organics (Brownlee et al., 2006; Brownlee, 2014). A future cryogenic sample return will be the only means of preserving both refractory and thermally labile components for laboratory analyses and for improving our understanding of the nature of cometary volatiles and organics (Bockelée-Morvan et al., 2021).

JAXA's Hayabusa spacecraft visited the S-type (silicaceous) asteroid 25143 Itokawa and collected regolith from its surface during two touchdowns in November 2005 (Yano et al., 2006). The sample capsule returned to Earth in June 2010. More than 1500 extraterrestrial particles (including olivine, pyroxene, feldspar, troilite, chromite, phosphates, Fe-Ni metal grains), with sizes ranging from 10 to 180 mm, were identified (Nakamura et al., 2011). Mineralogical and isotopic studies confirmed that Itokawa material is compositionally similar to ordinary (LL4–6) chondrites (Tsuchiyama et al., 2011; Yurimoto et al., 2011). The Hayabusa mission thus provided the first ground-truth for Earth-based observations of asteroids, and confirmed the link between S-type asteroids and ordinary chondrites which had been previously suggested by reflectance spectroscopy (Nakamura et al., 2011). The Hayabusa2 spacecraft investigated the C-type (carbonaceous) asteroid 162173 Ryugu from June 2018 to November 2019 and performed two touchdown

operations to collect a total of 5.4 g of material from the surface and sub-surface (Tachibana et al., 2022). In December 2020, the reentry capsule returned to Earth. Whereas the mineralogical, petrological, chemical, and isotopic characteristics of Ryugu samples are comparable to those of CI carbonaceous chondrites (Nakamura et al., 2022; Yokoyama et al., 2022), Ryugu samples appear to be more pristine than CIs recovered on Earth because they were not modified by the terrestrial environment (Kawasaki, 2022; Okazaki et al., 2022; Yada et al., 2021). In September 2023, NASA's OSIRIS-REx spacecraft returned a 121.6 g sample from the surface and subsurface of another C-type asteroid (101955 Bennu), thus providing the first opportunity for comparison of materials collected on two carbonaceous asteroids.

The *Martian Moons eXploration* (MMX) mission will be the third Japanese sample return mission from a small Solar System body. The MMX spacecraft is scheduled to be launched in 2026, orbit both Martian moons Phobos and Deimos, retrieve >10 g of Phobos regolith, and return to Earth in 2031. Phobos was chosen as the sampling target because it may contain material ejected from the surface of Mars (Ramsley and Head, 2013), and the returned Phobos regolith samples are expected to shed light on the origins of the Martian moons and the history of the Mars-moon system (Fujiya et al., 2021). The return of the sample tubes currently being collected in the vicinity of Jezero Crater by the Mars 2020 Perseverance rover as part of the NASA/ESA-led *Mars Sample Return* (MSR) program (Farley et al., 2020) is expected to provide the first Martian materials available for analysis in terrestrial laboratories (besides the Martian meteorites). These samples will engage laboratory-based scientists for decades to come and lead to paradigm-shifting discoveries in planetary sciences.

3. CONSTRAINTS FROM METEORITES ON THE PHYSICOCHEMICAL CONDITIONS OF THE EARLY SOLAR SYSTEM

3.1. Elemental compositions of the Solar System

Since the Sun is >99.8% of the mass of the Solar System, its composition can be used to define the bulk composition of the Solar System. The first quantitative measurement of the elements in the Sun's atmosphere was published by Russell (1929). These compositions reflect the elemental abundances of the *Solar photosphere*, the visible surface of the Sun. Early work assumed that the spectral lines used to determine the composition of the Solar photosphere originated in local thermodynamic equilibrium (LTE), thus the stellar atmosphere was modeled in a single dimension. Since the 2000s, increased computational power has allowed 3-D modeling of the Sun's atmosphere and non-LTE treatment of line formation. This type of Solar atmosphere model produces a more accurate representation of the *granularity* of the Sun's surface, where "granularity" refers to areas of convective upwelling of hot material and narrower regions of down-going cooler material (for a more detailed review, see McSween and Huss, 2022).

Scientists also used meteorites and Earth samples to constrain the abundance of the elements in the Solar System. These materials, however, often display compositional differences compared to the Sun which reflect changes caused by the chemical and physical processing of disk material as well as planet formation. Thus, samples must be carefully selected if they are to be used to constrain the composition of the Solar System. Kleiber (1885) reported the general composition of celestial objects in the form of a plane periodic system following atomic numbers. This was based on a compilation of element abundances in meteorites, the Sun, comets, fixed stars, and Earth. The synthesis of geochemical and cosmochemical information presented by Kleiber is thought to be the first published "cosmochemical" periodic table of elements. Using the periodic trends he observed, Kleiber concluded that cosmic bodies were not a consequence of a random contribution of the elements (for review, see Lodders and Fegley, 2015). In 1890, Lockyer wrote "The Meteoritic Hypothesis" in which he proposed that the visible celestial bodies are composed of meteorites or meteoritic vapor (Lockyer, 1890). The implication of Lockyer's observation is

that the composition of visible celestial objects could be determined by measuring the composition of meteorites (for review, see McSween and Huss, 2022). Just over 20 years later, it was observed that elements with even atomic numbers are more abundant than the adjacent odd-numbered elements in meteorites (Oddo, 1914) and in rocks that sampled the Earth's crust (Harkins, 1917). This pattern is now referred to as the Oddo-Harkins rule. The relative difference in element abundances creates a "zigzag abundance pattern" or "saw-tooth" pattern of the elemental composition of natural samples when plotted against their atomic number (Fig. 9). With the development of theories on nucleosynthesis during the 1930s–50s, it was subsequently recognized that odd nuclei are generally less stable than even nuclei, thus odd nuclei are not as abundant in nature as even nuclei.

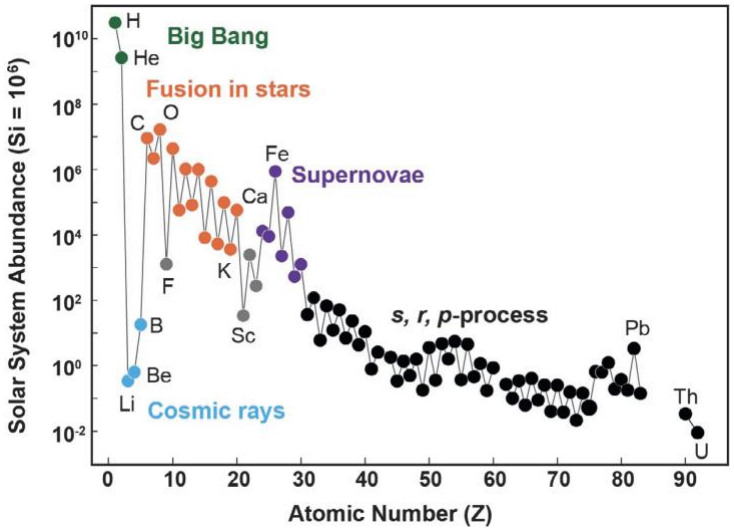

Figure 9: The present-day Solar System composition. The abundance of an element (silicon-normalized compositions, log Si = 10^6) is compared to its atomic number (Z). The nucleosynthetic processes that are responsible for the production of the elements are shown in different colors. These include the Big Bang, nuclear fusion in stars, cosmic ray interactions, slow and rapid (s- and r-processes) neutron capture processes, the p-process which produces isotopes predominantly by disintegration, and isotopes that are produced during explosive burning (i.e., supernova) (Burbidge et al., 1957). Data are from Lodders K (2021) Relative atomic solar system abundances, mass fractions, and atomic masses of the elements and their isotopes, composition of the solar photosphere, and compositions of the major chondritic meteorite groups. Space Science Reviews 217: 44.

Influential work by Goldschmidt saw the measurement and publication of the elemental composition of many terrestrial and meteoritic samples (Goldschmidt, 1937). A detailed review of this work is in McSween and Huss (2022). Briefly, Goldschmidt recognized that chondrites were unmelted rocks that could be used to probe the original compositions of the object from which they came. By dividing chondrites into silicate, metal, and sulfide components and measuring elemental abundances in each phase, he determined how elements partitioned between coexisting mineral phases. To describe the geochemical affinities of the elements, Goldschmidt proposed the terms *lithophile* (rock-loving), *siderophile* (iron-loving), *chalcophile* (sulfur-loving), *atmophile* (gas-loving), and *biophile* (organism-loving). Most of these terms are still used today, except for biophile which is infrequently used. Each element possesses one or more geochemical affinity (Fig. 10) that enables cosmochemists and geochemists to predict the partitioning of elements between different planetary reservoirs (i.e., mantle, core, atmosphere) and between different mineral phases. The geochemical affinity of each element is dependent on the oxidation state of the system. For example, chromium is a strongly lithophile element under redox conditions of the Earth's crust, however, under reduced conditions such as those found in iron meteorites, chromium is strongly chalcophile

entering almost exclusively into daubréelite ($FeCr_2S_4$) (Goldschmidt, 1937). Using his database, Goldschmidt calculated the "cosmic abundances" of 66 elements by using the weighted means of element concentrations in meteorite silicate (10 parts), metal (2 parts), and sulfide (1 part).

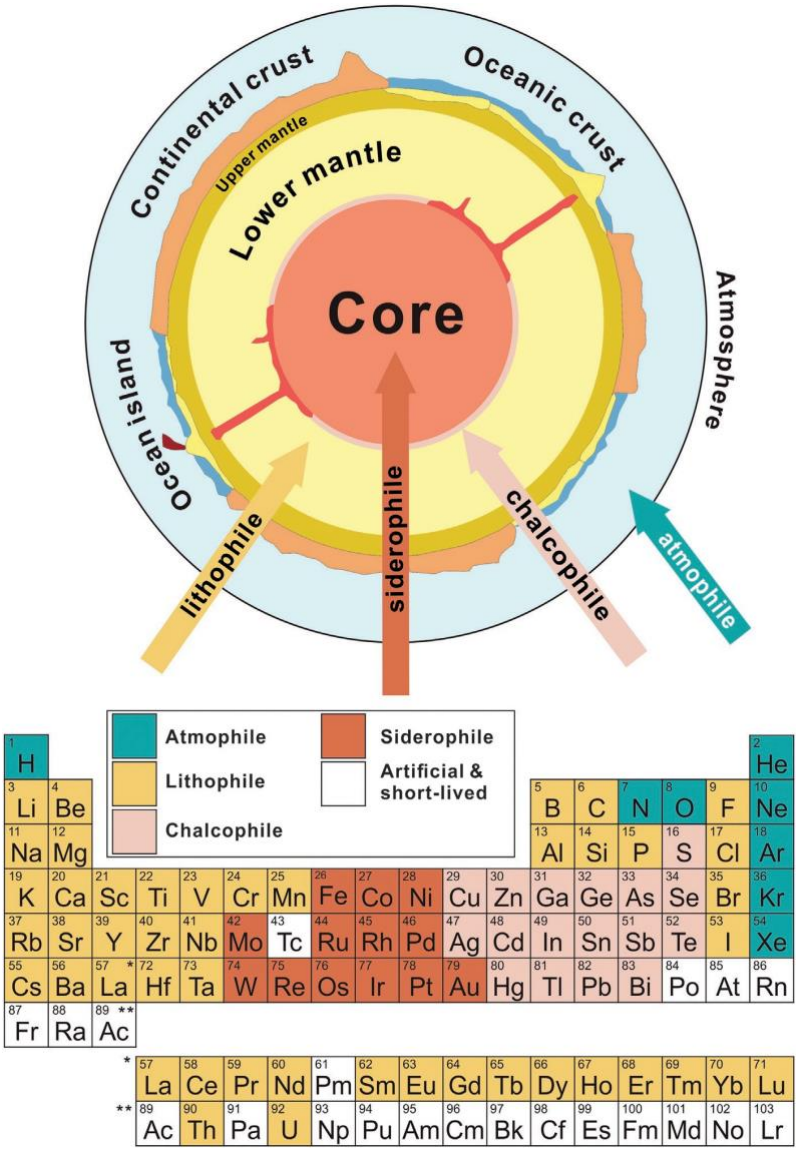

Figure 10: Goldschmidt (1937) classification of the elements and their preferential distribution between the Earth's major geochemical reservoirs: the core, mantle, and crust as well as the hydrosphere and atmosphere. The principal chemical behavior (atmophile, lithophile, chalcophile or siderophile) is indicated by the corresponding color. Artificial and short-lived elements are indicated in white.

Several years later, English astronomer Hoyle published two papers describing the nucleosynthesis of chemical elements heavier than He in stars (Hoyle, 1946, 1954). Around this time, Suess and Urey (1956) used meteorite and terrestrial rock compositions in addition to element abundance from stellar nucleosynthesis to estimate the cosmic abundances of elements that had been imprecisely measured or for which no empirical data was available. In the quest to identify the origin of the elements, Hoyle realized the importance of using datasets generated by cosmochemists, such as Goldschdmit, Suess, and Urey. Hoyle led a group of scientists to derive the basic principles of how elements are synthesized in the Universe and

published the seminal work in Burbidge et al. (1957), also known as the B^2FH paper. Cameron (1957) reported similar findings that same year. These groups recognized that the curvature and structure of the cosmic abundances of elements, now known as the *Solar System elemental abundance curve* (Fig. 9), reflect the different proportions of the Solar System's nucleosynthetic precursor material. Subsequent elemental data compilations have incorporated more precise and accurate data from meteorites and more accurate determinations of the composition of the Solar photosphere, such that the bulk composition of the Solar System is now well constrained (e.g., Cameron, 1973; Anders and Grevesse, 1989; Lodders and Fegley, 2023).

During the 1960s, Mason recognized that in terms of their bulk sample composition, the Ivuna-type (CI) carbonaceous chondrites have elemental compositions that closely resemble the Sun's photosphere (for a detailed review, see Mason, 1979). Samples retrieved by the Hayabusa2 mission from the C-type (carbonaceous) asteroid 162173 Ryugu have a chemical composition similar to CIs, but are even more pristine because they have not been modified by the Earth's atmosphere entry and recovery (Yokoyama et al., 2022). In Fig. 11, the bulk compositions of CI chondrites and Ryugu are compared with the composition of the present-day Solar photosphere (Lodders, 2021; Yokoyama et al., 2022). The resultant correlation has a 1:1 gradient for all elements except atmophile elements (H, He, C, N O, Ne) and Li. There is now better than 10% agreement between the elemental abundances derived from CI meteorites and Ryugu and those from Solar absorption line spectroscopy for most elements. The 1:1 relationship indicates that for most elements CI chondrites can be used to estimate the bulk elemental composition of the Solar System. As such, the CI chondrite composition is commonly used to "normalize" (i.e., divide by) sample data in cosmochemistry and geochemistry studies. The CI-normalization removes the zigzag pattern (Oddo-Harkins rule) of the elemental composition of natural samples and places major and trace elements on the same scale, even though they have markedly different relative abundances within a sample.

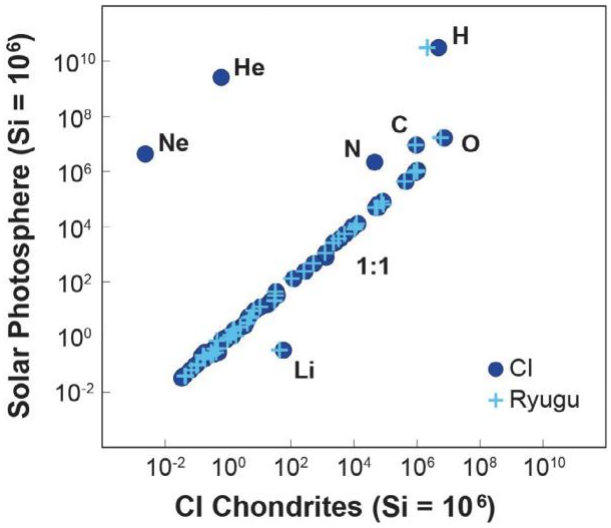

Figure 11: Elemental abundances in Ivuna-type (CI) carbonaceous chondrites, Ryugu, and the Solar photosphere. The abundance of an element is expressed as silicon-normalized composition (log Si = 10^6). Most elements follow a 1:1 ratio, whereas the highly volatile elements H, C, N, O, and the noble gases are distinctly lower in CI than in the Solar composition. The Solar depletion in Li is due to its processing in the Sun's nuclear burning cycle. Data sources: Lodders K (2021) Relative atomic solar system abundances, mass fractions, and atomic masses of the elements and their isotopes, composition of the solar photosphere, and compositions of the major chondritic meteorite groups. Space Science Reviews 217: 44 and Yokoyama et al. (2022) Samples returned from the asteroid Ryugu are similar to Ivuna-type carbonaceous meteorites. Science 379, eabn7850.

The temperature where half of an element is in the solid phase is called the *50% condensation temperature* (Wasson, 1985; Lodders, 2003). *Highly volatile elements* have 50% condensation temperatures <371 K, *volatile elements* < 665 K, *moderately volatile elements* between 1335 and 665 K, and *refractory elements* > 1335 K (for a gas of Solar composition at a total pressure of 10^{-4} bar; Lodders, 2003). The bulk composition of most chondrite parent bodies is fractionated relative to CI, and their abundance patterns generally correlate with condensation temperatures of the elements in a gas of Solar composition (assuming thermodynamic equilibrium between solids and gas phase). As chondritic meteorites are predominantly sourced from undifferentiated parent bodies, the bulk elemental compositions of chondrite groups provide snapshots of the compositions of their parent body, and, to a degree, the local composition of the disk at the time of accretion (for a detailed review, see Palme et al., 2014). Variations in elemental abundances between different chondrites reflect compositional variability in the disk and/or disequilibrium during the formation of solids from disk gas (i.e., condensation).

3.2. Oxygen fugacity of the Solar System recorded by meteorites and their components

In addition to constraining the composition of the Solar System, the chemical composition of meteorites and their mineralogy constrain the prevailing redox conditions in the disk. A key parameter is the *oxygen fugacity* (fO_2), which is a thermodynamic property related to the chemical potential of oxygen, quantitatively related to the redox state (i.e., *redox potential*) of a system. The redox state of meteorites is best indicated by the occurrence of Fe in different oxidation states. Iron can occur as a metal (Fe^0) alloyed with Ni and Co, as ferrous Fe (Fe^{2+}) in silicates, oxides, and sulfides, or as ferric Fe (Fe^{3+}) primarily in oxides (Rubin et al., 1988). The fO_2, therefore, controls the mole fractions of FeO, Fe_2O_3, and Fe components in silicate and metal phases and defines the thermodynamic stability of metal and sulfide phases (Righter et al., 2006). Other elements with valence states that are sensitive to redox formation conditions of planetary materials are Ti, V, Cr, and Eu in basalts, and Yb and possibly Sm in refractory condensates and extremely reduced materials (e.g., Simon et al., 2007; Hammouda et al., 2024 and refs. therein).

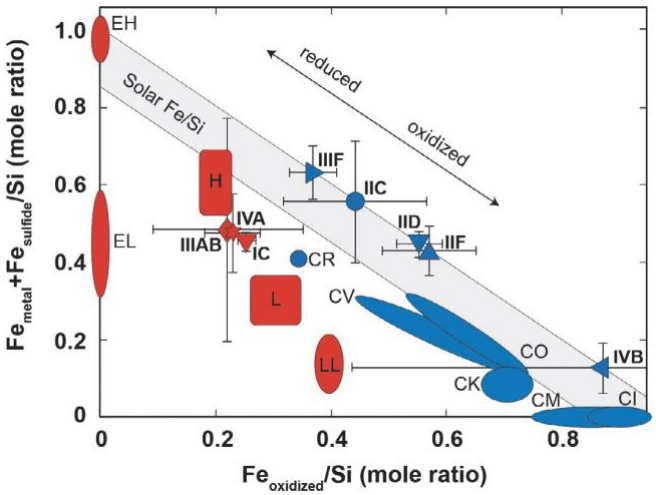

Figure 12: Modified Urey-Craig diagram indicating the abundances of reduced (metal and sulfide) and oxidized Fe normalized to Si for the major groups of enstatite (EH and EL), ordinary (H, L, and LL), and carbonaceous chondrites (CR, CV, CK, CO, CM, CI), and magmatic iron meteorites. Red symbols denote NC meteorite groups, and blue symbols the CC meteorite groups. CB and CH carbonaceous chondrites plot outside the compositions defined in the figure due to high metal enrichment. Figure based on Urey HC, Craig H (1953) The composition of the stone meteorites and the origin of the meteorites. Geochimica et Cosmochimica Acta 4: 36–82 and Hilton CD, Ash RD, Walker RJ (2022) Chemical characteristics of iron meteorite parent bodies. Geochimica et Cosmochimica Acta 318: 112–125.

The so-called *Urey-Craig diagram* (Urey and Craig, 1953) depicts the variation observed in chondrite groups between the proportions of reduced Fe as metal and bound in sulfide against oxidized Fe bound to O in silicates, all relative to Si (in molar abundances) (Fig. 12). Thus, the Urey-Craig diagram can be used to compare the redox state of a sample as recorded by its mineralogy. This diagram has since been expanded to include several magmatic iron meteorite groups (Hilton et al., 2022). The two chondrite groups with end-member compositions are the enstatite chondrites (EH), which are the most reduced (FeO in silicates is absent), and the CI chondrites, which are the most oxidized (metal and sulfides are absent). The Urey-Craig diagram indicates that chondrites preserve a record of a general redox gradient in the disk that may have been caused by variations in the C/O ratio or the relative proportions of H, C, and O in the disk (Righter et al., 2016). Enstatite and ordinary chondrites formed at relatively reducing conditions, whereas carbonaceous chondrites formed in a more oxidizing environment. Notably, NC iron meteorite parent bodies formed over a narrow range of fO_2, consistent with that recorded by NC chondrites (Bonnand and Halliday, 2018) (Fig. 12). The variation in fO_2 among the enstatite, ordinary, and Rumuruti chondrites is reflected by several mineralogical and bulk sample chemical properties, such as the elemental compositions of olivine, pyroxene, and kamacite, the bulk Fe# = FeO/(FeO + MgO), and the bulk FeO/(total Fe) ratio.

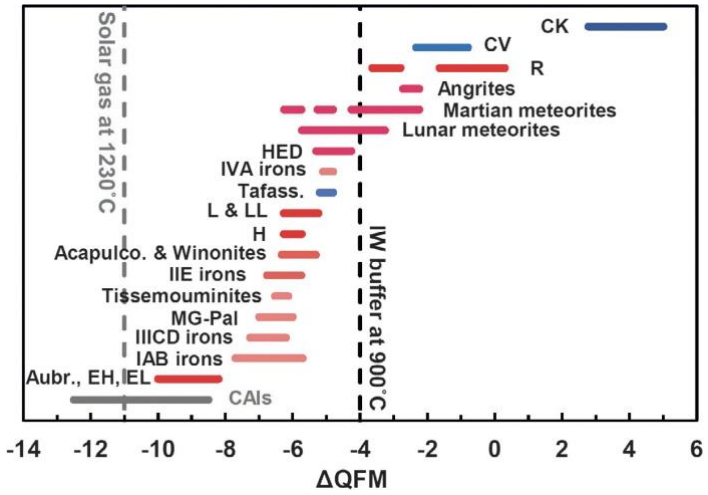

Figure 13: Relative variation in oxygen fugacity fO_2 (in log units relative to the quartz-fayalite-magnetite buffer, or QFM), between meteorite clans and groups. The Iron-Wüstite (IW) buffer at 900 ˚C is shown for reference. Data for CAIs are from Beckett and Grossman (1986), for Solar gas from Fegley Jr and Palme (1985), and for meteorite groups from Righter et al. (2006), Righter and Neff (2007), Bonnand and Halliday (2018), Ma et al. (2022), Stephant et al. (2023), and Hammouda et al. (2024). See text for further details. Figure modified from Ma M, Neumann W, Néri A, Schwarz WH, Ludwig T, Trieloff M, Klahr H, Bouvier A (2022) Early formation of primitive achondrites in an outer region of the protoplanetary disc. Geochemical Perspectives Letters 23: 33–37.

The oxidation state of meteorites and their CAIs varies greatly, with fO_2 changing over 18 log units (relative to the quartz- fayalite-magnetite or iron-wüstite oxygen buffers) (Fig. 13). As a result of changes in the conditions in which an object formed (including temperature), estimates of fO_2 may vary depending on mineral equilibria (assemblages) that are selected for the calculation. From their mineral assemblages and compositions, CAIs have estimated fO_2 close to that of the Solar gas at relevant temperatures (Beckett and Grossman, 1986; (Fegley Jr and Palme, 1985). Under such reduced conditions, elements typically present in oxidized form are reduced to a lower valence state. For example, Ti^{4+} is reduced to Ti^{3+}Evidence of transient oxidizing conditions accompanying thermal processing of nebular precursors is recorded in variations in Ti^{3+}/Ti^{tot} (measured by X-ray absorption spectroscopy) between minerals that were formed at different temperatures in CAIs (e.g. hibonite, pyroxene) (Simon et al., 2001, 2007) and within WLRs

formed around CAIs (Dyl et al., 2011). The presence of Si in metal (1.5–3.5 wt% in EH, compared to 0–2 wt% in EL), together with the presence of exotic (Mg, Ca, Mn, N-rich) sulfides in enstatite chondrites associated with FeO-poor enstatite, suggests a highly reduced environment of formation (Lin, 2022). Under such reduced conditions, the REE Eu, Yb, and possibly Sm may exist in 2+ reduced forms, which leads to elemental fractionation during mineral crystallization and melting. Reduction of Eu and Yb causes anomalies in REE patterns of oldhamites in enstatite-rich meteorites (EH and EL chondrites, aubrites, and ungrouped enstatite-rich achondrites) (Hammouda et al., 2022).

The fO_2 also provides valuable information about the chemical and thermal conditions under which a meteorite parent body evolved (e.g., differentiation, alteration, degassing). Partitioning experiments have shown a relation between the Eu/Gd ratios in clinopyroxene and plagioclase of compositions similar to those found in angrite meteorites with fO_2, which suggests that angrites crystallized at QFM ≈ −1 (McKay et al., 1994). Wadhwa (2001) used the Eu/Gd in augite (providing a proxy for the Eu^{2+}/Eu^{3+} ratio in the melt) as an oxybarometer for the mantle sources of Martian shergottites. The most depleted shergottites such as QUE 94201 indicate fO_2 formation conditions as low as the log QFM = −4 (or the IW buffer value) (Fig. 13) and oxidizing reactions (i.e., aqueous alteration) during crust formation (or evolution). The fO_2 of the Martian mantle, estimated using siderophile element abundances martian meteorites, is log QFM ≈ −5.2, which is similar in fO_2 to IIE irons and ordinary chondrites (Righter and Drake, 1996) and more reduced than the Earth's upper mantle (close to log QFM ≈ −4).

Differences in bulk mantle fO_2 between the terrestrial planets have influenced the gas species that were outgassed during the magma ocean stage and the mass and compositions of early planetary atmospheres (Gaillard et al., 2021; Zhang et al., 2017). Interactions of C-CO-CO_2 and H_2-H_2O with Fe metal in chondrites drive redox reactions (Righter et al., 2006). These reactions affect the redox state and partitioning of Fe and other redox sensitive elements during planetary differentiation and igneous processes, as summarized in Fig. 13. Several nominally lithophile elements behave as siderophile elements under very reduced conditions. The siderophile element abundances and P contents (0.5–1 wt%) measured in meteorites can be used to provide constraints on fO_2 of planetary mantles and core formation conditions and size (e.g., Mars; Righter and Drake, 1996) and iron meteorite parent bodies (Scott, 2020; Hilton et al., 2022). For magmatic irons, some additional assumptions must be made to constrain the fO_2 of their parent bodies, such as the silica and iron content of the chondritic groups to which the irons derive from, the size of the core, and volatile element budget related to their impact melting history (Wasson et al., 2006). High-pressure/high-temperature experiments and numerical simulations relevant to core formation conditions also indicate that elements such as H (Tagawa et al., 2021), He (Bouhifd et al., 2013), N (Dalou et al., 2019) or Cr (Bonnand et al., 2011) could be present in planetary cores under particular redox and high-pressure conditions. Another signature of these processes is the isotopic fractionation effects that are associated with element valence changes, coordination, and redox reactions at high temperatures for elements as heavy as U (Teng et al., 2017).

3.3. Isotopic composition of the Solar System

Since O and other volatile elements (H, C, N, noble gases) are strongly depleted in chondrites and even more so in achondrites and terrestrial rocks compared to the Solar reference, their Solar isotopic compositions are only preserved in the Sun itself or in the atmosphere of Jupiter, which gravitationally captured nebular gas prior to its dissipation. NASA's Genesis mission (Section "Sample return missions") permitted to precisely determine the isotopic ratios of O (McKeegan et al., 2011), N (Marty et al., 2011), and noble gases (Ne, Ar, Kr, Xe; Grimberg et al., 2006; Heber et al., 2009; Meshik et al., 2007; Wiens et al., 2007) of the Sun using captured Solar wind ions, which reflect that of the Sun's outer convective zone. Notably, the N isotopic composition of the present-day Sun (Marty et al., 2011) was found to be

indistinguishable from that of Jupiter's atmosphere which had been determined by infra-red spectroscopy (Fouchet et al., 2000; Fletcher et al., 2014) and mass spectrometry by the *Galileo Probe Mass Spectrometer* (Owen et al., 2001). The C isotopic composition of Genesis Solar wind samples could not be analyzed because the composition of the concentrator target had abundant C (i.e., SiC and diamond-like C). Lyons et al. (2018) more recently derived the C isotopic ratio of the Sun using data collected by the *Atmospheric Trace Molecule Spectroscopy Experiment* (ATMOS) carried on board the Space Shuttle in the mid-1990s.

The $^{3}He/^{4}He$ ratio of the Solar wind corresponds to the (D + ^{3}He)/^{4}He ratio of the nebular gas because D was converted to ^{3}He very early in Solar history. By assuming that Jupiter captured unfractionated nebular He, the pre-D-burning $^{3}He/^{4}He$ ratio of the Sun can be estimated based on data collected by the Galileo Probe (Geiss and Gloeckler, 1998; Mahaffy et al., 1998). Similarly, the Solar D/H ratio can be estimated by using the Galileo Probe measurements of the Jovian atmosphere. This ratio can also be calculated using the present-day Solar (D + ^{3}He)/^{4}He and $^{4}He/H$ ratios by subtracting the contribution of pre-D-burning ^{3}He (Geiss and Gloeckler, 1998). Importantly, H, C, N, and O trapped in chondrites, achondrites, comets, and the terrestrial planets have isotopic compositions that are markedly different from those of the nebular gas or Sun (see Broadley et al., 2022, for a recent review).

The isotopic composition of the Solar System for many lithophile, siderophile, and chalcophile elements is commonly defined using terrestrial rocks (e.g., Anders and Grevesse, 1989). This approach developed as a result of early models of Solar System formation that proposed the protoplanetary disk began in a hot gaseous state where all presolar solid material had been vaporized and then condensed/accreted with unfractionated isotopic compositions. With development of mass spectrometry and their increased availability, investigations during the 1950s and 1960s determined that meteorites and terrestrial rocks shared the same isotopic compositions for most non-volatile elements, except for small isotopic variations due to radioactive decay (Section "Solar System chronology from long-lived and short-lived radionuclides"), mass-dependent (Section "Mass-dependent isotope variations") or -independent isotopic fractionation effects (Section "Mass-independent isotope variations"). As analytical precision improved, however, it was observed that some meteorites also possessed small (ppm to e) isotopic variations that were linked to the heterogeneous distribution of presolar grains in the disk (Section "Nucleosynthetic isotope anomalies"). The small scale of these isotopic variations indicates that the protoplanetary disk was well-mixed, albeit imperfectly. The approach to defining the Solar System's isotopic composition using Earth, however, is being reassessed as the community's understanding of how these isotopic anomalies developed in the disk is refined.

4. DISK COMPOSITION AND EVOLUTION: INSIGHTS FROM METEORITE CHRONOLOGY AND ISOTOPIC VARIATIONS

4.1. Solar System chronology from long-lived and short-lived radionuclides

The chronology of events in the early Solar System can be derived from meteorites and their components by measuring the changes in the abundance of a radiogenic isotope produced by the decay of unstable, radioactive isotope nuclei over geological timescales. The *radioactive* (decay source or *parent*) and *radiogenic* (decay product or *daughter*) isotopes are two isotopes of different elements that are related through the process of nuclear disintegration. Readers are referred to Reiners et al. (2017) for a review of the principles of radioactive decay, analytical methods, diffusion, and radioactive systems used in geo-thermochronology. The changes in the abundance of radiogenic isotopes are used to study the timescales of geological, planetary, and cosmogenic processes (related to exposure to cosmic rays and early irradiation processes in space).

The abundance of parent and daughter isotopes in cogenetic minerals and samples must be correlated to constitute an *isochron* regression line, whose slope and intercept are related to time and the

initial isotopic composition of the radiogenic isotope and element, respectively (Fig. 14). The half-life ($t_{1/2}$) of a radioactive isotope is the time in years it takes for half of the atoms in a radioactive substance to decay into another element or isotope. It ranges from days for short-lived radioactive and cosmogenic isotopes to billions of years for long-lived radioactive isotopes (Tables 1 and 2). The decay constant, l, is the statistical notation of the probability of nuclei decay per year, $\lambda = \ln(2)/t_{1/2}$ (yr^{-1}). The rate of decay of a radioactive parent isotope (noted N) is proportional to the number of atoms of that isotope that are present in a system (see, for example, McSween and Huss (2022) for all decay equations). The parent isotope continues to exponentially decay until only trace amounts remain to be detected (after six half- lives), at which time the radioactive isotope is considered *extinct*. The half-life value of a radioactive isotope may vary in the literature as it may be measured by physical (particle) counting methods or calculated by comparing time differences between short-lived and/or long-lived radioactive systems in geological and planetary materials. Using this method, the half-life of ^{146}Sm was recently reinstated at 103 ± 5 Myr based on new ^{146}Sm-^{142}Nd isotopic measurements of meteorites and lunar samples of known ages (Fang et al., 2022).

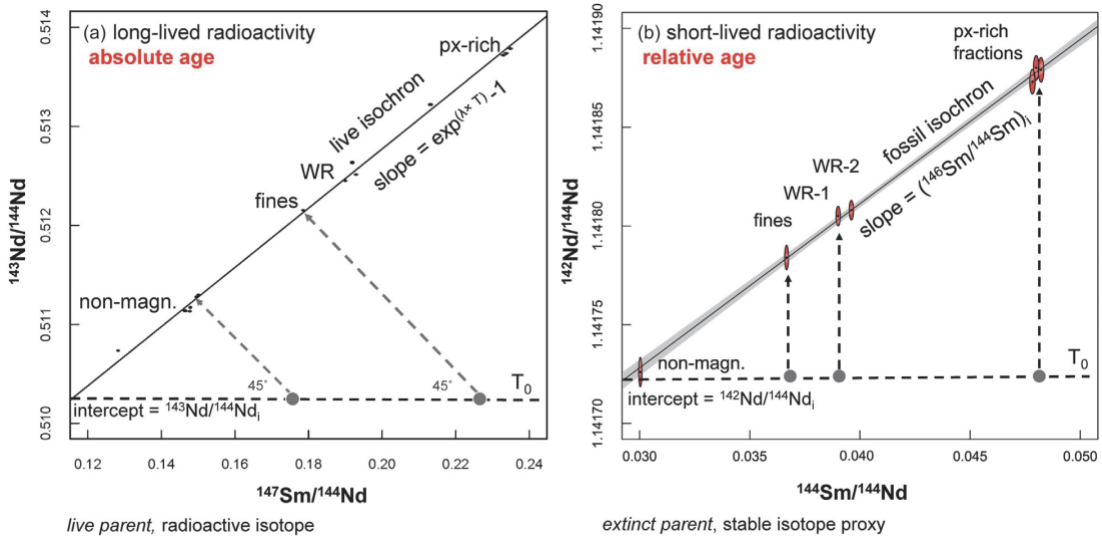

Figure 14: (a) Long-lived radioactivity (LLR) and (b) short-lived radioactivity (SLR) isochron age determinations. Examples are (a) the LLR ^{147}Sm-^{143}Nd and (b) the SLR and extinct ^{146}Sm-^{142}Nd system pairs for Erg Chech (EC) 002 (an ungrouped andesitic achondrite), redrawn using IsoplotR and data from Fang et al. (2022). The LLR system provides an absolute age (2s errors) of 4521 ± 143 Ma (n = 17 leachates and residues) with an intercept of $^{143}Nd/^{144}Nd_i$ = 0.50679 ± 0.00016, MSWD = 130. As ^{146}Sm is now extinct, the stable isotope proxy ^{144}Sm is used to establish the correlation between parent/daughter elemental ratio with the radiogenic isotopic ratios. For SLR, an age difference Δt between an object (N, which is the slope of the isochron) and an anchor (N_0) is calculated from the respective initial SLR abundances in these two objects using the isochron method and $\Delta t = 1/\lambda \times \ln(N/N_0)$. The ^{146}Sm-^{142}Nd age difference between EC 002 and CAIs of 0.5 ± 9.0 Myr is calculated using the $^{146}Sm/^{144}Sm_0$ determined in EC 002 (0.00831 ± 0.00031, with $^{142}Nd/^{144}Nd_i$ = 1.141479 ± 0.000013, MSWD = 0.84, n = 7) and CAIs (0.00823 ± 0.00044) from Marks et al. (2014) using the ^{146}Sm half-life value of 103 Myr (Fang et al., 2022).

4.1.1. Long-lived radioactive nuclides (LLR)

Meteorite absolute ages are time differences between a measured event and the present. Dates, however, are absolute times that are calculated from the ratio of a radioactive isotope and its daughter isotope using the law of radioactive decay and long-lived radioactive (LLR) systems. The most commonly employed LLR systems in high-temperature geochronology are ^{40}K-^{40}Ar, ^{87}Rb-^{87}Sr, ^{147}Sm-^{143}Nd, ^{176}Lu-^{176}Hf, ^{187}Re-^{187}Os, and ^{235,238}U-^{232}Th-^{206,207,208}Pb decay chains. With improvements in analytical techniques,

the radioactive systems ^{40}K-^{40}Ca and ^{138}La-^{138}Ce have recently been investigated in meteorites (e.g., Dai et al., 2023; Israel et al., 2020). For low-temperature applications (i.e., <1000 K), the U-Th-(Sm)-^{4}He dating system uses the alpha particles that accumulated over time due to the radioactive decay of ^{235,238}U and ^{232}Th isotopes and their intermediate short-lived daughter isotopes, with additional contribution from the alpha decay of ^{147}Sm (Reiners et al., 2017). ^{3}He/^{4}He ratios in U-rich minerals, are particularly useful in constraining the low-temperature history of chondrites and achondrites, which may be affected by possible re-heating due to shock and ejection events, within the 320–870 K temperature range (Min et al., 2017).

Table 1: Long-lived radionuclide systems used in geochronology.

Radioactive isotope	Radiogenic isotope	Decay type & branching decay probability	Half-life $t_{1/2}$ (±2σ Gyr)	Reference stable isotope for isochron	T_c (K)
^{40}K	^{40}Ar	N.C. (p ≈ 0.11)	12.040 ± 0.033	^{36}Ar	550 (orthoclase)
^{40}K	^{40}Ca	β^- (p ≈ 0.89)	1.399 ± 0.004 1.253 ± 0.003 (total)	^{44}Ca	1270 (plagioclase)
^{87}Rb	^{87}Sr	β^-	49.61 ± 0.16	^{86}Sr	670 (K-feldspar)
^{138}La	^{138}Ce	β^- (p ≈ 0.66)	103 ± 1 (total)	^{136}Ce, ^{142}Ce	n.a.
^{147}Sm	^{143}Nd	α	106.25 ± 0.38	^{144}Nd	>750 (garnet)
^{176}Lu	^{176}Hf	β^-	37.126 ± 0.139	^{177}Hf	>810 (garnet)
^{187}Re	^{187}Os	β^-	41.6 ± 0.02	^{188}Os	670 (pyrrhotite)
^{238}U	^{206}Pb	α ×8	4.4683 ± 0.0096	^{204}Pb	750 (apatite) 1250 (zircon)
^{235}U	^{207}Pb	α ×7	0.70381 ± 0.00476	^{204}Pb	
^{232}Th	^{208}Pb	α ×6	14.00 ± 0.67	^{204}Pb	
U-Th-(Sm)-He	^{4}He	α ×22		^{3}He	370 (apatite)

Half-life values are from Renne et al. (2011) for ^{40}K, from Villa et al. (2022) for ^{87}Rb and ^{147}Sm, from Kondev et al. (2021) for ^{138}La and ^{187}Re, weighted average value from Scherer et al. (2001) and Söderlund et al. (2004) for ^{176}Lu, and from Jaffey et al. (1971) for ^{232}Th, ^{235}U and ^{238}U (with updated uncertainty from Villa et al., 2022). The t_c are temperature estimates (in K) for closure to diffusion for selected mineral hosts at 200 K/Myr cooling rates (Reiners et al., 2017). n.a. = not available

While the LLR systems described above provide useful chronological constraints for geological events, they do not resolve the timescales of early Solar System processes and events ~4.57 Ga owing to insufficient age precision. Their principle weaknesses are (1) difficulties in obtaining sufficient spread in parent and daughter isotope ratios between mineral fractions and bulk-rock composition that are cogenetic, and (2) analytical challenges in determining the parent/daughter isotope ratio with high accuracy and precision (0.2–0.5%) using isotopic dilution methods. Additionally, there are uncertainties with some of the half-life values (e.g., ^{40}K, ^{87}Rb). Most LLR systems (except U-Th-Pb) are also limited in their application due to a lack of availf in situ analytical techniques. This is because isobaric interferences on parent and daughter isotopes are prevalent in existing methods. In situ analyses of single phases are, however, being developed with the advent of mass spectrometers equipped with collision reaction cells which can be coupled with laser ablation sampling systems (e.g., triple quadrupole ICP-MS or MC-ICP-MS; Hogmalm et al., 2017; Craig et al., 2021). In situ measurements of ^{87}Rb-^{87}Sr in K-rich feldspars and ^{176}Lu-^{176}Hf in Ca-phosphates or other REE-enriched minerals, which are fairly common igneous or metamorphic phases in meteorites, can now be carried out with enhanced precision and accuracy (Dauphas et al., 2022; Wu et al., 2023). Most applications of the LLR isotopic systems for early Solar System evolution are therefore related to relatively late planetary processes. The Rb-Sr and K-Ar systems in

feldspars and U-Pb in U-rich minerals such as apatites or zircons are particularly useful in tracing transient thermal events that may have reset the original chronological records of planetary materials due to their lower temperature of closure for diffusion (Table 1). Overall, the precision on absolute ages obtained with LLR systems that are based on the measurement of the parent/daughter isotope ratios and mineral and bulk-rock isochron methods (Fig. 14) is generally too low to resolve early Solar System events or to permit a comparison with relative ages obtained from short-lived systems. The LLR are powerful tracers of the formation of major planetary reservoirs. The parent and daughter elements of long-lived systems have different geochemical behaviors. Thus, radioactive and radiogenic isotope systems provide constraints on the physicochemical conditions and timing of planetary differentiation and the long-term evolution of their internal reservoirs. Also, these isotopic systems are preferentially hosted in certain mineral phases, which have distinct elemental diffusion rates and, consequently, different *closure temperatures* to diffusion (Table 1). The closure temperature to diffusion of a daughter element during a cooling path is the temperature of a sample at a time corresponding to its apparent date. In geochronology, LLR are thus commonly used for establishing the thermo-chronological path of metamorphic rocks (Reiners et al., 2017), and as such can provide pertinent information in cosmochemistry about the thermal and impact history of extraterrestrial materials. The diffusion parameters of radioactive and radiogenic elements in minerals of different compositions must be well known to model the thermal history of meteorites. While they can be measured in experiments and thermodynam- ically modeled for a given system and mineral (Table 1), diffusion parameters vary with composition, cooling rate, and grain size (Reiners et al., 2017).

The ^{238}U-^{206}Pb ($t_{1/2} \approx 4.468 \times 10^9$ yr) and ^{235}U-^{207}Pb ($t_{1/2} \approx 0.704 \times 10^9$ yr) decay schemes are unique as both share the same parent and final daughter elements (U and Pb). They can be combined together to provide the highest precision in geochronology. The half-lives of ^{238}U and ^{235}U were precisely determined by nuclear physicists (Jaffey et al., 1971) (Table 1). In situ SIMS or LA-(MC)ICP-MS are used to determine the ages of single U-rich mineral grains that generally contain little common Pb, such as zircon, baddeleyite, or apatite. A Concordia diagram reports radiogenic (noted as *) ratios of ^{238}U/^{206}Pb* against the ^{235}U/^{207}Pb* (Wetherill, 1956; White, 2020). This method verifies the closed-system behavior of a sample by using the position of the analytical point relative to the Concordia line (where the ^{238}U/^{206}Pb*and ^{235}U/^{207}Pb* dates are identical). Uranium-rich minerals, however, are relatively sparse and small in size in meteorites due to their (generally) ultramafic to mafic nature. Additionally, this method still relies on measuring parent/daughter isotopic ratios which is not precise enough to establish the timeline of early Solar System evolution.

Only the Pb-Pb radioactive decay scheme can produce absolute age dates with a precision better than 1 Myr (corresponding to a ~ 0.02% precision) and, thus, can resolve early Solar System processes such as the formation of CAIs, chondrules or achondrites (e.g., Amelin, 2008; Connelly et al., 2012; Reger et al.; 2023). The Pb-Pb isochron method is derived from the unique combination of the two U-Pb long decay chains and the in-growth of uranogenic Pb. The major advantage of the method is that it requires measuring the isotopic composition of only one element (Pb) to determine the radiogenic ^{207}Pb*/^{206}Pb* isotopic composition. This ratio is obtained independently from the elemental U/Pb ratio, which is determined at lower analytical precision (5–10%) using isotopic dilution methods. The ^{207}Pb/^{204}Pb vs ^{206}Pb/^{204}Pb conventional isochron method, for which the age is given by the slope of the isochron, was used to make the first accurate measurement of the ~4.55 Gyr age of the Earth based on the analysis of chondrites, iron meteorites, and terrestrial sediments (Patterson, 1956). The ^{207}Pb/^{206}Pb ratio is measured with better precision than the ^{207}Pb/^{204}Pb or ^{206}Pb/^{204}Pb ratios due to the higher abundances of ^{207}Pb and ^{206}Pb compared to ^{204}Pb (<1%). The ^{207}Pb/^{206}Pb ratio also changed rapidly in the early Solar System, by as much as ~0.7% per Myr at 4.57 Ga, due to the high abundances of ^{238}U and ^{235}U that were ~2 and ~6.5 times higher, respectively, than modern abundances. The ^{207}Pb/^{206}Pb vs ^{204}Pb/^{206}Pb inverse isochron method, where the age of a sample is given by the intercept, was subsequently introduced by Tera and Wasserburg (1972). A

major assumption underpinning this approach is that the system has a common initial isotopic composition and evolved with time as a closed system (Amelin, 2006). The initial common Pb composition can be measured on a U-free phase (e.g., feldspar, sulfide). The system (i.e., mineral, rock) may also be free of initial Pb which is indicated by low 204Pb contents and therefore highly radiogenic compositions (e.g., zircons, Pb-free silicate reservoir). Commonly for early Solar System objects, the the Canyon Diablo troilite is used as the reference material for the initial Pb isotopic composition of the Solar nebula (Tatsumoto et al., 1973). An early disturbance of the U-Th-Pb system via shock or aqueous alteration may still produce well-defined Pb-Pb linear arrays that are erroneously interpreted as single-stage evolution isochrons instead of mixing lines (Amelin, 2006; McSween and Huss, 2022). The thorogenic ^{208}Pb isotope systematics provide additional constraints on the long-term Th/U evolution of the samples and can shed light on potential heterogeneities of components (Blichert-Toft et al., 2020). Recent disturbances are not known to fractionate Pb isotopes, and, therefore, the age information from Pb radiogenic ingrowth should be preserved. Mixing of Pb isotopic components such as the initial and radiogenic Pb ingrowth of the sample with a terrestrial component can, however, cause disturbances and generate erroneous ages (Fig. 15). Samples, therefore, have to be acid-washed using multiple steps to remove potential common Pb phases and surface contamination due to weathering of the meteorite in the desert or from laboratory curation and preparation. Using this step-by-step leachate procedure, an internal Pb-Pb isochron using the most radiogenic steps can be obtained for a single phase (Amelin, 2006). Consequently, the ^{207}Pb*-^{206}Pb* has become the method of choice for age-dating early Solar System materials with very low abundances of common lead (monitored as ^{204}Pb) and high U/Pb ratios.

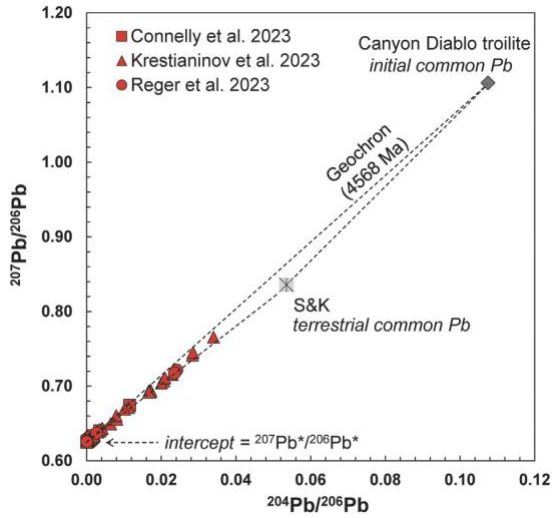

Figure 15: Schematic illustration of a Pb-Pb inverse isochron diagram using the Pb isotope data of all leachates and residues of mineral separates (pyroxene and plagioclase) and whole-rock samples of EC 002 from Connelly et al. (2023), Krestianinov et al. (2023), and Reger et al. (2023). The data show the potential contributions of two to three Pb isotopic components: initial common Pb such as Canyon Diablo IAB iron meteorite troilite or absence of initial common Pb, uranogenic Pb, and terrestrial common Pb contamination, which is defined by S&K = Stacey and Kramers (1975). A mixture of these three components would fall between the Geochron and S&K dashed lines. The average Pb-Pb age of EC 002 from the three studies above is 4565.93 ± 0.07 Ma, which is obtained from the ^{207}Pb*/^{206}Pb* radiogenic isotopic composition values obtained at the intercept where ^{204}Pb/^{206}Pb = 0 and using the respective measured U isotopic compositions. See text and data source references for further details.

The U isotopic composition serves as a reference parameter for various radiometric dating methods, including Pb-Pb dating. A modern ^{238}U/^{235}U = 137.88 was historically assumed to be constant across the Earth and the Solar System objects until slight excesses in ^{235}U were detected in bulk meteorites (Stirling

et al., 2005). Brennecka et al. (2010) determined the $^{238}U/^{235}U$ in various types of meteorites and in individual CAIs from the Allende meteorite and found a correlation between ^{235}U excesses and Th/U or Nd/U of the objects. Such U isotopic variations in CAIs would reduce Pb-Pb age determinations by up to 5 Myr relative to those using 137.88. The $^{238}U/^{235}U$ variations may also be explained, in part, by stable isotope fractionation effects associated with low-temperature or redox reactions that can modify the U isotopic composition of minerals (Stirling et al., 2007). Tissot et al. (2016) identified an unprecedented excess (~6%) of ^{235}U in an Allende CAI named Curious Marie. Owing to the magnitude of the excess, U kinetic isotopic fractionation during condensation cannot be responsible for the U isotopic variations measured in CAIs. The results of these studies together provided compelling evidence that ^{247}Cm (half-life of ~15.6 Myr; Table 2) was present in the early Solar System and contributed to the ^{235}U variations observed in bulk meteoritical samples. The initial abundance of $^{247}Cm/^{235}U$ of (7.0 1.6) × 10^{-5} relative to other SLR present in the early Solar System constrains the interval time between the last supernova-forming event of heavy r-process elements and incorporation into the solar nebula to ~100 Myr (consistent with earlier estimates from ^{129}I). Due to the presence of live ^{237}Cm for the first ~90 Myr of the Solar System, the $^{238}U/^{235}U$ of the samples analyzed must be measured for accurate Pb-Pb high-precision chronometry. While the composition of chondrules, bulk chondrites, and achondrites seemed originally relatively homogeneous with a $^{238}U/^{235}U$ of 137.786 0.013 (Connelly et al., 2012), variations have recently been resolved between individual chondrules (Bollard et al., 2019), achondrite mineral phases (Reger et al., 2023), and individual meteorites of a given group (Tissot et al., 2017).

4.1.2. Short-lived radioactive nuclides (SLR)

Evidence for the initial presence of short-lived radioactive nuclides (SLR) in the Solar System was established by isotopic analyses of meteorites (Table 2) (e.g., Davis, 2022 for a review). These radionuclides are now extinct, yet their decay products can be measured to infer the initial abundance and distribution of the parent SLR (Fig. 14b). The SLR provide key information about nucleosynthesis, the environment of the Sun at birth, and radiogenic heating sources of planetesimals. If a SLR was initially homogeneously distributed within the protoplanetary disk, it may be used to establish the chronology of events from condensation to planetary evolution. The secondary production within the Solar System of some of these SLR (^{10}Be, ^{14}C, ^{26}Al, and ^{36}Cl) due to exposure of materials to cosmic rays also provides information about irradiation processes and Solar activity. The cosmogenic production is, however, considered negligible in comparison to their initial abundances produced by nucleosynthesis to have any effect on their use in chronology. We refer the reader to the review by Davis (2022) and Section “From gas to dust to planetesimals” for further details on the initial abundances, origins, and principal applications in cosmochemistry of SLR systems.

As SLR are extinct isotopes, they provide relative dates of events that have been anchored onto an absolute time scale that was derived from LLR systems. Usually, the absolute U-Pb-Pb age and SLR systematics of CAIs are taken as time anchors for SLR as they mark t_0 for most systems (except for Fe-Ni as CAIs are nearly Fe-free, and Mn-Cr or I-Xe as CAIs are volatile-free). For other systems, basaltic meteorites such as angrites (D’Orbigny and Sahara 99,555 for Al-Mg, Mn-Cr, and Hf-W) or aubrites (Shallowater for I-Xe) may be used (Davis, 2022). Detailed chronological records for several SLR with half-lives particularly relevant to early Solar System formation (i.e., up to ~20 Myr; Table 2) and their comparison with absolute ages (U-corrected Pb-Pb ages, Section “Long-lived radioactive nuclides (LLR)”) have been a major focus of early Solar System chronology studies. The initial abundances have generally been well-established for SLR (except for ^{7}Be, ^{36}Cl, ^{97}Tc, ^{98}Tc, ^{99}Tc ^{126}Te, and ^{135}Ba) but there remains significant debate on their distribution among materials formed in different regions of the protoplanetary disk (Section “The particular case of ^{26}Al”). Chronological studies of meteorites, including ages obtained

from LLR (U-Pb-Pb, Ar-Ar) and SLR systems (Al-Mg, Mn-Cr, Hf-W, I-Xe), provide timescales of condensation, planetary accretion and differentiation, thermal and shock metamorphism, and volatile fractionation (Davis, 2022). Chronological records are also used to fit parameters of numerical modeling of the accretion time, size, and thermal evolution of meteorite parent bodies (e.g., Trieloff et al., 2003).

Table 2: Short-lived radionuclide systems used in cosmochemistry.

Radioactive isotope	Radiogenic isotope	Decay type and branching decay probability	Half-life $t_{1/2}$ (±2σ Myr)	Reference stable isotope for isochron	Initial abundance
^{7}Be	^{7}Li	β-	53.22 ± 0.06 (d)	^{9}Be	$(6.1 \pm 1.3) \times 10^{-3}$
^{10}Be	^{10}B	β-	1.3870 ± 0.0012	^{9}Be	$(7.3 \pm 1.7) \times 10^{-4}$
^{26}Al	^{26}Mg	β-	0.717 ± 0.024	^{27}Al	$(5.24 \pm 0.10) \times 10^{-5}$
^{36}Cl	^{36}Ar, ^{36}S	β- (p≈0.98), N.C. (p≈0.02)	0.3013 ± 0.0015	^{35}Cl	$(1.7–3.0) \times 10^{-5}$
^{41}Ca	^{41}K	β-	0.0994 ± 0.0015	^{40}Ca	4×10^{-9}
^{53}Mn	^{53}Cr	β-	3.7 ± 0.4	^{55}Mn	$(7 \pm 1) \times 10^{-6}$
^{60}Fe	^{60}Ni	β-	2.62 ± 0.04	^{56}Fe	$(1.01 \pm 0.27) \times 10^{-8}$
^{92}Nb	^{92}Zr	β-	34.7 ± 2.4	^{93}Nb	$(1.66 \pm 0.10) \times 10^{-5}$
^{97}Tc	^{97}Mo	β-	4.21 ± 0.16	^{92}Mo	$<1 \times 10^{-6}$
^{98}Tc	^{98}Ru	β-	4.2 ± 0.3	^{96}Ru	$<2 \times 10^{-5}$
^{107}Pd	^{107}Ag	β-	6.5 ± 0.3	^{108}Pd	$(5.9 \pm 1.3) \times 10^{-5}$
^{126}Sn	^{126}Te	β-	0.23 ± 0.014	^{124}Sn	$<3 \times 10^{-6}$
^{129}I	^{129}Xe	β-	16.14 ± 0.12	^{127}I	$(1.35 \pm 0.02) \times 10^{-4}$
^{135}Cs	^{135}Ba	β-	1.33 ± 0.19	^{133}Cs	$<2.8 \times 10^{-6}$
^{146}Sm	^{142}Nd	α	103 ± 5	^{144}Sm	$(8.40 \pm 0.32) \times 10^{-3}$
^{182}Hf	^{182}W	β-	8.9 ± 0.09	^{180}Hf	$(1.018 \pm 0.043) \times 10^{-4}$
^{205}Pb	^{205}Tl	β-	17 ± 0.9	^{204}Pb	$(1.8 \pm 1.2) \times 10^{-3}$
^{244}Pu	^{232}Th	fission	81.3 ± 0.3	^{238}U	$(7.7 \pm 0.6) \times 10^{-3}$
^{247}Cm	^{235}U	α, 3×	15.6 ± 0.5	^{235}U	$(7.0 \pm 1.6) \times 10^{-5}$

Half-lives in million years (Myr), except ^{7}Be in days (d), are taken from Kondev et al. (2021). Initial abundances for SLR are taken from Davis (2022 and refs. therein) and Tissot et al. (2016) for the ^{247}Cm/^{235}U initial abundance.

4.1.3. The particular case of ^{26}Al

Aluminum-26 is a short-lived isotope that decays to magnesium-26 with a half-life of 717,000 years (Kondev et al., 2021). It is an essential isotope used in a wide range of scientific studies, from cosmology, astrophysics, and nuclear physics to space and planetary science. The gamma-ray emissions associated with decaying ^{26}Al are observed throughout our galaxy by telescopes (Gounelle, 2015). By mapping the abundance of this isotope in our galaxy, astronomers have gained insights into the dynamics of stellar nucleosynthesis and interstellar gas. It is proposed that ^{26}Al originates principally from production in massive stars (25–120 $M_{\odot}$, with contribution from rarer, very massive stars that are up to 300 $M_{\odot}$) as well as irradiation and exposure to cosmic rays (Martinet et al., 2022). Its injection into the Solar molecular cloud must have occurred rapidly after production for it to be preserved in the Solar System. Bulk (digested sample) and in situ (individual mineral phase) measurements of Al/Mg and Mg isotopic compositions of refractory inclusions in CV3 chondrites establish together that the initial *canonical abundance* of ^{26}Al in the Solar System corresponds to a ^{26}Al/^{27}Al ratio of 5.24 (0.10) × 10^{-5} (2s) (Jacobsen et al., 2008; MacPherson et al., 2010). Because of discrepancies found between absolute U-corrected ^{207}Pb-^{206}Pb and

relative ^{26}Al-^{26}Mg ages of CAIs and chondrules (e.g., Kita et al., 2013; Bollard et al., 2019; Gregory et al., 2020; Krestianinov et al., 2023), there has been significant debate, however, in interpreting the initial abundance and distribution of ^{26}Al in other planetary materials that formed at different times and in different regions of the protoplanetary disk. The heterogeneous or homogeneous distribution and possible late addition of ^{26}Al in the protoplanetary disk (as proposed by Bollard et al., 2019) needs to be resolved before confidently using the ^{26}Al-^{26}Mg short-lived radionuclide system for chronological applications (Section "From gas to dust to planetesimals" for further discussion).

4.2. Mass-dependent isotope variations

Physical processes and chemical reactions can result in mass-dependent isotopic variations in planetary materials that scale with the mass difference between the isotopes involved. These isotopic variations are measured using different types of mass spectrometers, depending on the nature of the sample and the precision required for the analysis.

Two types of mass-dependent isotope effects must be considered for cosmochemical applications. First, mass-dependent fractionation effects occur in all mass spectrometers during ion formation, extraction, transmission, separation, and/or detection. This *instrumental mass fractionation* (or *mass bias*), which results in a difference of the measured isotope ratio from the true isotope ratio in a sample, can be corrected in different ways that depend on the type of mass spectrometric method employed. For example, standard-sample bracketing is used for correcting for mass bias in MC-ICP-MS studies because instrumental fractionation is predominantly a function of the physics of ion extraction from the plasma rather than the chemical behavior of the element (Albarède et al., 2015). In TIMS measurements, mass fractionation depends on the chemistry of the element being analyzed, and it also differs from sample to sample; thus, correction requires a pair of invariant stable isotopes in the element of interest and measuring the deviation of that isotope ratio from some assumed value (Carlson, 2014). Matrix-matched reference materials are used for SIMS measurements because sputtering may produce significant mass-dependent isotope fractionation of secondary ions, the magnitude of which depends on the chemical and structural environment of the analyzed area of the sample (Marin-Carbonne et al., 2022).

The second type of mass-dependent fractionation refers to the degree of *natural* or *intrinsic* isotope fractionation of major or trace elements, and provides important constraints on processes in the disk and during planetary accretion and evolution. Mass-dependent fractionation was first recognized for the *traditional* stable isotopes of the light elements H, C, N, O, and S in both geo- and cosmochemistry (for review, see Stern and Wiemann, 2021). Groundbreaking developments in plasma source mass spectrometry now permit high-precision analyses of so-called *non-traditional* stable isotopes (i.e., stable isotopes of elements other than the aforementioned light ones, including Mg, Si, Fe; Johnson et al., 2004; Teng et al., 2017). For both traditional and non-traditional stable isotopes, mass-dependent fractionation may occur during equilibrium and kinetic processes for which the mass fractionation laws differ (Young et al., 2002). The resulting isotopic variations are typically reported in d units, as parts per thousands (*per mil*, %) deviations from a universally accepted (terrestrial) standard; by convention, the heavier isotope is the numerator, whereas the lighter isotope is the denominator of the isotope ratio of interest. For O, for example, δ^{17}O and δ^{18}O values are generally reported, where $\delta^{i}O = [(^{i}O/^{16}O)_{sample}/(^{i}O/^{16}O)_{sample} - 1] \times 1000$, and SMOW is Standard Mean Ocean Water. Analogous definitions can be written for δD, δ^{13}C, δ^{15}N, and isotope systems of heavier elements.

Equilibrium isotope fractionation is linked to processes that lead to a bidirectional isotope exchange between two different phases or molecular species (i.e., compounds) that have a common element, without any net chemical reaction (*sensu stricto* it only occurs in a closed, well-mixed system in thermodynamic

equilibrium). For an in-depth treatment of the theoretical, quantum-mechanical background, the reader is referred to Schauble (2004) and citations therein, including the classical papers by Bigeleisen and Mayer (1947) and Urey (1947). The magnitude of equilibrium fractionation between two compounds decreases with increasing temperature (as $1/T$ at low temperatures and as $1/T^2$ at room temperature and above), and it is largest for light elements because of the greater relative mass difference between their isotopes (scaling roughly as $[(m_{heavy} - m_{light})/ (m_{light}m_{heavy})]$. Furthermore, the heavy isotope will preferentially partition into the site with the stiffest chemical bonds. The magnitude of fractionation during isotopic exchange between two compounds A and B, can be expressed as an *equilibrium constant*, but more useful is the *fractionation factor* $a_{A-B} = R_A/R_B$, where R_A and R_B are the isotope ratios (e.g., $^{18}O/^{16}O$) of compounds A and B. The a_{A-B} values generally differ by just a few percent from the equal-energy value of 1.00, except for exchange reactions involving H isotopes, where a_{A-B} values may be as large as 4 at room temperature. Isotope fractionation between two compounds, therefore, is often also reported as $D_{A-B} \approx 1000 \times \ln(a_{A-B})$ or $D_{A-B} = 1000 \times (a_{A-B} - 1)$ that magnify the difference between a_{A-B} and 1.00.

The other mass-dependent mechanism resulting in stable isotope fractionation is *kinetic isotope fractionation*. It is usually associated with fast, unidirectional, or incomplete chemical or physical processes such as bond-breaking dissociation reactions or diffusion. Kinetic isotope fractionation due to bond-breaking reactions is temperature sensitive due to the effect of isotopic substitution on activation energies required to reach a transition state. Light isotopes, being more reactive, will generally be concentrated in the end product of the reaction. Inverse kinetic effects, where heavy isotopes are preferentially concentrated in the transition state or reaction product, may occur if the transition state is more strongly bound than the reactant. Diffusion effects result from higher velocities of lighter isotopes at constant kinetic energy. This class of kinetic transport phenomena can lead to large isotope fractionations even at high temperatures.

4.2.1. Mass-dependent fractionation of oxygen isotopes in planetary materials

Oxygen is the major constituent of rocky planets and the third most abundant element in the Solar System, as determined by spectroscopic measurements of the Solar photosphere (Section "Elemental composition of the Solar System"). Oxygen isotopes in planetary materials provide fundamental insights into cosmochemical processes occurring in the protoplanetary disk and during planetary processes. Nonetheless, the O isotopic signature of the Sun, presumably the best proxy for the initial O isotopic composition of the Solar System, remained essentially unknown until NASA's Genesis Discovery Mission collected samples of the Solar wind and returned them to Earth for laboratory analysis in 2004 (Section "Sample return missions"). The O isotopic composition of the Solar wind, which was captured in the Genesis Concentrator target and analyzed using the MegaSIMS (a hybrid secondary ion microscope-accelerator mass spectrometer at the University of California, Los Angeles), first had to be corrected for mass-dependent fractionation induced by the Concentrator during ion implantation and by the mass spectrometer during analysis. The corrected values then had to be adjusted by considering that during the formation and acceleration of the Solar wind, O isotopes in the Solar wind were mass-dependently fractionated by ~22 to 34% per atomic mass unit toward a lighter composition (Heber et al., 2012). Thus, photospheric O was found to have an isotopic composition of $\delta^{18}O = -58.5\%$ and $\delta^{17}O = -59.1\%$ (McKeegan et al., 2011) (Fig. 16a). This result demonstrates that the Sun is highly enriched in ^{16}O compared to Earth, the Moon, Mars, and bulk meteorites.

On an O three-isotope diagram ($\delta^{17}O$ vs $\delta^{18}O$), terrestrial materials such as silicate rocks and minerals evolve along a line with a slope of ~0.52. The slope of this *terrestrial fractionation line* (TFL) reflects the relative mass difference between the isotope pairs $^{17}O/^{16}O$ and $^{18}O/^{16}O$, and illustrates that mass-dependent fractionation effects result in the $\delta^{18}O$ value changing by slightly less than twice that of the $\delta^{17}O$

value. Deviations from this reference line are conventionally expressed as $\Delta^{17}O \approx \delta^{17}O - 0.52 \times \delta^{18}O$. Equilibrium or kinetic processes, however, result in slightly different triple isotope fractionations, and published slope factors of the TFL range from 0.509 (the lower limit for kinetic fractionation; Matsuhisa et al., 1978) to 0.5305 (the theoretical upper limit at high temperature; Young et al., 2002). The range in possible mass-dependent fractionation laws should be considered when seeking to identify sub-per mil deviations from mass dependency, particularly for cosmochemical applications for which the TFL serves as a fundamental benchmark. For example, the $\delta^{17}O$– $\delta^{18}O$ arrays for Earth and the Moon are virtually indistinguishable (Wiechert et al., 2001; Cano et al., 2020; Greenwood et al., 2018; Herwartz et al., 2014; Young et al., 2016) (Fig. 16b). High-precision oxygen isotope analyses together with well-constrained mass fractionation lines, therefore, are required for both terrestrial and lunar samples to prove the existence or absence of a minor terrestrial-lunar $\Delta^{17}O$ difference. This, in turn, is crucial for assessing the degree of material mixing that occurred during the Giant Impact responsible for the Earth-Moon system and for tracing the origin of the impactor (see Canup et al., 2023 for a review).

Similar to volcanic rocks returned from the Moon, meteorites that have chemical and mineralogical compositions and textures that are typical of large-scale melting and differentiation on their parent bodies—including Martian meteorites, HEDs, angrites, aubrites, and main-group pallasites—generally record restricted O isotopic variations, with samples falling on mass-dependent fractionation arrays with a slope of ~0.52 that are parallel to the TFL (Clayton and Mayeda, 1996; Greenwood et al., 2017) (Fig. 16b). The restricted compositions can be explained by the fact that melting and the formation of a magma ocean tend to homogenize O isotopes on the parent body, while melt differentiation and crystallization smear them along a mass-dependent fractionation line. If isotopic equilibrium is maintained during magmatic evolution, the distinct O isotopic composition of co-existing mafic minerals in achondrites (e.g., pyroxene-olivine) can be used to estimate the temperature of magmatic systems; this requires knowledge of the mineral-mineral O isotope fractionation factor (e.g., $D_{px-ol} \approx 1000 \times \ln(a_{px-ol})$) as a function of temperature. This approach, referred to as *oxygen isotope thermometry*, permitted to calculate the temperature of the magma chamber for two Martian meteorites (i.e., ~1430 ˚C for SaU 008 and ~ 1200 ˚C for DaG 476; Ali et al., 2018), and to establish the physicochemical conditions of magma production in the mantle of Mars. Such temperature determinations may also be made for other achondrites and lunar basalts to constrain the history of igneous systems on differentiated asteroids and the Moon.

Oxygen isotope thermometry can also be used to constrain the temperature of aqueous alteration on chondritic parent bodies. Alteration temperatures can be estimated using the mass-dependent O isotopic fractionation between a secondary mineral and an aqueous fluid, which requires knowing the initial O isotopic composition of the fluid. Additionally, thanks to the advances of in situ techniques (e.g., SIMS), alteration temperatures can also be estimated using the O isotopic fractionation between two cogenetic phases that precipitated from the same parent fluid in isotopic equilibrium (e.g., Zheng, 2011). Based on this approach, the temperature of aqueous alteration on the C-type asteroid Ryugu was determined. The O isotopic compositions of co-precipitated dolomite and magnetite in samples returned by the Hayabusa2 mission (Section "Sample return missions") was initially inferred to record an equilibration temperature of 37 ± 10 ˚C, which falls within the temperature range of 10–150 ˚C previously estimated for aqueous alteration on the CI chondrite parent body (Yokoyama et al., 2022). Additional O and C isotope measurements of calcite and dolomite grains, however, lead Fujiya et al. (2023) to argue that calcite precipitated over a wide range of temperatures and oxygen fugacities, as reflected by significant $\delta^{18}O$– $\delta^{13}C$ variations (Fig. 16a), whereas dolomite formed later at equilibrium. These results demonstrate that mass-dependent oxygen isotope variations have the potential to record complex alteration reactions and provide key constraints on the physicochemical conditions of aqueous alteration on chondritic asteroids.

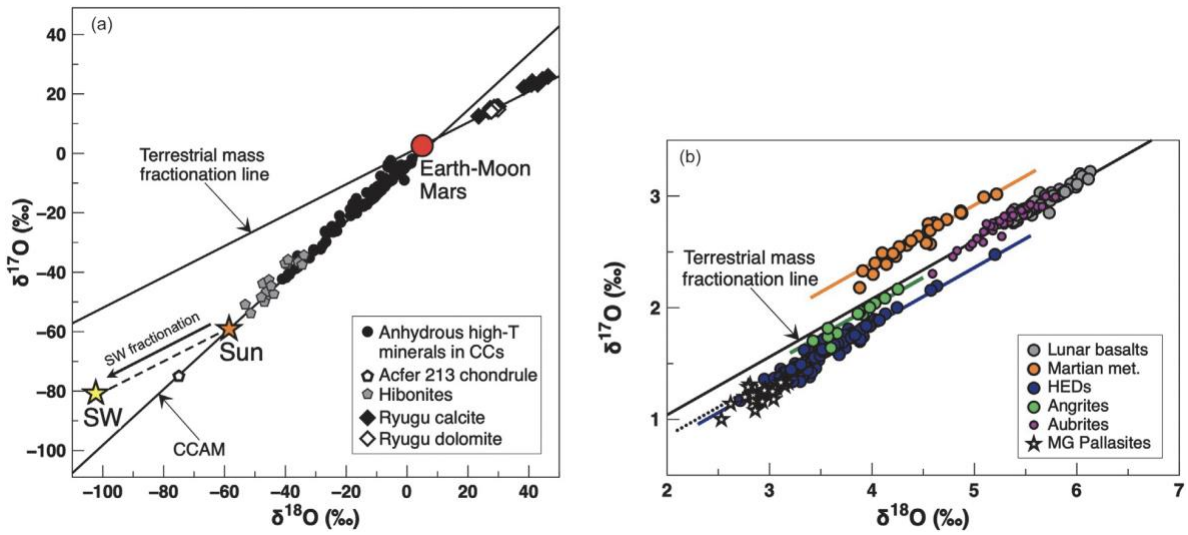

Figure 16: Oxygen three-isotope diagrams (note the change of scale between the two panels). (a) Anhydrous high-temperature minerals (i.e., CAIs) in carbonaceous chondrites define a linear correlation with a slope of ~1, referred to as the *carbonaceous chondrite mineral line* (CCAM). A chondrule of the Acfer 214 CH3 carbonaceous chondrite and platy hibonite grains fall onto the same line. Mass-independent O isotope variations in these early-formed solids likely result from mixing between a ^{16}O-rich (Solar) component and ^{16}O-poor water ice. The O isotopic composition of the Sun (derived from the Solar wind (SW) value) falls onto the extension of the CCAM. Oxygen isotope variations in carbonates (calcite and dolomite) of the asteroid Ryugu result from temperature changes during precipitation from ^{17,18}O-enriched water. (b) Differentiated achondrites (including Martian meteorites, HEDs, angrites, aubrites) and main-group pallasites follow mass-dependent fractionation arrays with a slope of ~0.52 that are parallel to the terrestrial mass fractionation line. The O isotopic composition of lunar basalts is virtually indistinguishable from the terrestrial signature. Panel (A) Data sources: Clayton RN, Grossman L, Mayeda TK (1973) A component of primitive nuclear composition in carbonaceous meteorites. *Science* 182: 485–488, Clayton RN, Onuma N, Grossman L, Mayeda TK (1977) Distribution of the pre-solar component in Allende and other carbonaceous chondrites. *Earth and Planetary Science Letter*s 34: 209–224, Kobayashi S, Imai H, Yurimoto H (2003 New extreme 16O-rich reservoir in the early solar system. *Geochemical Journal* 37: 663–669, Liu M-C, McKeegan K, Goswami JN, Marhas KK, Sahijpal S, Ireland TR, Davis AM (2009) Isotopic records in CM hibonites: Implications for timescales of mixing of isotope reservoirs in the solar nebula. *Geochimica et Cosmochimica Acta* 73: 5051–5079, McKeegan KD, Kallio APA, Heber VS, Jarzebinski G, Mao PH, Coath CD, Kunihiro T, Wiens RC, Nordholt JE, Moses RW, Jr, Reisenfeld DB, Jurewicz AJG, Burnett DS, 2011. The oxygen isotopic composition of the Sun inferred from captured solar wind. *Science* 332: 1528–1532, Fujiya W et al. (2023) Carbonate record of temporal change in oxygen fugacity and gaseous species in asteroid Ryugu. *Nature Geoscience* 16: 675–682. Panel (B) Data sources: Clayton RN, Mayeda TK (1996) Oxygen isotope studies of achondrites. *Geochimica et Cosmochimica Acta* 60: 1999–2017., Franchi IA, Wright IP, Sexton AS, Pillinger CT (1999) The oxygen-isotopic composition of Earth and Mars. *Meteoritics and Planetary Science* 34: 657–661, Wiechert U, Halliday AN, Lee D-C, Snyder GA, Taylor LA, Rumble D (2001) Oxygen isotopes and the Moon-forming giant impact. *Science* 294: 345–348, Herwartz D, Pack A, Friedrichs B, Bischoff A (2014) Identification of the giant impactor Theia in lunar rocks. *Science 344* (6188): 1146–1150., Young ED, Koh IE, Warren PH, Rubie DC, Jacobson SA, Morbidelli A (2016) Oxygen isotopic evidence for vigorous mixing during the Moon-forming giant impact. *Science* 351(6272): 493–496, Greenwood RC, Burbine TH, Miller MF, Franchi IA (2017) Melting and differentiation of early-formed asteroids: The perspective from high precision oxygen isotope studies. *Geochemistry* 77(1): 1–43, Greenwood RC, Barrat J-A., Miller MF, Anand M, Daupha N, Franchi IA, Sillard P, Starkey NA (2018) Oxygen isotopic evidence for accretion of Earth's water before a high-energy Moon-forming giant impact. *Science Advances* 4(3): eaao5928, Cano EJ, Sharp ZD, Shearer CK (2020) Distinct oxygen isotope compositions of the Earth and Moon. *Nature Geoscience* 13: 270–274.

4.2.2. Mass-dependent fractionation of non-traditional isotopes in planetary materials

Determining the extent of mass-dependent fractionation recorded by non-traditional isotopes in planetary materials has been the focus of various recent studies addressing planetary accretion and evolution. Besides O, the next most abundant elements in rocky planets are Mg, Si, and Fe. Small, but significant fractionations of their isotopes by high-temperature cosmochemical processes can now be detected thanks to high-precision mass spectrometric analyses. By measuring the Mg isotopic composition of a range of chondrites and achondrites (including Martian meteorites, diogenites, and an angrite), Hin et al. (2017) found that differentiated planetary bodies have higher δ^{25}Mg values than chondritic asteroids. These observations imply that during the accretion of low-mass planetesimals, high-temperature events (i.e., planetary collisions) led to substantial evaporation from melt ponds or magma oceans, and the isotopically light vapor phase subsequently escaped to space. Vapor-melt isotopic fractionation and vapor loss may also explain the heavy Si isotope enrichment (high δ^{30}Si) of the angrite parent body observed by Dauphas et al. (2015). Furthermore, vaporization and loss of isotopically-light Fe during the Moon-forming giant impact was considered by Poitrasson et al. (2004) as a mechanism to explain the heavier Fe isotopic composition of Earth and the Moon compared to Mars and Vesta. More recent studies, however, have revealed that Fe isotopes will also fractionate as a result of other high-temperature planetary processes such as core formation. The Fe isotope system has been of particular interest for tracing high-temperature processes such as magmatic differentiation and core formation because of the ubiquity of iron in planetary reservoirs, its variable oxidation states, and electronic spin transitions at very high pressure (Lin et al., 2005). Following the discovery of a heavy-Fe-isotope enrichment (i.e., higher δ^{57}Fe) in iron meteorites compared to chondrites as well as in pallasite metals compared to co-existing olivines (Poitrasson et al., 2005), Elardo et al. (2019) proposed that impurities (e.g., high concentrations of Ni and S) in Fe-alloys result in metallic bond stiffening and preferential incorporation of heavy Fe isotopes into alloys compared to silicate melt at equilibrium. Consequently, the silicate mantles of differentiated planetary bodies are expected to be isotopically light compared to chondrites. Samples from the silicate portions of the Moon, Mars, and Vesta, however, do not show the expected light Fe isotope signature, possibly because partial melting and crust formation erased the isotope signature generated by core-mantle differentiation (Elardo and Shahar, 2017). Importantly, other experimental studies indicate that Ni does not influence metal-silicate Fe isotope fractionation, and that other factors may control the extent of Fe isotopic fractionation effects observed in planetary materials (Kubik et al., 2022). The larger pressure during core formation on Mars-sized bodies may also limit Fe isotope fractionation (Ni et al., 2022). Overall, the Fe isotopic signature of achondrites, irons, and stony-irons may be the result of one or several planetary processes, including planetary accretion, giant impacts, core-mantle differentiation, disproportionation of ferrous iron to ferric iron and metal at very high pressure in large bodies like Earth, and subsequent magmatic processing (Kubik et al., 2022).

4.3. Mass-independent isotope variations

Mass-independent (or *non-mass-dependent*) *isotope fractionation* results from specific nuclear or chemical processes for which the extent of isotope separation is not proportional to the difference in the masses of the isotopes involved. In planetary materials, mass-independent isotope effects were first recognized for S and O (i.e., elements with more than two isotopes that permit to resolve mass-independent from mass-dependent effects) (Clayton et al., 1973; Hulston and Thode, 1965). While mass-independent S isotope variations in meteorites are widespread, their magnitude is small (i.e., typically sub-permil) (Labidi et al., 2017). In stark contrast, following the falls of the Allende and Murchison meteorites in 1969, Clayton et al. (1973) discovered that δ^{17}O– δ^{18}O values in anhydrous, high-temperature phases (i.e., CAIs) of

carbonaceous chondrites are remarkably different from terrestrial rocks, with depletions of up to 35% for both values. The O isotopic compositions defined a linear correlation with a slope close to unity, rather than falling on a mass-dependent array with a slope of ~0.52 in $\delta^{17}O$– $\delta^{18}O$ space (Fig. 16a). More precise measurements, using not only Allende CAIs but also Allende chondrules and dark inclusions (i.e., materials with distinct forma- tional and secondary histories), led to the refinement of the $\delta^{17}O$– $\delta^{18}O$ slope to 0.94 0.01 (2*s*) (Clayton et al., 1977); this reference line is referred to as the *carbonaceous chondrite anhydrous mineral line* (CCAM; Fig. 16a). Based on the results of a UV laser ablation study of a single coarse-grained type B CAI from Allende, it was later proposed that unaltered CAI minerals define a $\delta^{17}O$– $\delta^{18}O$ line with a slope of exactly 1 (the so-called *Young and Russell line*, Y&R) (Young and Russell, 1998). SIMS analysis of chondrules from the ungrouped C2 chondrite Acfer 094 carbonaceous chondrite established a third, distinct slope ~1 line, known as the *primitive chondrule minerals* (PCM) line, which falls between the CCAM and Y&R lines (Ushikubo et al., 2012). While the CCAM line has been suggested to result from secondary alteration processes that displaced primary O isotopic compositions from the slope-1 line via mass-dependent fractionation processes (Young and Russell, 1998), the underlying mechanisms controlling the slope of these different lines remain debated. The magnitude of O isotope variations in planetary materials are now recognized to extend from $\delta^{17}O \approx \delta^{18}O \approx -75\%$ in a chondrule of the Acfer 214 CH3 carbonaceous chondrite (Kobayashi et al., 2003) (Fig. 16a) to $\delta^{17}O \approx \delta^{18}O \approx +180\%$ in the aqueously altered matrix of Acfer 094 (Sakamoto et al., 2007; Vacher et al., 2021).

Understanding the process(es) that resulted in mass-independent O isotope variations in the earliest-formed solids of the Solar System remains a fundamental issue in cosmochemistry. Clayton et al. (1973) concluded that carbonaceous chondrites contain a ^{16}O-rich dust component of interstellar origin, produced by stellar nucleosynthetic processes such as He burning or explosive C burning. Admixture of this ^{16}O-rich exotic dust with ^{16}O-poor water would produce a slope of 1 in a O three-isotope diagram (Clayton and Mayeda, 1984). Such ^{16}O-rich presolar grains, however, are rare in meteorites (Nittler, 2003), and isotopic variations of other elements (e.g., Mg, Si, Ca, Ti) are much smaller and uncorrelated with those of O (Clayton, 1993). Solar wind samples collected by NASA's Genesis mission finally revealed that the O isotopic composition of the Sun and, by inference, the Solar nebula, is ^{16}O-rich and lies along the CAI trend (McKeegan et al., 2011) (Fig. 16a). The prevailing view is now that the most ^{16}O-rich CAIs and hibonite (i.e., a refractory Ca-aluminate) therein preserve the O isotopic signature of the nebular gas from which they condensed. Starting from this Solar O isotopic composition, a chemical process in the nebula or the precursor molecular cloud led to mass-independent O isotope fractionation. Production of ^{16}O-depleted components may be related to isotope-selective self-shielding during ultraviolet photolysis of CO (Clayton, 2002). The preferentially released ^{17}O and ^{18}O then interacted with H-rich nebular gas in the outer Solar System to form isotopically heavy water ice, which was transported toward the inner Solar System where the isotopic anomaly was transferred to silicates and silicate precursors, with the exception of CAIs. Concurrently, CO self-shielding can also generate ^{13}C-rich C-bearing molecules; hence, this process may explain the difference between Solar ($\delta^{13}C = -48 \pm 7\%$; Lyons et al., 2018) and planetary ($\delta^{13}C \approx -5$ 15%; Mikhail and Füri, 2019) C isotopic compositions, as well as the ^{13}C-enrichment of C-bearing molecular ices that asteroid Ryugu appears to have accreted (Fujiya et al., 2023).

Other chemical mechanisms have been proposed to explain the O isotope variations in planetary materials, including molecule- symmetry-driven fractionations similar to those involved in the synthesis of ozone (Chakraborty et al., 2013; Thiemens and Heidenreich, 1983). For such reactions, grain surfaces may play a key catalytic role, as demonstrated by laboratory experiments (Robert et al., 2021). In grains condensed from plasmas, substantial mass-independent fractionation (i.e., >1000%) has not only been produced for O but also for Ti and Mg isotopes (Robert et al., 2020, 2021). Based on these results, Thiemens and Lin (2021) recently questioned whether the Solar photospheric O isotopic composition can be used as

a proxy for the Solar nebula; they assumed, instead, that the nebula had values of $\delta^{18}O$ = +5% and $\delta^{17}O$ = +2.5%. In this scenario, symmetry-dependent gas-to-solid chemical reactions (such as the reaction SiO + OH = SiO_2 + H; Chakraborty et al., 2013) produced both isotopically heavy and light reservoirs, with an endmember at $\delta^{17}O = \delta^{18}O \approx -50\%$ that is preserved in CAIs. Irrespective of the origin of mass-independent O isotope variations, isotopic heterogeneities were eventually propagated into larger-sized bodies, such as asteroids and planets, and triple O isotope measurements have become a key tool for meteorite classification and for identifying meteorite groups of common provenances (Greenwood et al., 2017; Ireland et al., 2020).

Other mass-independent isotope effects in meteorites and lunar samples result from spallation or neutron capture. *Spallation* results from exposure to galactic cosmic rays (GCR) and Solar cosmic rays (SCR) in space and/or on Earth where high-energy particles (i.e., protons, neutrons, and other charged particles) collide with atomic nuclei (O, Al, Ca, Mg, S, Si, and first-row transition metals) causing them to break apart into new stable or radioactive isotope nuclei and emitted particles. Production of so-called *cosmogenic* (or *spallogenic*) isotopes mainly depends on the total duration of exposure to cosmic rays in space, with very limited or negligible production on Earth. Consequently, measurements of the relative proportions of cosmogenic stable or radioactive isotopes that were produced in space and on Earth (e.g., ^{10}Be, ^{14}C, ^{26}Al, ^{36}Cl, ^{41}Ca, ^{53}Mn, ^{60}Co, noble gases ^{3}He, ^{21}Ne, ^{38}Ar) can be used to estimate the *cosmic ray exposure* (CRE) age as well as transfer time, terrestrial age (time since the fall event), and pre-atmospheric radius of a meteorite (Eugster et al., 2006; Herzog, 2003). Calculated CRE ages can then be used to correct other isotope systems in planetary materials that have been affected by cosmogenic nuclide contributions (e.g., D/H ratios in lunar samples; Füri et al., 2017). The CRE ages derived from ^{21}Ne concentrations have also been used to obtain interstellar lifetimes of SiC presolar grains going back to 4 ± 2 Myr and up to 3 ± 2 Gyr before the formation of the Solar System (Heck et al., 2020).

Neutron capture effects by thermal or epithermal neutrons (with different energies) modify the isotopic composition of elements with large cross-sections to neutrons in planetary materials with long-term exposure. Such effects have to be carefully assessed against isotopic anomalies inherited from nucleosynthetic signatures in meteorites (Section "Nucleosynthetic isotope anomalies"). Since ^{149}Sm and ^{158}Gd are the isotopes with the largest cross-section, anti-correlations of ^{149}Sm/^{152}Sm with ^{150}Sm/^{152}Sm and of ^{157}Gd/^{160}Gd with ^{158}Gd/^{160}Gd in long-term exposed meteorites, lunar, or planetary samples are typically used as neutron monitors for corrections (Hidaka et al., 2000). Neutron capture effects also create shifts in the ratios of other isotopes with smaller cross- sections; therefore, the measured isotopic compositions for many systems (e.g., Mo, Ru, Nd, Hf, W) in lunar samples, CAIs, and meteorites must be corrected prior to interpretation (Bermingham et al., 2018a,b; Bouvier and Boyet, 2016; Fischer-Gödde et al., 2015; Kruijer et al., 2012; Sprung et al., 2010; Worsham et al., 2019). For metal-rich meteorites, Os and Pt isotopes are used to correct isotopic data for neutron capture effects (Cook et al., 2020; Hunt et al., 2017; Kruijer et al., 2013; Spitzer et al., 2021a,b; Walker, 2012; Worsham et al., 2017).

4.4. Nucleosynthetic isotope anomalies

Nucleosynthetic or *genetic* isotope anomalies recorded by meteorite components (CAIs, AOAs, chondrules, etc.), bulk meteorites, and some planets (Earth, Mars) developed from the uneven distribution of presolar grains in the disk. These part-per-million scale isotopic anomalies are much smaller than what is recorded by individual presolar grains because these grains have been mixed with ISM-processed dust, which is isotopically non-anomalous.

Many refractory elements and some volatile elements have reported bulk meteorite nucleosynthetic anomalies in one or more of their isotopes. This includes isotopes of Ne, Kr, Xe, K, Ca, Ti, Cr, Fe, Ni, Zn, Sr, Zr, Mo, Ru, Pd, Ba, Nd, Sm, Er, Yb, Hf, W, and Pt. Nucleosynthetic Os isotope anomalies have been reported, however, they are considered to be a consequence of localized thermal processes on the ureilite

parent body rather than a reflection of the heterogeneous distribution of Os isotopes in the Solar System (Goderis et al., 2016). For a review of nucleosynthetic isotope anomalies in meteorites and their components and their link to establish Earth's building blocks, see Bermingham and Meyer (2024).

The cause of the heterogeneous distribution of presolar grains in the disk is an active area of research. Two general mechanisms have been proposed. (1) Presolar grains were heterogeneously distributed in the molecular cloud, and this heterogeneity was inherited by the Solar System (Dauphas et al., 2002). The late injection of supernova material followed by inefficient homogeni- zation (e.g., Qin et al., 2011) is a potential mechanism by which the heterogeneous distribution of presolar grains in the disk developed. (2) Initially, presolar grains were homogeneously distributed throughout the molecular cloud and the protoplanetary disk, however, by virtue of disk-based dust decoupling processes these grains became heterogeneously distributed. Decoupling processes include thermal processing of labile phases in presolar grains (Trinquier et al., 2009). This requires the highly selective destruction of thermally labile phases, which can occur due to a susceptibility to chemical reactions or vaporization at high temperatures (i.e., volatility-controlled gas-dust decoupling). Alternatively, small grains, which had a different isotopic composition to coarse grains, may have become segregated in the disk via "size-sorting" or "grain type-sorting" (Dauphas et al., 2008, 2010; Regelous et al., 2008).

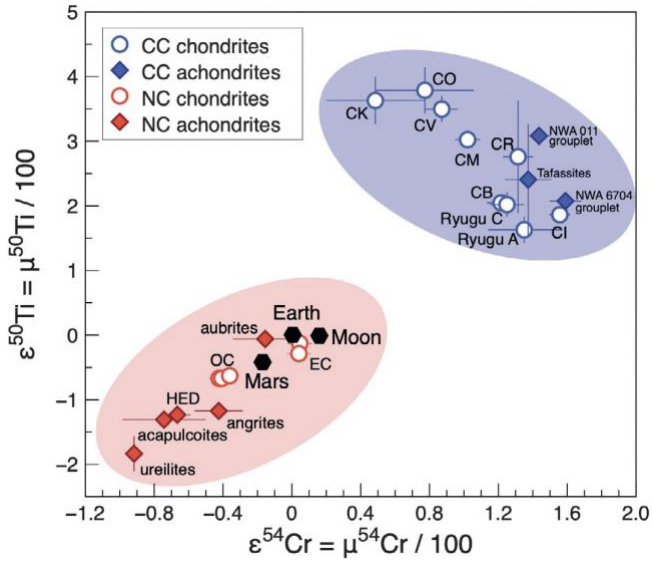

Figure 17: Variation in $^{50}Ti/^{47}Ti$ and $^{54}Cr/^{52}Cr$ (expressed in ε- or μ-units) between chondrites (open symbols) and achondrites (filled symbol) in comparison to Earth, Moon, and Mars (black hexagons). NC- and CC-type bodies are represented in red and blue, respectively. Ryugu samples were collected at the surface (A) and subsurface (C) of the C-type asteroid by JAXA's Hayabusa2 mission. Modified from Warren PH (2011) Stable-isotopic anomalies and the accretionary assemblage of the Earth and Mars: A subordinate role for carbonaceous chondrites. *Earth and Planetary Science Letters* 311: 93–100, Ma M, Neumann W, Néri A, Schwarz WH, Ludwig T, Trieloff M, Klahr H, Bouvier A (2022) Early formation of primitive achondrites in an outer region of the protoplanetary disc. *Geochemical Perspectives Letters* 23: 33–37, and Yokoyama T, et al. (2022) Samples returned from the asteroid Ryugu are similar to Ivuna-type carbonaceous meteorites. *Science* 379: eabn7850, including data sources therein.

A top-level division in bulk meteorites defined by their nucleosynthetic isotope anomalies was identified by Warren (2011). This division is based on a ubiquitous isotopic dichotomy among planetary materials that is evident in interelement isotopic compar- isons (e.g., $\mu^{54}Cr$ vs $\mu^{50}Ti$; Fig. 17). The CC group is defined by high $\mu^{54}Cr$ and $\mu^{50}Ti$ and is separated by a gap from the NC group, which has low $\mu^{54}Cr$ and $m^{50}Ti$. Hints of what now is recognized as the NC-CC dichotomy were observed prior to Warren (2011)

(e.g., Trinquier et al., 2007). Since 2011, the NC-CC dichotomy has been extended to almost all meteorite groups and most isotopic systems which exhibit nucleosynthetic isotope anomalies (Section "Meteorite classification"). Several highly volatile to moderately volatile elements also show a NC-CC dichotomy in isotopic compositions (N in some iron meteorites (Grewal et al., 2021); Zn (Steller et al., 2022; Savage et al., 2022; Martins et al., 2023)).

5. SAMPLE-BASED CONTRAINTS ON SOLAR SYSTEM FORMATION

5.1. From gas to dust to planetesimals

5.1.1. Chronology of chondritic components

5.1.1.1. Refractory inclusions

The oldest known objects that formed in the Solar System are refractory inclusions. They are identified as either hibonite-rich CAIs (PLACs), FUN inclusions, or "normal" CAIs (see Section "Calcium-aluminum-rich inclusions" for further definition). Placing chronological constraints on the formation of PLACs and FUN inclusions is challenging owing to their rarity in meteorites, generally small sizes, large nucleosynthetic anomalies, and depletion in radioactive elements that are commonly used for dating (i.e., U, Fe, Mn). In addition, they lack evidence of ^{26}Al or have abundances that are lower than the canonical value ($^{26}Al/^{27}Al_0 \approx 5.24 \times 10^{-5}$; Table 2) at the time of their formation which has been interpreted to indicate that they formed before the injection of ^{26}Al into the Solar nebula (Jacobsen et al., 2008). On the other hand, most normal CAIs contain evidence for the presence of ^{26}Al, which suggests these refractory inclusions formed while ^{26}Al was present in the canonical abundance (Table 2). The detection of ^{26}Al in the earliest formed solids in the Solar System implies a rapid timescale for the injection and homogenization of ^{26}Al within the refractory inclusion formation region. Most refractory inclusions share some compositional similarities, with close to Solar ^{16}O-rich isotopic compositions and Si, Mg, and Ca stable isotopic compositions that indicate similar formation environments and extensive evaporation processes (Williams et al., 2017; Kööp et al., 2020).

Due to the low U contents (sub-ppb to ~20 ppb U) of refractory inclusions, only large (>100 mg) individual CAIs from CV3 chondrites can provide absolute chronological constraints using U-corrected Pb-Pb chronometry. Large masses have to be dissolved to measure the $^{238}U/^{235}U$ ratio to the high precision that is required for the Pb-Pb age correction (Section "Long-lived radioactive nuclides (LLR)"). The U-corrected Pb-Pb ages of individual CAIs are 4567.18 ± 0.21 Ma for an Allende SJ101 forsterite-bearing CAI (Amelin et al., 2010), with a $^{26}Al/^{27}Al_0$ of $(5.20 \pm 0.53) \times 10^{-5}$ (MacPherson et al., 2017), and 4567.30 ± 0.16 Ma for the average of three fine-grained 22E, 31E, and 32E CAIs from Efremovka which is not accompanied by in situ ^{26}Al-^{26}Mg data but has bulk CAI model ^{26}Al abundances that are consistent with the canonical value (Connelly et al., 2012). These U-corrected ages are consistent with previously reported uncorrected ages for CAIs from Allende and Efremovka (Amelin et al., 2002; Jacobsen et al., 2008) with an assumed $^{238}U/^{235}U$ ratio of 137.88. An older age of 4567.94 ± 0.31 Ma with $^{26}Al/^{27}Al_0$ of $(4.9 \pm 0.53) \times 10^{-5}$ is reported for a compact Type A (unmelted) CAI from NWA 6991 (Bouvier et al., 2011; Wadhwa et al., 2014). The 0.76 ± 0.37 Myr difference between U-corrected Pb-Pb ages of CAIs is distinctly longer than the range of in situ ^{26}Al-^{26}Mg ages of type A to type B CAIs that spanover ~0.2 Myr (Kita et al., 2013). The origin of this discrepancy between radioactive systems is unclear and could be related to the complex condensation, melting, aqueous alteration, and thermal history of CAIs and their CV3 chondrite hosts, as well as acid-wash (leaching) step selection made for Pb-Pb age calculations (Desch et al., 2023).

5.1.1.2. Chondrules

Chondrules are a major component of chondrites and are intimately linked to planetary formation processes (Section “Chondrules"). Based on their chemical compositions, chondrules may have been a major contributor to the planetary building blocks (Alexander, 2022). It is unclear, however, if they formed in the protoplanetary disk via nebular and/or planetary processes (see Russell et al., 2018 for a review). Determining the time and location of chondrule formation events, particularly in comparison to CAIs, provides critical constraints on the evolution of the protoplanetary disk and earliest stages of planetary formation (e.g. Connelly et al., 2012). The in situ ^{26}Al-^{26}Mg chronology of chondrules from NC and CC primitive chondrites indicates a main and extended period of chondrule formation between 1.5 and 4 Myr after CAIs in the NC and CC regions (Villeneuve et al., 2009; Fukuda et al., 2022). Most chondrule ages of unequilibrated ordinary chondrites (UOC, sub-types 3.00–3.05) that are based on analyses of mesostasis-olivine assemblages are well-constrained between 1.8 and 2.2 Myr after CAIs (Siron et al., 2022). A minority of UOC chondrules (~10%) and spinel- olivine-rich chondrules in NC and CC chondrites, however, indicate earlier formation ages, reducing the gap to ~0.7 Myr between the formation of refractory inclusions and chondrules (Villeneuve et al., 2009; Piralla et al., 2023). Chondrule ages from primitive CO, CV, and a CM2.9 indicate a resolvable delay in chondrule formation between 2.2 and 3.0 Myr after CAIs, with the CR chondrules showing distinct formation episodes that last until 4 Myr after CAIs (see compilation in Fukuda et al., 2022 and refs. therein). Younger metal-rich chondrules from the CH-CB chondrites are related to large planetary collision events 4–5 Myr after CAIs (Krot et al., 2005a,b).

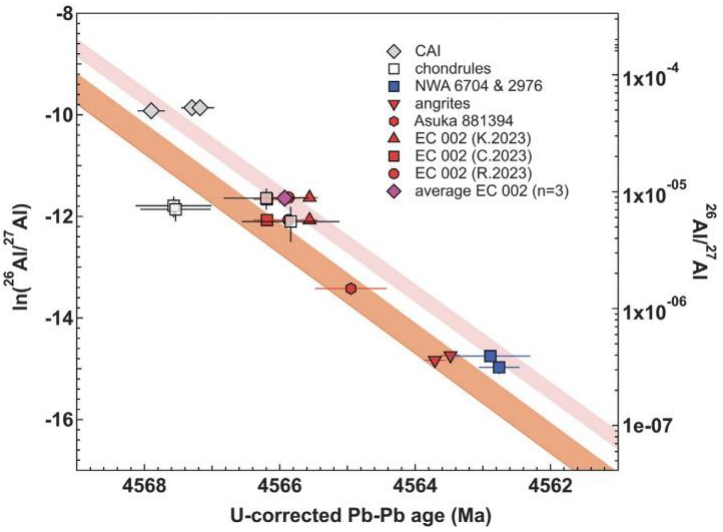

Figure 18: The ^{26}Al/^{27}Al ratio (in natural log scale) at the time of isotopic closure vs U-corrected ^{207}Pb-^{206}Pb ages of individual CAIs (Amelin et al., 2010; Bouvier et al., 2011; Connelly et al., 2012), chondrules (Bollard et al., 2019), and achondrites (Sahara 99555 and D’Orbigny angrites, Asuka 881397, EC 002, and ungrouped achondrites NWA 6704 and NWA 2976) for which both systems have been measured in the same samples. For EC 002, the U-corrected Pb-Pb ages from three independent studies (Reger et al., 2023; Connelly et al., 2023; Krestianinov et al., 2023) are plotted both against the reported ^{26}Al/^{27}Al ratio obtained by MC-ICP-MS solution measurements (~8.65×10^{-6} by Connelly et al., 2023 and ~8.89×10^{-6} by Fang et al., 2022 and Reger et al., 2023) and by in situ SIMS (~5.72×10^{-6}) measurements, respectively. NC- and CC-type achondrites are shown in red and blue, respectively, except for the weighted average Pb-Pb age for EC 002, which is indicated in pink. The shaded areas represent the decay of ^{26}Al (slope of −0.967) over time using EC 002 weighted average (pink) or angrite (orange) Pb-Pb ages as anchors, respectively. Modified from Krestianinov E, Amelin Y, Yin Q-Z, Cary P, Huyskens MH, Miller A, Dey S, Hibiya Y, Tang H, Young, ED (2023) Igneous meteorites suggest Aluminium-26 heterogeneity in the early Solar Nebula. *Nature Communications* 14: 4940.

The absolute U-corrected Pb-Pb chronology of chondrules may provide additional temporal constraints independently of the distribution of ^{26}Al. Analytical methods have improved with advances in extensive step-by-step leaching methods to obtain internal Pb-Pb isochrons of individual chondrules. This replaces the previously standard approach of conducting analyses of pooled chondrules with different individual ages (Amelin et al., 2002; Bouvier et al., 2007). The average measured ^{238}U/^{235}U of three individual chondrules from the CV3.6 Allende chondrite is equal to 137.786 ± 0.013, similar to the composition of bulk chondrites (Connelly et al., 2012). Six chondrules from the LL3.10 NWA 5697 chondrite have a ^{238}U/^{235}U ratio that varies from 137.755 ± 0.025 to 137.807 ± 0.033, corresponding to a Pb-Pb age adjustment of −0.33 ± 0.26 to +0.22 ± 0.34 Myr instead to using the average Solar present-day value of 137.786 (Bollard et al., 2019) (Fig. 18). Using the measured or average U isotopic ratios, individual chondrules from LL (NWA 5697), CV (Allende), and CR (NWA 6043 and NWA 7655) chondrites have Pb-Pb ages ranging from 4567.61 ± 0.54 Ma to 4563.24 ± 0.62 Ma, including ~4567.3 Ma ages for two CV and CR chondrules (Connelly et al., 2012; Bollard et al., 2019). Therefore, unlike the Al-Mg systematics, the Pb-Pb ages of individual chondrules indicate that they started to form as early as CAIs when compared against the CAI average age of 4567.30 ± 0.16 Ma from Connelly et al. (2012), and OC and CR chondrules continued to form over an extended period of time (Bollard et al., 2019). Only four of the U-corrected Pb-Pb dated chondrules from NWA 5697 have corresponding in situ Al-Mg systematics (Fig. 18). The ^{26}Al-^{26}Mg ages of these four chondrules are inconsistent with their Pb-Pb ages (Bollard et al., 2019). The mismatch between the Al-Mg and Pb-Pb age differences compared to CAIs is interpreted to be a consequence of a reduced abundance of ^{26}Al (~9–30% relative to the canonical value) in thermally-processed chondrule precursors, similarly to what has been proposed for the angrite parent body (Schiller et al., 2015), that formed within the inner protoplanetary disk (Bollard et al., 2019).

5.1.2. Chronology of planetary differentiation

Magmatic iron meteorites sample the metallic cores of differentiated planetesimals that formed within the NC and CC regions (Section “Iron meteorites”). The ^{182}Hf-^{182}W and ^{107}Pd-^{107}Ag systematics (Table 2) of these parent bodies constrain the chronology of core formation. The Hf-W and Pd-Ag SLR systems comprise parent and daughter elements that behave differently during differentiation. During metal-silicate segregation (i.e., core formation), siderophile W preferentially partitions into the metallic core, leaving lithophile Hf in the silicate mantle (Fig. 10). The highly siderophile Pd and siderophile/chalcophile Ag are fractionated via the separation of S-rich liquid from metal during core segregation, with Ag preferentially partitioning into S-rich phases such as troilite. These elements also fractionate during volatile depletion events because Pd and Ag have significantly different condensation temperatures of ~1324 and ~996 K, respectively. The isotopic compositions of W and Pd are presumed to have remained constant after fractionation, only to be modified in iron meteorites by neutron-capture effects during exposure to cosmic rays (Section “Mass-independent isotope variations”). Thus, after correction of the W and Ag isotopic compositions for neutron capture effects using Os or Pt isotopes, the radiogenic W and Ag isotopic compositions of iron meteorites provide a record of core formation and cooling (e.g., Kruijer et al., 2014b; Hunt et al., 2022; Tornabene et al., 2023). Once corrected, the Hf-W ages of magmatic iron meteorites from the IIAB, IIIAB, IVA, IVB, and IID groups span from ~0.7 to ~2.9 My after CAI formation (e.g., Kruijer et al., 2017). The core formation ages can be further used in thermal modeling using a chondritic source to constrain the ages of parent body accretion and major impact events on their parent bodies. The modeled accretion ages of magmatic iron meteorite parent bodies are 0.2 ± 0.2 Myr and 1.0 ± 0.2 Myr after CAIs in the NC and CC region, respectively (Kleine et al., 2020, and refs. therein) (Fig. 19). These estimates for some iron meteorite parent bodies have been revised based on corrections made on the ^{182}W isotopic compositions due to neutron capture effects, physical parameters used for the parent bodies,

or additional chronological constraints (Neumann et al., 2018; Spitzer et al., 2021a). The Pd-Ag systematics of IIAB, IIIAB, and IVA irons indicate protracted cooling and impact histories until ~8 to 12 Myr after CAIs that may be associated with a later timing of gas dissipation in the Solar nebula (i.e., in comparison to 4 Myr as proposed by Wang et al., 2017) or the early giant planet instability (Hunt et al., 2022) (Fig. 20).

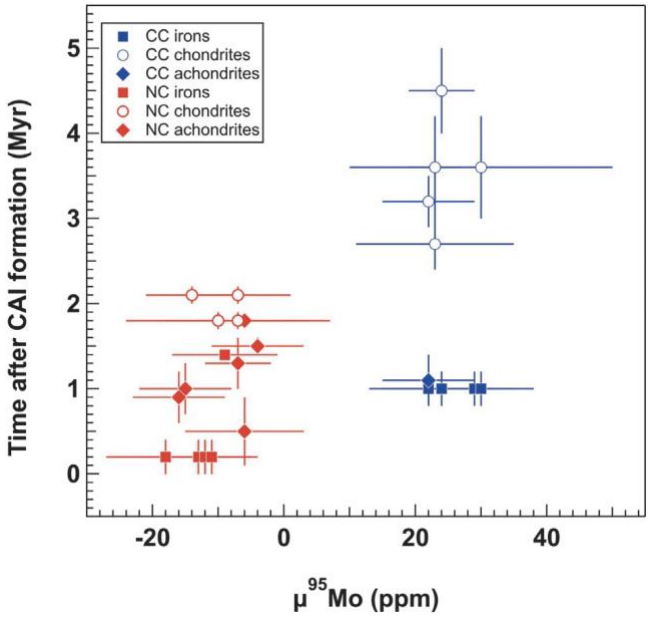

Figure 19: Accretion ages of meteorite parent bodies compared with their genetic ^{95}Mo isotopic anomalies. Figure modified from Kleine T, Budde G, Burkhardt C, Kruijer T, Worsham E, Morbidelli A, Nimmo F (2020) The non-carbonaceous–carbonaceous meteorite dichotomy. *Space Science Reviews* 216: 1–27, using the Tafassasset parent body accretion age from Ma et al. (2020).

The timing of igneous processes is constrained from U-Pb-Pb isotopic studies of achondrites for high-precision absolute LLR timescales, while other systems such as Rb-Sr, Sm-Nd or Lu-Hf provide additional constraints on the formation and long-term evolution of silicate reservoirs. For SLR chronometry, the ^{26}Al-^{26}Mg system is often complemented by ^{182}Hf-^{182}W and ^{53}Mn-^{53}Cr systematics. The parent bodies of most achondrites and irons formed within 10 Myr after CAIs. Only the cumulate eucrites indicate an extended period, up to 50 Myr after CAIs, of plutonic magmatism activity on the HED clan parent body (Bouvier et al., 2015).

One relatively small group of achondrites has received significant attention as a possible anchor for relative ages obtained by several SLR systems (Al-Mg, Mn-Cr, Hf-W). The angrites, particularly the volcanic or "quenched" angrites (e.g., D'Orbigny, Sahara 99555), formed between 4 and 5 Myr after CAIs and cooled rapidly enough after crystallization to provide synchronous records between different chronometers. Quenched angrites also lack evidence of major shock effects, which could potentially have modified their primary chemical and isotopic signatures. Plutonic angrites formed ~7 Myr after the quenched angrites (after ^{26}Al was extinct), and cooled more slowly than the quenched angrites as shown by their coarse-grained textures and slightly younger U-Pb phosphate ages (Amelin et al., 2011). The U-corrected Pb-Pb ages of the quenched (and also plutonic) angrites are concordant with their Hf-W and Mn-Cr systematics (Kruijer et al., 2014a) which supports the idea that ^{182}Hf and ^{53}Mn were homogeneously distributed in the formation regions of CAIs and of the angrite parent body. The initial ^{182}Hf/^{180}Hf$_0$ was constrained at $(1.018 \pm 0.043) \times 10^{-4}$ by an internal isochron of CAIs (Kruijer et al., 2014a) (Table 2). The initial ^{53}Mn/^{55}Mn$_0$ of the Solar System was calculated at $(7 \pm 1) \times 10^{-6}$ using the U-corrected Pb-Pb ages

and SLR systematics of quenched and plutonic angrites and a possible range of CAI ages (Table 2) (Tissot et al., 2017). The initial ^{26}Al abundances for individual quenched angrites vary, however, between studies and correspond to an age adjustment of ~0.3 Myr (Spivak-Birndorf et al., 2009; Schiller et al., 2015). Initial $^{26}Al/^{27}Al_0$ abundances as low as $(1.3 \pm 0.2) \times 10^{-5}$ (~30% of the canonical value) have been suggested for the angrite parent body formation reservoir, similar to the upper value proposed for chondrules (Schiller et al., 2015; Bollard et al., 2019 and refs. therein). These discrepancies raise questions about the significance of the Pb-Pb ages of CAIs, or of the ^{26}Al-^{26}Mg systematics in angrites to be used as anchors for constraining t_0 (Tissot et al., 2017).

Desch et al. (2023) used a statistical approach based on literature SLR and LLR chronometry of CAIs, chondrules, and angrites to constrain the age of the Solar System (t_0) to a value of 4568.4 ± 0.2 Ma. Using a similar approach, Piralla et al. (2023) also proposed an older age of ~4568.7 Ma for Solar System formation. An older t_0 age than the reported ages for CAIs suggests that CAI Pb-Pb ages may have been reset by subsequent thermal events. Alternatively, the U-corrected Pb-Pb ages of angrites could be at least ~0.3 Myr younger due to the higher $^{238}U/^{235}U$ of whole-rock samples (related to phosphates as the main U carrier) used to correct the Pb-Pb ages that are obtained from leached pyroxenes with lighter U isotopic compositions (Tissot et al., 2017).

Ages for igneous activity on planetesimals indicate that ^{26}Al was an important radioactive heat source for the first few million years of Solar System history. By contrast, recent estimates of the initial abundance of ^{60}Fe (Table 2) indicate that it was probably too low in abundance to make a critical contribution to planetary heating (O'Neill et al., 2020). The initial abundance of ^{26}Al is a critical parameter to constrain numerical models of planetary accretion and differentiation. If ^{26}Al was present in lower than canonical values such as $(1.5–2.5) \times 10^{-5}$, it would restrict the period of accretion of differentiated planetesimal to within the first 100,000 yr after CAIs to reach melting temperature and a magma ocean stage. Aluminum-26 may have been heterogeneously distributed within the protoplanetary disk by being modified over time by inward moving ^{26}Al-rich dust of Solar CI composition from the outer to the inner disk. If so, there is no chronological significance of the ^{26}Al difference in abundance between unrelated objects (Bollard et al., 2019).

As alternatives to CAIs and angrites, other possible samples to anchor early Solar System chronology have been sought. Three ungrouped achondrites (GRA 06128; NWA 11119, EC 002) with evolved and alkaline-rich composition (e.g., Srinivasan et al., 2018; Barrat et al., 2021) sample NC asteroids. These samples have formation ages that indicate even earlier crust formation timescales (within 2–3 Myr after CAIs) compared to NC basaltic angrites and eucrites (~3 to 10 Myr after CAIs). Independent studies of the EC 002 ungrouped achondrite have reported the oldest crystallization ages for an achondrite using Al-Mg, Mn-Cr, Sm-Nd (Fig. 14), and U-corrected Pb-Pb ages (e.g., Barrat et al., 2021; Fang et al., 2022). The age estimates, however, vary outside their reported uncertainties for the different radionuclide systems. The two reported ^{53}Mn-^{53}Cr internal isochron studies for EC 002 provide inconsistent relative ages of 1.0 ± 0.9 to 2.1 ± 0.9 Myr after CAIs (Anand et al., 2022; Zhu et al., 2022). The $^{26}Al/^{27}Al$ initial abundances obtained by in situ SIMS and solution analysis MC-ICP-MS correspond to ~2.1 and ~1.8 Myr crystallization ages after CAIs, respectively. The Pb-Pb ages vary from 4565.56 ± 0.12 Ma (including whole-rock and mineral separate leachates and residues, using $^{238}U/^{235}U = 137.829 \pm 0.005$; Krestianinov et al., 2023), to 4565.87 ± 0.30 Ma (pyroxene leachates and residue, using $^{238}U/^{235}U = 137.766 \pm 0.027$; Reger et al., 2023), and 4566.19 ± 0.20 Ma (whole-rock leachates and residue, using $^{238}U/^{235}U = 137.813 \pm 0.010$; Connelly et al., 2023) (Fig. 18). The difference in U-corrected Pb-Pb ages of EC 002 may be explained by the variability in U isotopic compositions measured in unleached and leached whole-rocks and leached pyroxene samples (Reger et al., 2023). The difference in measured $^{238}U/^{235}U$ causes a ~0.66 Myr offset on Pb-Pb age calculations. Additionally, variations in the deconvolution of the three Pb isotopic

components and their corresponding $^{207}Pb^{*}/^{206}Pb^{*}$ isotopic compositions may explain the 0.63 ± 0.23 Myr gap on two reported Pb-Pb ages with similar U isotopic compositions (contributing to a difference of only ~0.17 Myr in the Pb-Pb age correction) (Fig. 14). Different events may be recorded by the Pb-Pb and SLR systems such as Al-Mg or Mn-Cr, which have different closure temperatures to diffusion (Neumann et al., 2023). For instance, the presence of xenolithic minerals may explain some of the age discrepancies observed between leached pyroxene compared to whole-rock Pb-Pb and also Mn-Cr systematics (Anand et al., 2022). Moreover, the assumption that basaltic achondrites cooled rapidly enough to synchronize all the LLR and SLR chronometers and that they evolved without secondary disturbances (i.e., thermal metamorphism, aqueous alteration, impact events) may be incorrect. A protracted cooling history may explain part of the age offsets that are now observed with high-precision chronology. It is, therefore, critical to further investigate the LLR and SLR systematics of EC 002 and other achondrites that crystallized within 5 Myr after CAIs to better constrain the formation age of the Solar System and the initial abundance and spatial distribution of ^{26}Al within the Solar nebula.

5.1.3. Timescales of secondary processes

Water ice accreted by primitive asteroids in association with the heat generated by the accretion process and by ^{26}Al decay caused aqueous alteration and/or fluid-assisted metamorphism (e.g., Vacher and Fujiya, 2022). Aqueous alteration is recorded to various degrees in all major chondrite groups, except for the enstatite chondrites. Parent body-based alteration produced secondary minerals that include hydrous phyllosilicates (principally serpentines and smectite clays), carbonates, sulfates, oxides (magnetite), fayalite, and secondary sulfides. Their O isotopic compositions can be used as a paleothermometer to constrain the temperatures of aqueous alteration (Section "Mass-dependent fractionation of oxygen isotopes in planetary materials"). Aqueous alteration took place at <373 K between 1.8 and 6.8 Myr after CAIs on Ryugu's parent body (Yokoyama et al., 2022; McCain et al., 2023), similar to what has been found for carbonaceous chondrites (particularly CI). Substantial uncertainties on reported Mn-Cr dates result from the lack of appropriate matrix-matched standards for in situ SIMS measurements of dolomite to determine the Mn/Cr ratios accurately.

Thermal metamorphism on chondrite parent bodies is associated with temperatures between 700 and 1300 K. Secondary minerals such as Ca-phosphates and feldspar formed during this process. Since the U-Pb closure temperature in phosphate is relatively lower than in other minerals (Table 1), the Pb-Pb ages of phosphates can be younger than those of pyroxene in slowly-cooled metamorphosed (types 4–6) chondrites and achondrites (e.g., Bouvier et al., 2007; Reger et al., 2023). Complemen- tary to other chronometers, the U-Pb ages of Ca-phosphates found in chondrites and achondrites provide constraints on the post-crystallization and long-term (10–100 Myr) cooling histories of their parent bodies (Trieloff et al., 2003; Neumann et al., 2023). For example, the Ca-phosphate Pb-Pb ages in types 4–6 H ordinary chondrites indicate a rapid formation period, which suggests that the H chondrite parent body formed within 2–3 Myr after CAIs (Trieloff et al., 2003), and cooled faster than LL and L ordinary chondrite parent bodies due to its smaller size (Bouvier et al., 2007).This information can, in turn, be used to model accretion ages and planetesimal sizes. In shocked meteorites, the Ar-Ar ages and U-Pb ages in Ca-phosphates are often used together to depict the impact history of planetary samples (Walton et al., 2023).

5.2. What Solar System events are preserved in the NC-CC dichotomy?

The Solar System events recorded by the NC-CC isotopic dichotomy remain puzzling. Due to the ubiquity of meteorite samples being either NC or CC, the dichotomy is considered to be the expression of a fundamental and widespread process that was active in the early Solar System. Warren (2011) conjectured that the bimodality may be an extreme manifestation of the effects of episodic (i.e., temporal) accretion of

early solids in the disk. Alternatively, the compositional differences between NC and CC could reflect an accretion location (i.e., spatial) difference. Some of the CC considered by Warren (2011) are hydrous (CI, CM), yet several others are anhydrous (e.g., CK, CO, CV). Nevertheless, because both anhydrous and hydrous carbonaceous chondrites parent bodies share similar CC genetics, that study speculated it was likely all carbonaceous chondrites originally accreted in the outer Solar System, perhaps beyond Jupiter.

The interpretation that NC meteorites originate from the inner Solar System (sunward relative to Jupiter) and CC bodies accreted in the outer Solar System is now a commonly held assumption in many models that attempt to explain the origin of the NC-CC dichotomy and early disk evolution. It is also an increasingly common practice to use the genetic signature of a parent body to "cosmolocate" its accretion location in the disk, where the inner Solar System is the putative NC region and the outer Solar System is the CC region.

Distinguishing between a temporal and/or spatial origin for the NC-CC dichotomy requires constraints on parent body genetics and the timescales of parent body accretion (e.g., Desch et al., 2018; Kruijer et al., 2017; Sugiura and Fujiya, 2014). Towards this goal, Kruijer et al. (2017) combined nucleosynthetic Mo isotope anomalies with Hf-W metal segregation ages of iron meteorites to report that the NC group formed <0.4 Ma after CAI formation and the CC group formed ~0.9 Ma after CAI formation. Using this age difference, that study inferred an early formation age of Jupiter, which separated the inner and outer Solar System for several million years. Subsequently, Hilton et al. (2019) reported that the Hf-W-derived accretion ages of previously unanalyzed CC iron parent bodies were not resolved from the accretion ages of NC parent bodies, thereby removing the generalized constraint that NC and CC parent bodies had distinct ages. In a review, Kleine et al. (2020) summarized published data to conclude that there is an age overlap between NC and CC parent bodies but that chondrite parent bodies accreted after iron meteorite parent bodies, starting at ~1.8 Myr after CAIs in the NC region, and continued to accrete until at least ~4 Myr after CAI formation in the CC reservoir (Fig. 19). Although a strict age distinction between NC and CC parent bodies is no longer present in the currently available dataset, it is still a common interpretation that Jupiter (Warren, 2011; Kruijer et al., 2017) or a different physical barrier such as a pressure bump (Brasser and Mojzsis, 2020) or an early-formed snow line (Lichtenberg et al., 2021) developed within 1 Myr in the disk and segregated the two regions.

Studies have since investigated several different ways by which the NC and CC regions developed different isotopic composi- tions. Using Mo isotopic compositions of meteorites and meteorite components, Budde et al. (2016), Kruijer et al. (2017), Poole et al. (2017), and Worsham et al. (2017) proposed that the isotopic difference between NC and CC bodies was caused by the addition of *r*- and/or *p*-process material to the CC region. Stephan and Davis (2021) presented a detailed study of published Mo isotope data from meteorites that were renormalized in a manner which allows for a meaningful comparison between *s*-, *r*-, and *p*-process contributions observed in the Mo isotopic composition of presolar SiC grains. The Mo isotopic variations in meteorites and their components were found to be mainly controlled by *s*-process enrichments or depletions relative to a terrestrial composition. Ek et al. (2020) and Frossard et al. (2021) proposed models to explain isotopic variations of volatile and refractory elements over time in which ISM grains in the NC region were preferentially destroyed by thermal gradients that produced a relative enrichment of *s*-process-enriched presolar SiC grains.

By using meteoritic data to constrain numerical models of disk processes, Desch et al. (2018) recognized the role CAIs play in defining the bulk NC or CC composition of a meteorite parent body. The study proposed that the early (<1 Ma) formation of Jupiter opened a gap and created a pressure maximum in which CAIs were trapped and carbonaceous chondrites formed. Subsequently, CAIs were depleted from the inner Solar System by aerodynamic drag which resulted in the isotopic difference between NC and CC parent bodies. Alexander (2019a,b) used a sample-based approach to demonstrate that different mixtures

of four meteorite components can reproduce most bulk elemental and isotopic compositions of CC meteorites. These four components include a 'chondrule' (or chondrule precursor) component, the CC-RI component that has a refractory inclusion-like bulk composition, anhydrous and reduced but otherwise CI-like matrix, and water with comparatively high $\Delta^{17}O$ and $\delta^{18}O$ values. Building on these studies by adding new nucleosynthetic isotope data, Burkhardt et al. (2019) concluded that mixing compositions similar to CAIs into an NC-like composition could generate the chemical and isotopic composition of the CC reservoir.

To constrain the redox conditions of the NC-CC regions, Rubin (2018) reported that the differences in chemical and physical properties between NC and CC meteorites indicate the high concentration of Ni and refractory siderophile elements in CC irons could be a byproduct of the high oxidation state of the carbonaceous precursors. Hilton et al. (2022) came to a similar conclusion regarding the oxidation state of CC irons by using the absolute abundances of highly siderophile elements (HSE) projected for parent body cores. The projected HSE absolute abundances are variable and generally higher in CC bodies compared to NC bodies. That study concluded that these chemical fingerprints may indicate the CC parent bodies formed under conditions which were overall more oxidizing than those of the NC environment. Broadly, the CC-type chondrites contain higher abundances of oxidized Fe and hydrous minerals compared to NC-type chondrites (Urey and Craig, 1953; Wood, 2005; Yoshizaki et al., 2021; Hilton et al., 2022) (Figs. 12 and 13), which supports the interpretation that the CC reservoir was located outboard of the NC reservoir. The relative position of these locations to Jupiter, however, remains unconstrained by these studies.

Numerical models of astrophysical disk processes have begun to be used to identify the origins of variations in the meteorite data. Several variants of an "infall" model have been proposed. These models are based on the idea that the isotopic difference between NC and CC is caused by a change in the composition of infalling material from the molecular cloud into the disk in a manner that modified the inner and outer disk compositions differently (e.g., Burkhardt et al., 2019; Nanne et al., 2019; Spitzer et al., 2020; Kleine et al., 2020). The feasibility of infall models depends on the likelihood of a change in the isotopic composition of infalling material to specific locations in the protoplanetary disk during specific times of parent body accretion.

Numerical models of astrophysical disk processes have also provided alternatives to the central role of Jupiter in constructing the NC and CC reservoirs. Brasser and Mojzsis (2020) used dynamical simulations to show that the growth of Jupiter via pebble accretion was not fast enough to cause the NC-CC region separation. As an alternative, a pressure maximum in the disk near Jupiter's location was proposed to have created a ringed structure similar to those detected by the telescope ALMA (e.g., protoplanetary disks around Elias 27, IM Lup, and WaOph 6, Huang et al., 2018; Herbig Ae star HD 163296, Isella et al., 2016; HD 169142 Fedele et al., 2017; Herbig Ae star MWC 480, Liu et al., 2019). This type of pressure maximum is predicted to have almost completely prevented pebbles from the Jovian region from reaching the terrestrial zone, thus restricting communication between the NC and CC regions. Lichtenberg et al. (2021) used numerical models to investigate how the evolution of the disk influenced the timing of protoplanet formation. It was found that migration of the water snow line could generate two distinct bursts of planetesimal formation which sample different source regions, presumptively the NC and CC regions. Applying astronomical observations of ring- and gap-like structures in their dust distributions to the origin of NC-CC regions, Izidoro et al. (2021) found that these structures are associated with pressure bumps trapping dust particles at specific locations which can lead to planetesimal formation. Assuming the existence of pressure bumps near the silicate sublimation line (at T ~ 1400 K), water snow line (at T ~ 170 K) and CO snow line (at T ~ 30 K), the authors' numerical simulations demonstrated that dust piles up at the bumps lead to the formation of up to three rings of planetesimals (near 1 au, between ~3–4 and ~10–20 au, and a ring between ~20 and ~45 au). Their simulations show that the evolution of the innermost ring

can describe the orbital structure of the inner Solar System as well as cause the different isotopic signatures of Earth, Mars, and different meteorites. These models remove the central role of Jupiter in the development of the NC-CC regions. As direct evidence of the cause of the NC-CC isotopic dichotomy is yet to be identified, however, its origin remains debated.

5.3. The applicability of the NC-CC isotopic dichotomy to tracing Earth's accretion

Despite the debate about what Solar System history is preserved by the NC-CC isotopic dichotomy, numerous studies use the dichotomy to constrain the origin and composition of Earth's building blocks. This is done by attempting to match the genetic composition of Earth to a mixture of meteorite groups that have been classified as NC or CC. Based on a coincidence in genetic composition and the geochemical (siderophile/lithophile/atmophile) and cosmochemical (refractory/volatile) nature of a given element, an inference can be drawn about the NC or CC nature of Earth's building blocks at different stages of accretion as well as the relative timing of volatile element accretion. This approach relies on several assumptions.

First, the genetic and volatile element composition of a meteorite reflects that of its parent body's bulk composition. Due to the limited amount of material available for analysis, the genetic composition of a meteorite sample, which is inferred to be that of its parent body, is often defined by less than a few grams of material. At this scale, over- or under-sampling of chondritic components can lead to an apparent genetic variability in meteorites from a common parent body (e.g., Ca, Valdes et al., 2021; Mo, Budde et al., 2016). Parent body alteration can also mobilize presolar components and modify the genetic composition on a small sampling scale (e.g., Os, Yokoyama et al., 2011). Although these issues should be monitored for, consistency is generally observed in the genetic composition of samples from a common parent body based on large data compilations (e.g., Burkhardt et al., 2019; Warren, 2011). By contrast, very small amounts of material (a few to a few tens of milligrams) are needed for volatile element (H, C, N, noble gases) analyses. At this sampling scale, substantial variability in the volatile content and isotopic composition is observed for any given chondrite group (Broadley et al., 2022; Pearson et al., 2006; Vacher et al., 2020) and for samples returned from one single asteroid (e.g., Ryugu; Okazaki et al., 2022). This demonstrates that aqueous alteration and/or thermal metamorphism can strongly affect the volatile element distribution at the small sampling scale used to constrain the composition of a given parent body, and presents a challenge to defining the volatile element and isotopic composition of a parent body.

Second, the genetic and volatile element composition of a parent body reflects the composition of the disk from which it accreted. The genetic composition of a parent body is assumed to reflect the composition of the disk feeding zones from which it was made. Exposure of the parent body (or its meteors) to cosmic rays can modify the genetic composition if the isotopes have large neutron cross sections. In genetic studies, however, these shifts are monitored and corrected using neutron dosimeters (e.g., Sm, Gd, Os, Pt; see Section "Mass-independent isotope variations"). Almost all parent bodies can be classified as either NC or CC, thus there is little evidence in the meteorite collection for collisional mixing between NC and CC bodies, despite this being a common physical process in the early Solar System. Only one ungrouped iron meteorite (Nedagolla) has been reported to have an isotopic composition that does not fall within either the NC or CC group consistently for all of its nucleosynthetic isotopic compositions (Spitzer et al., 2021a,b). This composition has been interpreted as the first isotopic evidence for early collisional mixing of NC and CC bodies as a result of Jupiter's growth. Additionally, some Allende (CV) and Karoonda (CK) chondrules also appear to plot in between the NC and CC fields in μ^{54}Cr vs μ^{50}Ti space, interpreted to result from outward transport of inner Solar System materials (Williams et al., 2020). The presence of CC-type xenoliths in NC meteorite breccias (including enstatite and ordinary chondrites, HEDs, and polymict ureilites) provides a textural evidence of mixing of the two reservoirs during a major perturbation of the asteroid belt caused by the giant planet orbital instability within 100 Myr (Goodrich et al., 2021).

Regardless of the evidence of some early mixing between NC and CC reservoirs, the assumption that the genetic composition of a parent body reflects the composition of the disk from which it accreted is supported by most published data.

It is unclear how the distribution of volatiles in the feeding zone of planetesimals developed as the physicochemical conditions in the disk evolved during the first few million years of Solar System history. The stability of water ice, organics, and reduced phases (nitrides, carbides, graphite), as well as the efficiency of their accretion on planetary bodies, was mainly governed by temperature and redox conditions in the protoplanetary disk (Bermingham et al., 2020; Broadley et al., 2022). The evolving temperature structure of the disk led to the migration of the snow line and other condensation fronts, which not only affected the distribution of ice and icy dust grains but likely also controlled the accretion of planetesimals at specific locations and times in the disk (Izidoro et al., 2021). Nevertheless, it is presumed that NC planetesimals formed under relatively hot and reducing conditions, where water existed in the disk predominantly in vapor form. Conversely, CC planetesimals accreted under relatively colder and more oxidizing conditions in the outer regions of the disk, where water was present in the form of ice or icy dust grains.

Third, NC bodies accreted in the inner Solar System and are relatively depleted in volatile elements compared to CC bodies which accreted in the outer Solar System. Despite this commonly held assumption, the abundance of the major volatiles H, C, and N cannot directly be linked to the NC-CC signature of planetary building blocks. This is because these volatiles are predominantly carried by phases distinct from presolar grains, such as fluid-derived phyllosilicates, soluble and insoluble organic matter, nitrides, carbides, and graphite. Whereas matrix-poor NC bodies (i.e., ordinary and enstatite chondrites) are indeed depleted in H, C, and N compared to matrix-rich CC bodies (i.e., CI and CM carbonaceous chondrites), some carbonaceous chondrite groups (e.g., CV and CK) are also volatile-poor (Bermingham et al., 2020; Broadley et al., 2022; Vacher et al., 2020). Piani et al. (2020) demonstrated that enstatite chondrites contain significant quantities of H which may have provided most of Earth's water during accretion. Noble gases are, in part, hosted by various presolar grains (i.e., so-called *planetary* noble gas components in chondrites) but the light noble gas (He, Ne) budget of chondritic dust grains is dominated by the Solar-wind derived component, implanted at the grain surface during irradiation (Okazaki et al., 2022). Depending on the irradiation conditions in the protoplanetary disk (e.g., Solar wind flux, disk opacity, turbulence), dust grains from both the NC- and CC-reservoirs (akin to those collected on the silicaceous and carbonaceous chondrites Itokawa and Ryugu, respectively; Nagao et al., 2011; Okazaki et al., 2022) may have contained considerable amounts of Solar He, Ne, and Ar. Consequently, Earth could have accreted Solar He and Ne from irradiated chondritic dust after the dispersion of nebular gas (Péron et al., 2018). Although using the genetic composition of a meteorite to trace the origin of volatiles on Earth requires a demonstrated link between the genetic composition of a parent body and its volatile element composition, this link is yet to be robustly established.

Fourth, the genetic composition of Earth can be related to different stages of its accretion history. Earth likely formed from the accretion of building blocks sourced from different heliocentric distances (e.g., Kokubo and Ida, 1998), but their proportions remain debated (e.g., Schiller et al., 2018; Dauphas et al., 2024). The processes of accretion, melting, differentiation, and plate tectonics homog- enized most of the genetic signatures of Earth's individual building blocks. Earth, the Moon, and enstatite meteorites have almost indistinguishable isotopic compositions for many elements (e.g., O, Ca, Nd, Ti, Sr, Cr, Zr). Dauphas (2017), however, demonstrated that lithophile and siderophile elements can be used to constrain the isotopic nature of Earth's accreting material through time. The lithophile element composition of the BSE reflects the accumulated genetic composition of Earth's major building blocks, and points to material that was isotopically most similar to NC enstatite meteorites (Dauphas, 2017). The moderately siderophile Mo and

highly siderophile Ru present in the BSE, however, were likely added during two different stages of Earth's accretion. The dominant portion of Mo in the BSE was established during the final 10–20% of Earth's accretion, possibly coincident with closing stages of core segregation (Dauphas et al., 2004) (Fig. 2f). On the other hand, the Ru budget of the BSE was predominantly set during the final 0.5–2 wt% of Earth's accretion (i.e., late accretion) (Chou, 1978; Walker, 2009; Dauphas, 2017; Kimura et al., 1974) (Fig. 2g). Thus, the Mo and Ru isotopic compositions of the BSE provide complementary genetic information of participating building blocks during Earth's final stages of accretion. In addition, both Mo and Ru are commonly used as genetic tracers that discriminate between NC and CC origins (e.g., Bermingham et al., 2018a; Budde et al., 2016; Fischer-Gödde et al., 2015; Poole et al., 2017; Worsham et al., 2017).

The proportion of NC and CC material accreted by Earth remains debated. The NC-CC nature of Earth's final major building blocks has been investigated by examining the relationship between the Mo and Ru isotopic compositions of meteorites and the BSE composition. The nucleosynthetic isotope compositions correlate in what is known as the "cosmic Mo-Ru isotope correlation" (Dauphas et al., 2004). The correlation indicates that Mo and Ru isotopic anomalies in meteorites are caused by the uneven distribution of the same type of presolar carriers (likely *s*-process enriched carriers). Using BSE Mo and Ru isotopic compositions derived from laboratory standards, Dauphas et al. (2004) found that this composition fell on the cosmic Mo-Ru isotope correlation at a position that is now recognized as having NC genetics (Bermingham et al., 2018a,b). Dauphas et al. (2004) inferred the Earth's feeding zone(s) did not substantially change during the latter stages of Earth's accretion (from the Moon-forming event to late accretion), because if there was a change, the BSE estimate would not fall on the cosmic Mo-Ru isotope correlation. Based on a global suite of terrestrial samples, the Ru isotopic composition of the modern BSE was estimated to be most similar to that of NC parent bodies (Bermingham and Walker, 2017). Some Eoarchean rocks, however, have since been reported to possess enrichments in m^{100}Ru relative to estimates for the modern BSE, a composition that is not found in bulk meteorites (Fischer-Gödde et al., 2020). Fischer-Gödde et al. (2020) concluded that during late accretion, Ru was added by CC-dominated volatile-rich material from the outer Solar System which lowered the Ru isotopic composition of the mantle to the modern BSE estimate. By contrast, the μ^{97}Mo composition of the modern BSE was found to be most similar to NC meteorites (Bermingham et al., 2018a), implying that the final 10–20 wt% of Earth's accretion (including materials added by the final 0.5–2 wt% of late accretion) was dominated by NC materials, similar to findings by Dauphas et al. (2004). Subsequently, the μ^{94}Mo- μ^{95}Mo composition of the BSE was reported to be a mix of NC and CC materials, such that Earth accreted 46 ± 15% of CC material during the final 10–20 wt% of its formation (Budde et al., 2019). That study concluded Earth accreted carbonaceous bodies late in its growth history, probably through the Moon-forming impact.

The isotopic composition of H and N in the terrestrial mantle appears consistent with an NC (i.e., enstatite chondrite-like) source, without a contribution of CC-type material (Piani et al., 2020). A late addition of CI-like material is, however, required to explain the H and N isotope ratios in Earth's surficial reservoirs (atmosphere and oceans). The relative timing of this addition cannot yet be tied to the constraints from siderophile elements, but it must have occurred sufficiently late during Earth's formation to prevent homogenization between the mantle and surface.

Fifth, the volatile isotopic composition in Earth's primitive (i.e., relatively undegassed) mantle reflects the composition of the volatiles that were present in the accreted material, and a coincidence in composition with known chondrite groups allows tracing the origin of terrestrial volatiles. When cosmochemical endmembers are compared to trace the origin of Earth's volatiles, potential isotopic fractionation effects caused by planetary accretion and growth are rarely considered. Moreover, the importance of differentiated planetesimals, with volatile cargos differing from those of chondrites, providing material to Earth remains debated (Hirschmann et al., 2021). Secondary ion mass spectrometric

analyses have revealed that enstatite achondrites (i.e., aubrites) are significantly H-depleted compared to chondrites as a result of extensive water loss during parent body heating and melting (Peterson et al., 2023). Impact-induced devolatilization during accretion may have also led to water loss (Tyburczy et al., 1990). These processes likely modified the H isotopic composition of any accreted water, and preferential incorporation of light H into the core during differentiation further affected the D/H ratio of Earth's mantle (Wu et al., 2018). In the case of N, experimental studies have revealed that, depending on the redox conditions and N speciation, magma ocean degassing could have resulted in significant (kinetic) isotopic fractionation between vapor and silicate melt (Dalou et al., 2022). The magnitude and direction of N isotopic fractionation during core-mantle differentiation remains debated. Grewal et al. (2022) argued that the N isotopic composition of Earth's silicate mantle reflects that of the accreted material based on the observation of limited N isotopic fractionation between silicate and alloy melts. Further research is required to assess whether the isotopic similarity between major volatiles in Earth's present-day mantle and enstatite chondrites directly reflects the source region of volatiles in the protoplanetary disk, or if planetary processes overprinted the initial isotopic composition of terrestrial volatiles.

The isotopic anomalies of meteorites provide genetic links that can be used to establish the nature of the Earth's building blocks at different stages of its accretion (e.g., Dauphas, 2017). It is, however, not a simple task to deduce the composition of the Earth and other terrestrial planets and the origin of volatiles by using genetics. The accessible part of the Earth's mantle appears to be depleted in Si (the most abundant element after O) compared to all known chondrite groups. This disconnect highlights the difficulty in building Earth from the known collection of meteorite samples. Moreover, planetary heating and collisional effects may have significantly modified the budget of volatile elements and the stable isotopic signatures for both volatile (e.g., H, Zn, K, Se; Sossi et al., 2018) and refractory elements (e.g., Si, Mg; Hin et al., 2017). Collisional effects may be responsible for a change in Sm/Nd ofthe bulk Earth and differentiated planetesimals which can explain ^{142}Nd excesses in the Earth's mantle and achondrites relative to chondrites (Frossard et al., 2022). Consequently, the budget in refractory elements within Earth's silicate layers would be modified. These issues combined are likely a significant part of the reason why no model is yet to entirely satisfy the elemental budgets and the NC and CC genetic history of Earth's building blocks. Earth is an end-member of the NC group. Earth shows a much stronger depletion of moderately to highly volatile elements compared to chondrites. The available collection of extraterrestrial samples is missing representants from the most inner part of the Solar System which are required to reconcile Earth's formation models based on elemental and isotopic compositions. New meteorite discoveries and future planetary missions, combined with observations and experimental constraints, will hold important answers to these unresolved questions in cosmochemistry.

6. SUMMARY AND OUTLOOK

Meteorites are classified into different groups based on their mineralogy, chemical composition, and distinct mass-independent O isotopic compositions. In addition to these defining characteristics, nucleosynthetic isotope anomalies are present in bulk meteorites and their components. These isotopic anomalies have been identified for many elements which are composed of isotopes synthesized in different nucleosynthetic events and possess different chemical characteristics. This suggests that a range of presolar grains and physical processes were involved in planetary formation over the lifetime of the Solar nebula. In addition to the distinct genetic signatures of a meteorite being used to establish relations between different parent bodies, nearly all planetary materials belong to two main reservoirs, CC and NC, which are separated by a gap in isotopic composition. The NC-CC isotopic dichotomy reflects a fundamental process that resulted in the isolation of two different planetary formation reservoirs. How the dichotomy developed, however, remains under investigation.

The earliest solids formed in the Solar System were the refractory inclusions, which are found in chondrites. The formation of normal CAIs (with a canonical ^{26}Al initial abundance) is dated between 4567 and 4568 Ma by U-corrected Pb-Pb chronology and from relative ^{26}Al abundances anchored against various NC and CC achondrites of known crystallization U-Pb ages. The range of absolute ages of normal CAIs is much larger than their corresponding Al-Mg relative ages, suggesting a possible disturbance in the U-Pb systematics of CAIs that may be associated with high temperature resetting events or other aqueous and thermal processes on chondrite parent bodies. Age dates obtained from the ^{26}Al-^{26}Mg system appear to be inconsistent with other SLR and U-corrected Pb-Pb age dates of CAIs, chondrules, and achondrites. The initial abundance and distribution of ^{26}Al among planetary formation reservoirs within the protoplanetary disk has to be established for the Al-Mg system to be used as a high-resolution chronometer and for thermal modeling of planetary differentiation as ^{26}Al was the main radioactive heat source for the first five million years of planetary formation.

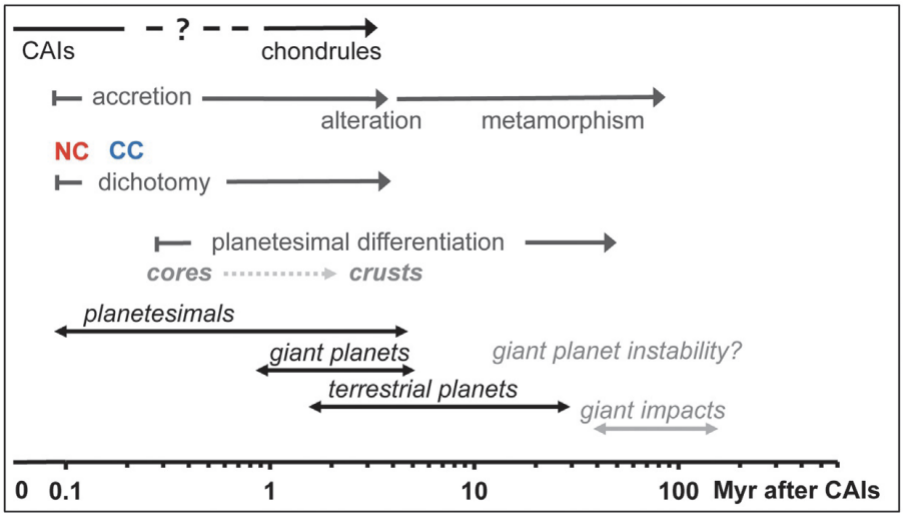

Figure 20: Chronology of early Solar System events in a nutshell, highlighting key planetary formation processes starting 4.57 Gyr ago. The ^{26}Al-^{26}Mg chronology of CAIs indicates rapid condensation and melting of the inclusions within 100 kyr, and chondrule formation events from ~1.5 to 4 Myr after CAIs. The significance of intermediate Pb-Pb absolute ages of four individual chondrules is questioned (see Fig. 18). Timescales of planetary differentiation from core to crust formation are based on the radiometric ages of iron and achondrite meteorites. Accretion ages of NC and CC meteorite parent bodies (from Fig. 19) provide constraints on the formation and duration of the dichotomy until CC asteroids were implanted into the inner Solar System to form the asteroid belt. The formation of the asteroid belt has been suggested to be related to the giant planet instability, whose timing is still debated but may have occurred between the first few Myr to 100 Myr after CAIs. The periods of formation of planetesimals, giant planets, and terrestrial planets as well as of giant impacts and late accretion are also shown. See text for further information.

The thermo-chronological records of meteorites and their components, from their formation to secondary events, can be used to better interpret the significance of age dates and constrain the formation history of meteorite parent bodies. For example, the ^{182}Hf-^{182}W systematics of meteorites reveal early metal-silicate segregation ages, which can be used to model accretion times of planetesimals. Iron meteorite parent bodies formed within 0.2 ± 0.2 Myr after CAIs in the NC region to 1.0 ± 0.2 Myr after CAIs in the CC region. Detailed chronological records of achondrite and primitive achondrite meteorite parent bodies point to early to slightly later modeled ages of 0.1–1.5 Myr after CAIs (e.g., Budde et al., 2015; Ma et al., 2022; Neumann et al., 2023). These planetesimals formed before chondrules (i.e., and chondrite parent bodies) that have reported individual Al-Mg ages between 1.6 and 4 Myr after CAIs (Fig. 20). Rare chondrules

have been dated as early as 0.7 Myr after CAIs. Late chondrule formation in the CR (up to 4 Myr after CAIs), CH, and CB regions (up to 5 Myr after CAIs) may be associated with large impact events. The younger chondrule ages provide minimum accretion ages for the respective chondrite parent bodies, which formed either contemporarily or later than achondrite planetesimals. Chondrite parent bodies formed when ^{26}Al was almost extinct, contributing to minimal thermal heating to preserve their primary compositional and textural characteristics. Aqueous alteration in CI parent bodies and Ryugu started contemporaneously to accretion from ~1 and lasted until 5 Myr after CAIs, as indicated by Mn-Cr systematics of secondary minerals. Basaltic magmatism extended to 12 Myr after CAIs on the angrite parent body to 50 Myr after CAIs on the HED parent body. Late crystallization ages together with slower cooling rates for cumulate meteorites suggest that angrites and eucrites originate from planetesimals with radii >100 km in order to sustain protracted periods of internal heating and magmatism. Some of these magmatic events may also be related to large planetary impacts and re-melting of planetary crusts.

Significant questions remain about where the NC and CC regions were located in the disk, and if they can be linked to regions without or with water ice, respectively. What effect did the three-dimensional movement of condensation fronts in the disk have on the distribution of volatiles in the feeding zones for the terrestrial planets? To what extent can the NC and CC genetics be used to trace the source of terrestrial volatiles? What planetary materials are missing from the existing meteorite collection, but are critical to successfully tracing the source(s) of terrestrial building blocks and volatiles? In part, these questions will persist until the interplay between chemical and physical processes in the protoplanetary disk is further understood. As a new era of space exploration begins, unprecedented observations made by ALMA and the James Webb Space Telescope will provide revolutionary new insights into the formation of solar systems and exoplanets. On-going and planned sample-return missions and meteorite recovery programs will also provide a new and much-needed diversity of cosmochemical materials, which planetary scientists can study to answer some of the most profound questions about our origins.

Acknowledgments

The authors thank Hope A. Tornabene, Ran Zhao, Philip Reger, and Jan Leitner for their help with developing the figures and fruitful discussions. Laurence Garvie is thanked for providing the photograph of the Allende slab. We also thank the Editor Sujoy Mukhopadhyay for his invitation and support, as well as the time of one anonymous reviewer who provided detailed comments and suggestions. A.B. acknowledges support from UBT and BGI. K.R.B. acknowledges support from NSF award 2220922 and NASA award 80NSSC20K0997. Co-funded by the European Union (ERC, IRONIS, 101087562, awarded to E.F.). Views and opinions expressed are however those of the author(s) only and do not necessarily reflect those of the European Union or the European Research Council. Neither the European Union nor the granting authority can be held responsible for them.

REFERENCES

Adachi I, Hayashi C, and Nakazawa K (1976) The gas drag effect on the elliptic motion of a solid body in the primordial solar nebula. *Progress of Theoretical Physics* 56: 1756–1771.

Albarède F, Albalat E, and Télouk P (2015) Instrumental isotope fractionation in multi-collector icp-ms. *Journal of Analytical Atomic Spectrometry* 30: 1736–1742.

Alexander CMO (2019a) Quantitative models for the elemental and isotopic fractionations in chondrites: The carbonaceous chondrites. *Geochimica et Cosmochimica Acta* 254: 277–309.

Alexander CMO (2019b) Quantitative models for the elemental and isotopic fractionations in the chondrites: The non-carbonaceous chondrites. *Geochimica et Cosmochimica Acta* 254: 246–276.

Alexander CMD (2022) An exploration of whether Earth can be built from chondritic components, not bulk chondrites. *Geochimica et Cosmochimica Acta* 318: 428–451.

Ali A, Jabeen I, Nasir SJ, and Banerjee NR (2018) Oxygen isotope thermometry of DaG 476 and SaU 008 Martian meteorites: implications for their origin. *Geosciences* 8: 15.

Amelin Y (2006) The prospect of high-precision Pb isotopic dating of meteorites. *Meteoritics and Planetary Science* 41: 7–17.

Amelin Y, Krot AN, Hutcheon ID, and Ulyanov AA (2002) Lead isotopic ages of chondrules and calcium-aluminum–rich inclusions. *Science* 297: 1678–1683.

Amelin Y (2008) U-Pb ages of angrites. *Geochimica et Cosmochimica Acta* 72: 221–232.

Amelin Y, Kaltenbach A, Iizuka T, Stirling CH, Ireland TR, Petaev M, and Jacobsen SB (2010) U-Pb chronology of the Solar System's oldest solids with variable $^{238}U/^{235}U$. *Earth and Planetary Science Letters* 300: 343–350.

Amelin Y, Kaltenbach A, and Stirling CH (2011) The U-Pb systematics and cooling rate of plutonic angrite NWA 4590. In: *Lunar Planet. Sc. Conf. XLII, A#1682*.

Anand A, Kruttasch PM, and Mezger K (2022) ^{53}Mn-^{53}Cr chronology and $\varepsilon^{54}Cr$-$\Delta^{17}O$ genealogy of Erg Chech 002: The oldest andesite in the solar system. *Meteoritics & Planetary Science* 57: 2003–2016.

Anders E and Grevesse N (1989) Abundances of the elements: Meteoritic and solar. *Geochimica et Cosmochimica Acta* 53: 197–214.

Barrat J-A, Jambon A, Yamaguchi A, Bischoff A, Rouget M-L, and Liorzou C (2016) Partial melting of a C-rich asteroid: Lithophile trace elements in ureilites. *Geochimica et Cosmochimica Acta* 194: 163–178.

Barrat J-A, Chaussidon M, Yamaguchi A, Beck P, Villeneuve J, Byrne DJ, Broadley MW, and Marty B (2021) A 4,565-My-old andesite from an extinct chondritic protoplanet. *Proceedings of the National Academy of Sciences of the United States of America* 118: e2026129118.

Beckett J and Grossman L (1986) Oxygen fugacities in the solar nebula during crystallization of fassaite in Allende inclusions. *Lunar and Planetary Science* XVII: 36–37.

Benedix GK, McCoy TJ, Keil K, Bogard DD, and Garrison DH (1998) A petrologic and isotopic study of winonaites: Evidence for early partial melting, brecciation, and metamorphism. *Geochimica et Cosmochimica Acta* 62: 2535–2553.

Benedix GK, McCoy TJ, Keil K, and Love SG (2000) A petrologic study of the IAB iron meteorites: Constraints on the formation of the IAB-Winonaite parent body. *Meteoritics and Planetary Science* 35: 1127–1141

Benedix GK, Lauretta DS, and McCoy TJ (2005) Thermodynamic constraints on the formation conditions of winonaites and silicate-bearing IAB irons. *Geochimica et Cosmochimica Acta* 69: 5123–5131.

Benedix GK, Haack H, and McCoy TJ (2014) 1.7—Iron and stony-iron meteorites. In: Holland HD and Turekian KK (eds.) *Treatise on Geochemistry*, 2nd edn., pp. 267–285. Oxford: Elsevier.

Bennett N, Sio C, Schauble E, Lesher C, Wimpenny J, and Shahar A (2022) Iron isotope evidence of an impact origin for main-group pallasites. *Geochemical Perspectives Letters* 23: 6–10.

Bermingham KR and Walker RJ (2017) The ruthenium isotopic composition of the oceanic mantle. *Earth and Planetary Science Letters* 474: 466–473.

Bermingham KR, Worsham EA, and Walker RJ (2018a) New insights into Mo and Ru isotope variation in the nebula and terrestrial planet accretionary genetics. *Earth and Planetary Science Letters* 487: 221–229.

Bermingham KR, Gussone N, Mezger K, and Krause J (2018b) Origins of mass-dependent and mass-independent Ca isotope variations in meteoritic components and meteorites. *Geochimica et Cosmochimica Acta* 226: 206–223.

Bermingham KR, Füri E, Lodders K, and Marty B (2020) The NC-CC isotope dichotomy: Implications for the chemical and isotopic evolution of the early solar system. *Space Science Reviews* 216: 133. https://doi.org/10.1007/s11214-020-00748-w

Bermingham KR and Meyer BS (2024) Nucleosynthetic Isotope Anomalies in Cosmochemistry and Geochemistry. *Oxford Research Encyclopedia of Planetary Science*. https://doi.org/ 10.1093/acrefore/9780190647926.013.144.

Bigeleisen J and Mayer MG (1947) Calculation of equilibrium constants for isotopic exchange reactions. *The Journal of Chemical Physics* 15: 261–267.

Binzel RP and Xu S (1993) Chips off of asteroid 4 Vesta: Evidence for the parent body of basaltic achondrite meteorites. *Science* 260(5105): 186–191.

Bischoff A, Scott ER, Metzler K, and Goodrich CA (2006) Nature and origins of meteoritic breccias. In: Lauretta DS and McSween, Jr. HY (eds.) *Meteorites and the Early Solar System*, Vol. II, pp. 679–712. University of Arizona Press.

Bischoff A, Bannemann L, Decker S, Ebert S, Haberer S, Heitmann U, Horstmann M, Klemm KI, Kraemer AK, and Lentfort S (2022) Asteroid 2008 TC3, not a polymict ureilitic but a polymict C1 chondrite parent body? Survey of 249 Almahata Sitta fragments. *Meteoritics & Planetary Science* 57: 1339–1364.

Bland P, Zolensky M, Benedix G, and Sephton M (2006) Weathering of chondritic meteorites. In: *Meteorites and the Early Solar System II*, Vol. 1, pp. 853–867.

Blichert-Toft J, Göpel C, Chaussidon M, and Albarède F (2020) Th/U variability in Allende chondrules. *Geochimica et Cosmochimica Acta* 280: 378–394.

Blum J and Wurm G (2008) The growth mechanisms of macroscopic bodies in protoplanetary disks. *Annual Review of Astronomy and Astrophysics* 46: 21–56.

Bockelée-Morvan D, Filacchione G, Altwegg K, et al. (2021) AMBITION—Comet nucleus cryogenic sample return. *Experimental Astronomy* 54: 1077–1128.

Boesenberg JS, Davis AM, Prinz M, Weisberg MK, Clayton RN, and Mayeda TK (2000) The pyroxene pallasites, Vermillion and Yamato 8451: Not quite a couple. *Meteoritics & Planetary Science* 35: 757–769.

Bollard J, Kawasaki N, Sakamoto N, Olsen M, Itoh S, Larsen K, Wielandt D, Schiller M, Connelly JN, Yurimoto H, and Bizzarro M (2019) Combined U-corrected Pb-Pb dating and ^{26}Al-^{26}Mg systematics of individual chondrules—Evidence for a reduced initial abundance of ^{26}Al amongst inner Solar System chondrules. *Geochimica et Cosmochimica Acta* 260: 62–83.
Bonal L, Quirico E, Bourot-Denise M, and Montagnac G (2006) Determination of the petrologic type of CV3 chondrites by Raman spectroscopy of included organic matter. *Geochimica et Cosmochimica Acta* 70: 1849–1863.
Bonnand P and Halliday AN (2018) Oxidized conditions in iron meteorite parent bodies. *Nature Geoscience* 11: 401–404.
Bonnand P, Parkinson IJ, James RH, Karjalainen A-M, and Fehr MA (2011) Accurate and precise determination of stable Cr isotope compositions in carbonates by double spike MC-ICP-MS. *Journal of Analytical Atomic Spectrometry* 26: 528–535.
Boss AP (1995) Collapse and fragmentation of molecular cloud cores. II. Collapse induced by stellar shock waves. *The Astrophysical Journal* 439: 224.
Bouhifd M, Jephcoat AP, Heber VS, and Kelley SP (2013) Helium in Earth's early core. *Nature Geoscience* 6: 982–986.
Bouvier A and Boyet M (2016) Primitive Solar System materials and Earth share a common initial ^{142}Nd abundance. *Nature* 537: 399–402.
Bouvier A, Blichert-Toft J, Moynier F, Vervoort JD, and Albarède F (2007) Pb-Pb dating constraints on the accretion and cooling history of chondrites. *Geochimica et Cosmochimica Acta* 71: 1583–1604.
Bouvier A, Brennecka GA, and Wadhwa M (2011) Absolute chronology of the first solids in the Solar System. In: *Workshop on the Formation of the First Solids in the Solar System, LPI Contribution 1639, Abs. #9054*.
Bouvier A, Blichert-Toft J, Boyet M, and Albarède F (2015) ^{147}Sm-^{143}Nd and ^{176}Lu-^{176}Hf systematics of eucrite and angrite meteorites. *Meteoritics & Planetary Science* 50: 1896–1911.
Brasser R (2013) The formation of Mars: Building blocks and accretion time scale. *Space Science Reviews* 174: 11–25.
Brasser R and Mojzsis S (2020) The partitioning of the inner and outer Solar System by a structured protoplanetary disk. *Nature Astronomy* 4: 492–499.
Brearley AJ and Jones RH (1998) Chondritic meteorites. In: Papike JJ (ed.) *Planetary Materials*. Washington, D.C: Mineralogical Society of America. Chapter 3.
Brennecka G, Weyer S, Wadhwa M, Janney PE, Anbar AD, and Zipfel J (2010) ^{238}U/^{235}U variations in meteorites: Extant ^{247}Cm and implications for Pb-Pb dating. *Science* 327: 449–451.
Broadley MW, Bekaert DV, Piani L, and Füri E (2022) Origin of life-forming volatile elements in the inner Solar System. *Nature* 611: 245–255. https://doi.org/10.1126/science.abo0431
Brownlee DE (2004) Comets. In: Davis AM (ed.) *Treatise on Geochemistry*, Vol. 1, pp. 663–688. Amsterdam: Elsevier.
Brownlee D (2014) The Stardust mission: Analyzing samples from the edge of the solar system. *Annual Review of Earth and Planetary Sciences* 42: 179–205.
Brownlee DE, Tsou P, Anderson JD, Hanner MS, Newburn RL, Sekanina Z, Clark BC, Hörz F, Zolensky ME, Kissel J, McDonnell JAM, Sandford SA, and Tuzzolino AJ (2003) Stardust: Comet and interstellar dust sample return mission. *Journal of Geophysical Research: Planets* 108(E10): 8111.
Brownlee D, et al. (2006) Comet 81P/Wild 2 under a microscope. *Science* 314: 1711–1716.
Buchwald VF (1975) *Handbook of Iron Meteorites: Their History, Distribution, Composition, and Structure, in 3 volumes*. Berkley, CA: University of California Press.
Budde G, Kruijer TS, et al. (2015) Planetesimal differentiation revealed by the Hf–W systematics of ureilites. *Earth and Planetary Science Letters* 430: 316–325.
Budde G, Burkhardt C, Brennecka GA, Fischer-Gödde M, Kruijer TS, and Kleine T (2016) Molybdenum isotopic evidence for the origin of chondrules and a distinct genetic heritage of carbonaceous and non-carbonaceous meteorites. *Earth and Planetary Science Letters* 454: 293–303.
Budde G, Burkhardt C, and Kleine T (2019) Molybdenum isotopic evidence for the late accretion of outer Solar System material to Earth. *Nature Astronomy* 3: 736–741.
Burbidge ME, Burbidge GR, Fowler GW, and Hoyle F (1957) Synthesis of the elements in stars. *Reviews of Modern Physics* 29: 547–650.
Burkhardt C, Dauphas N, Hans U, Bourdon B, and Kleine T (2019) Elemental and isotopic variability in solar system materials by mixing and processing of primordial disk reservoirs. *Geochimica et Cosmochimica Acta* 261: 145–170.
Burnett, D.S., and Genesis Science Team (2011) Solar composition from the Genesis Discovery Mission. *Proceedings of the National Academy of Sciences of the United States of America* 108: 19147–19151.
Buseck PR (1977) Pallasite meteorites—mineralogy, petrology and geochemistry. *Geochimica et Cosmochimica Acta* 41: 711–740.
Cameron AGW (1957) *Stellar Evolution, Nuclear Astrophysics, and Nucleogenesis*, 2nd edn. Chalk River, Ontario, Canada: Atomic Energy of Canada Ltd. (Technical Report No. CRL-41 (2nd Ed.); AECL-454).
Cameron AG (1973) Abundances of the elements in the solar system. *Space Science Reviews* 15: 121–146. Cameron A and Truran J (1977) The supernova trigger for formation of the solar system. *Icarus* 30: 447–461.
Cano EJ, Sharp ZD, and Shearer CK (2020) Distinct oxygen isotope compositions of the Earth and Moon. *Nature Geoscience* 13: 270–274.
Canup RM, Righter K, Dauphas N, Pahlevan K, Cuk M, Lock SJ, Stewart ST, Salmon J, Rufu R, and Nakajima M (2023) Origin of the Moon. *Reviews in Mineralogy and Geochemistry* 89: 53–102.
Carlson RW (2014) Thermal ionization mass spectrometry. In: Holland HD and Turekian KK (eds.) *Treatise on Geochemistry*, 2nd edn, Vol. 15, pp. 337–354. Amsterdam: Elsevier.
Cartier C and Wood BJ (2019) The role of reducing conditions in building Mercury. *Elements* 15: 39–45.
Chabot NL and Haack H (2006) Evolution of asteroidal cores. In: Lauretta DS and McSween HY (eds.) *Meteorites and the Early Solar System II*, pp. 747–771. University of Arizona Press.
Chakraborty S, Yanchulova P, and Thiemens MH (2013) Mass-independent oxygen isotopic partitioning during gas-phase SiO_2 formation. *Science* 342: 463–466.
Chou C-L (1978) Fractionation of siderophile elements in the Earth's upper mantle. In: *Proc. Lunar Planet. Sci. Conf. 9th*, pp. 219–230.
Clayton RN (1993) Oxygen isotopes in meteorites. *Annual Review of Earth and Planetary Sciences* 21: 115–149.
Clayton RN (2002) Self-shielding in the solar nebula. *Nature* 415: 860–861.
Clayton RN and Mayeda TK (1978) Genetic relations between iron and stony meteorites. *Earth and Planetary Science Letters* 40: 168–174.
Clayton RN and Mayeda TK (1984) The oxygen isotope record in Murchison and other carbonaceous chondrites. *Earth and Planetary Science Letters* 67: 151–161.
Clayton RN and Mayeda TK (1996) Oxygen isotope studies of achondrites. *Geochimica et Cosmochimica Acta* 60: 1999–2017.

Clayton RN, Grossman L, and Mayeda TK (1973) A component of primitive nuclear composition in carbonaceous meteorites. *Science* 182: 485–488.
Clayton RN, Onuma N, Grossman L, and Mayeda TK (1977) Distribution of the pre-solar component in Allende and other carbonaceous chondrites. *Earth and Planetary Science Letters* 34: 209–224.
Connelly JN, Bizzarro M, Krot AN, Nordlund A, Wielandt D, and Ivanova MA (2012) The absolute chronology and thermal processing of solids in the solar protoplanetary disk. *Science* 338: 651–655.
Connelly J, Bollard J, Amsellem E, Schiller M, Larsen K, and Bizzarro M (2023) Evidence for very early planetesimal formation and $^{26}Al/^{27}Al$ heterogeneity in the protoplanetary disk. *The Astrophysical Journal Letters* 952: L33.
Cook DL, Leya I, and Schönbächler M (2020) Galactic cosmic ray effects on iron and nickel isotopes in iron meteorites. *Meteoritics & Planetary Science* 55: 2758–2771.
Corrigan CM, Zolensky ME, Dahl J, Long M, Weir J, Sapp C, and Burkett PJ (1997) The porosity and permeability of chondritic meteorites and interplanetary dust particles. *Meteoritics & Planetary Science* 32: 509–515.
Craig G, Wehrs H, Bevan DG, Pfeifer M, Lewis J, Coath CD, Elliott T, Huang C, Lloyd NS, and Schwieters JB (2021) Project Vienna: A novel precell mass filter for collision/reaction cell MC-ICPMS/MS. *Analytical Chemistry* 93: 10519–10527.
Curran NM, Nottingham M, Alexander L, Crawford IA, Füri E, and Joy KH (2020) A database of noble gases in lunar samples in preparation for mass spectrometry on the Moon. *Planetary and Space Science* 182: 104823. https://doi.org/10.1016/j.pss.2019.104823
Dai W, Moynier F, Fang L, and Siebert J (2023) K-Ca dating and Ca isotope composition of the oldest Solar System lava, Erg Chech 002. *Geochemical Perspectives Letters* 24: 33–37.
Dalou C, Füri E, Deligny C, Piani L, Caumon M-C, Laumonier M, Boulliung J, and Edén M (2019) Redox control on nitrogen isotope fractionation during planetary core formation. *Proceedings of the National Academy of Sciences of the United States of America* 116: 14485–14494. https://doi.org/10.1073/pnas.1820719116
Dalou C, Deligny C, and Füri E (2022) Nitrogen isotope fractionation during magma ocean degassing: Tracing the composition of early Earth's atmosphere. *Geochemical Perspectives Letters* 20: 27–31. https://doi.org/10.7185/geochemlet.2204
Dauphas N (2017) The isotopic nature of the Earth's accreting material through time. *Nature* 541: 521–524.
Dauphas N and Pourmand A (2011) Hf-W-Th evidence for rapid growth of Mars and its status as a planetary embryo. *Nature* 473: 489–492.
Dauphas N, Marty B, and Reisberg L (2002) Molybdenum evidence for inherited planetary scale isotope heterogeneity of the protosolar nebula. *APJ* 565: 640–644.
Dauphas N, Davis AM, Marty B, and Reisberg L (2004) The cosmic molybdenum–ruthenium isotope correlation. *Earth and Planetary Science Letters* 226: 465–475.
Dauphas N, Cook DL, Sacarabany A, Fröhlich C, Davis AM, Wadhwa M, Pourmand A, Rauscher T, and Gallino R (2008) Iron 60 evidence for early injection and efficient mixing of stellar debris in the protosolar nebula. *The Astrophysical Journal* 686: 560–569.
Dauphas N, Remusat L, Chen JH, Roskosz M, Papanastassiou DA, Stodolna J, Guan Y, Ma C, and Eiler JM (2010) Neutron-rich chromium isotope anomalies in supernova nanoparticles. *The Astrophysical Journal* 720: 1577–1591.
Dauphas N, Poitrasson F, Burkhardt C, Kobayashi H, and Kurosawa K (2015) Planetary and meteoritic Mg/Si and d^{30}Si variations inherited from solar nebula chemistry. *Earth and Planetary Science Letters* 427: 236–248.
Dauphas N, Hopp T, Craig G, Zhang ZJ, Valdes MC, Heck PR, Charlier BLA, Bell EA, Harrison TM, Davis AM, Dussubieux L, Williams PR, Krawczynski MJ, Bouman C, Lloyd NS, Tollstrup D, and Schwieters JB (2022) In situ ^{87}Rb–^{87}Sr analyses of terrestrial and extraterrestrial samples by LA-MC-ICP-MS/MS with double Wien filter and collision cell technologies. *Journal of Analytical Atomic Spectrometry* 37: 2420–2441.
Dauphas N, Hopp T, and Nesvorný D (2024) Bayesian inference on the isotopic building blocks of Mars and Earth. *Icarus* 408: 115805.
Davis AM (2011) Stardust in meteorites. *Proceedings of the National Academy of Sciences of the United States of America* 108: 19142–19146.
Davis AM (2022) Short-lived nuclides in the early solar system: Abundances, origins, and applications. *Annual Review of Nuclear and Particle Science* 72: 339–363.
Davis AM and Olsen EJ (1991) Phosphates in pallasite meteorites as probes of mantle processes in small planetary bodies. *Nature* 353: 637–640.
Desch SJ and Connolly HC Jr (2002) A model of the thermal processing of particles in solar nebula shocks: Application to the cooling rates of chondrules. *Meteoritics & Planetary Science* 37: 183–207.
Desch SJ, Kalyaan A, and Alexander CMO (2018) The effect of Jupiter's formation on the distribution of refractory elements and inclusions in meteorites. *APJS* 238: 11.
Desch SJ, Dunlap DR, Dunham ET, Williams CD, and Mane P (2023) Statistical chronometry of meteorites. I. A test of ^{26}Al homogeneity and the Pb-Pb age of the solar system. *Icarus* 402: 115607.
Dodd R Jr, Van Schmus W, and Koffman D (1967) A survey of the unequilibrated ordinary chondrites. *Geochimica et Cosmochimica Acta* 31: 921–951.
Drouard A, Gattacceca J, Hutzler A, Rochette P, Braucher R, Bourlès D, Team A, Gounelle M, Morbidelli A, and Debaille V (2019) The meteorite flux of the past 2 my recorded in the Atacama Desert. *Geology* 47: 673–676.
Dyl KA, Simon JI, and Young ED (2011) Valence state of titanium in the Wark–Lovering rim of a Leoville CAI as a record of progressive oxidation in the early Solar Nebula. *Geochimica et Cosmochimica Acta* 75: 937–949.
Ek M, Hunt AC, Lugaro M, and Schönbächler M (2020) The origin of s-process isotope heterogeneity in the solar protoplanetary disk. *Nature Astronomy* 4: 273–281.
El Goresy A, Dubrovinsky L, Sharp TG, and Chen M (2004) Stishovite and post-stishovite polymorphs of silica in the Shergotty meteorite: Their nature, petrographic settings versus theoretical predictions and relevance to Earth's mantle. *Journal of Physics and Chemistry of Solids* 65: 1597–1608.
Elardo SM and Shahar A (2017) Non-chondritic iron isotope ratios in planetary mantles as a result of core formation. *Nature Geoscience* 10: 317–321.
Elardo SM, Shahar A, Mock TD, and Sio CK (2019) The effect of core composition on iron isotope fractionation between planetary cores and mantles. *Earth and Planetary Science Letters* 513: 124–134.
Eugster O, Herzog GF, Marti K, and Caffee MW (2006) Irradiation records, cosmic-ray exposure ages, and transfer times of meteorites. In: Lauretta DS and McSween HY (eds.) *Meteorites and the Early Solar System II*, pp. 829–851. University of Arizona Press.
Fang L, Frossard P, Boyet M, Bouvier A, Barrat J-A, Chaussidon M, and Moynier F (2022) Half-life and initial Solar System abundance of ^{146}Sm determined from the oldest andesitic meteorite. *Proceedings of the National Academy of Sciences of the United States of America* 119: e2120933119.

Farley KA, et al. (2020) Mars 2020 mission overview. *Space Science Reviews* 216: 142.
Fedele D, Carney M, et al. (2017) ALMA unveils rings and gaps in the protoplanetary system HD 169142: Signatures of two giant protoplanets. *Astronomy & Astrophysics* 600: A72.
Fegley Jr B and Palme H (1985) Evidence for oxidizing conditions in the solar nebula from Mo and W depletions in refractory inclusions in carbonaceous chondrites. *Earth and Planetary Science Letters* 72: 311–326.
Fischer RA and Ciesla FJ (2014) Dynamics of the terrestrial planets from a large number of N-body simulations. *Earth and Planetary Science Letters* 392: 28–38.
Fischer-Gödde M, Burkhardt C, Kruijer TS, and Kleine T (2015) Ru isotope heterogeneity in the solar protoplanetary disk. *Geochimica et Cosmochimica Acta* 168: 151–171.
Fischer-Gödde M, Elfers B-M, Münker C, Szilas K, Maier WD, Messling N, Morishita T, Van Kranendonk M, and Smithies H (2020) Ruthenium isotope vestige of Earth's pre-late-veneer mantle preserved in Archaean rocks. *Nature* 579: 240–244.
Fletcher LN, Greathouse TK, Orton GS, Irwin PGJ, Mousis O, Sinclair JA, and Giles RS (2014) The origin of nitrogen on Jupiter and Saturn from the $^{15}N/^{14}N$ ratio. *Icarus* 238: 170–190.
Fouchet T, Lellouch E, Bézard B, Encrenaz T, Drossart P, Feuchtrgruber H, and de Graauw T (2000) ISO-SWS observations of Jupiter: Measurement of the ammonia tropospheric profile and of the $^{15}N/^{14}N$ isotopic ratio. *Icarus* 143: 223–243.
Frisch PC, Redfield S, and Slavin JD (2011) The interstellar medium surrounding the Sun. *Annual Review of Astronomy and Astrophysics* 49: 237–279.
Frossard P, Boyet M, Bouvier A, Hammouda T, and Monteux J (2019) Evidence for anorthositic crust formed on an inner solar system planetesimal. *Geochemical Perspectives Letters* 11: 28–32.
Frossard P, Guo Z, Spencer M, Boyet M, and Bouvier A (2021) Evidence from achondrites for a temporal change in Nd nucleosynthetic anomalies within the first 1.5 million years of the inner solar system formation. *Earth and Planetary Science Letters* 566: 116968.
Frossard P, Israel C, Bouvier A, and Boyet M (2022) Earth's composition was modified by collisional erosion. *Science* 377: 1529–1532.
Fujiya W, Furukawa Y, Sugahara H, Koike M, Bajo K, Chabot NL, Miura YN, Moynier F, Russell SS, Tachibana S, Takano Y, Usui T, and Zolensky ME (2021) Analytical protocols for Phobos regolith samples returned by the Martian Moons eXploration (MMX) mission. *Earth, Planets and Space* 73: 120.
Fujiya W, et al. (2023) Carbonate record of temporal change in oxygen fugacity and gaseous species in asteroid Ryugu. *Nature Geoscience* 16: 675–682.
Fukuda K, Tenner TJ, Kimura M, Tomioka N, Siron G, Ushikubo T, Chaumard N, Hertwig AT, and Kita NT (2022) A temporal shift of chondrule generation from the inner to outer Solar System inferred from oxygen isotopes and Al-Mg chronology of chondrules from primitive CM and CO chondrites. *Geochimica et Cosmochimica Acta* 322: 194–226.
Füri E, Deloule E, and Trappitsch R (2017) The production rate of cosmogenic deuterium at the Moon's surface. *Earth and Planetary Science Letters* 474: 76–82. https://doi.org/10.1016/j.epsl.2017.05.042
Gaillard F, Bouhifd M, Füri E, Malavergne V, Marrocchi Y, Noack L, Ortenzi G, Roskosz M, and Vulpius S (2021) The diverse planetary ingassing/outgassing paths produced over billions of years of magmatic activity. *Space Science Reviews* 217: 1–54. https://doi.org/10.1007/s11214-021-00802-1
Gattacceca J, Bonal L, Sonzogni C, and Longerey J (2020) CV chondrites: More than one parent body. *Earth and Planetary Science Letters* 547: 116467.
Gattacceca J, McCubbin FM, Grossman J, Bouvier A, Bullock E, Chennaoui Aoudjehane H, Debaille V, D'Orazio M, Komatsu M, Miao B, and Schrader DL (2021) The Meteoritical Bulletin, No. 109. *Meteoritics & Planetary Science* 56: 1626–1630.
Gattacceca J, McCubbin FM, Grossman JN, Schrader DL, Chabot NL, D'orazio M, Goodrich C, Greshake A, Gross J, and Joy KH (2023) The Meteoritical Bulletin, No. 111. *Meteoritics & Planetary Science* 58: 901–904.
Geiss J and Gloeckler G (1998) Abundances of deuterium and helium-3 in the protosolar cloud. *Space Science Reviews* 84: 239–250.
Geiss J, Eberhardt P, Bühler F, and Meister J (1970) Apollo 11 and 12 Solar wind composition experiments: Fluxes of He and Ne isotopes. *Journal of Geophysical Research, Space Physics* 75: 5972–5979.
Geiss J, Bühler F, Cerutti H, Eberhardt P, Filleux CH, Meister J, and Signer P (2004) The Apollo SWC experiment: Results, conclusions, consequences. *Space Science Reviews* 110: 307–335.
Goderis S, Chakrabarti R, Debaille V, and Kodolányi J (2016) Isotopes in cosmochemistry: Recipe for a Solar System. *Journal of Analytical Atomic Spectrometry* 31: 841–862.
Golabek GJ and Jutzi M (2021) Modification of icy planetesimals by early thermal evolution and collisions: Constraints for formation time and initial size of comets and small KBOs. *Icarus* 363: 114437.
Goldberg E, Uchiyama A, and Brown H (1951) The distribution of nickel, cobalt, gallium, palladium and gold in iron meteorites. *Geochimica et Cosmochimica Acta* 2: 1–25.
Goldschmidt VM (1937) The principles of distribution of chemical elements in minerals and rocks. The seventh Hugo Müller Lecture, delivered before the Chemical Society on March 17th, 1937. *Journal of the Chemical Society* : 655–673.
Goldstein JI and Michael JR (2006) The formation of plessite in meteoritic metal. *Meteoritics & Planetary Science* 41: 553–570.
Goldstein JI, Scott ERD, and Chabot NL (2009) Iron meteorites: Crystallization, thermal history, parent bodies, and origin. *Geochemistry* 69: 293–325.
Goodrich CA and Delaney JS (2000) Fe/Mg-Fe/Mn relations of meteorites and primary heterogeneity of primitive achondrite parent bodies. *Geochimica et Cosmochimica Acta* 64(1): 149–160.
Goodrich CA, Sanborn ME, Yin Q-Z, Kohl I, Frank D, Daly RT, Walsh KJ, Zolensky ME, Young ERD, Jenniskens P, and Shaddad MH (2021) Chromium isotopic evidence for mixing of NC and CC reservoirs in polymict ureilites: Implications for dynamical models of the early Solar System. *The Planetary Science Journal* 2: 13.
Gounelle M (2015) The abundance of ^{26}Al-rich planetary systems in the Galaxy. *Astronomy & Astrophysics* 582: A26. Greaves JS (2005) Disks around stars and the growth of planetary systems. *Science* 307: 68–71.
Greenwood RC (2006) Oxygen isotope variation in stony-iron meteorites. *Science* 313: 1763–1765.
Greenwood RC, Barrat J-A, Scott ER, Haack H, Buchanan PC, Franchi IA, Yamaguchi A, Johnson D, Bevan AW, and Burbine TH (2015) Geochemistry and oxygen isotope composition of main-group pallasites and olivine-rich clasts in mesosiderites: Implications for the "Great Dunite Shortage" and HED-mesosiderite connection. *Geochimica et Cosmochimica Acta* 169: 115–136.
Greenwood RC, Burbine TH, Miller MF, and Franchi IA (2017) Melting and differentiation of early-formed asteroids: The perspective from high precision oxygen isotope studies. *Geochemistry* 77(1): 1–43.

Greenwood RC, Barrat J-A, Miller MF, Anand M, Dauphas N, Franchi IA, Sillard P, and Starkey NA (2018) Oxygen isotopic evidence for accretion of Earth's water before a high-energy Moon-forming giant impact. *Science Advances* 4(3): eaao5928.
Gregory T, Luu T-H, Coath CD, Russell SS, and Elliott T (2020) Primordial formation of major silicates in a protoplanetary disc with homogeneous $^{26}Al/^{27}Al$. *Science Advances* 6: eaay9626.
Grewal DS, Dasgupta R, and Marty B (2021) A very early origin of isotopically distinct nitrogen in inner Solar System protoplanets. *Nature Astronomy* 5: 356–364.
Grewal DS, Sun T, Aithala S, Taylor H, Dasgupta R, Yeung LY, and Schauble EA (2022) Limited nitrogen isotopic fractionation during core-mantle differentiation in rocky protoplanets and planets. *Geochimica et Cosmochimica Acta* 338: 347–364.
Grimberg A, Baur H, Bochsler P, Bühler F, Burnett DS, Hays CC, Heber VS, Jurewicz AJG, and Wieler R (2006) Solar wind neon from Genesis: Implications for the lunar noble gas record. *Science* 314(5802): 1133–1135.
Grossman L (1972) Condensation in the primitive solar nebula. *Geochimica et Cosmochimica Acta* 36: 597–619.
Grossman JN and Brearley AJ (2005) The onset of metamorphism in ordinary and carbonaceous chondrites. *Meteoritics & Planetary Science* 40: 87–122.
Haack H and McCoy TJ (2003) Iron and stony-iron meteorites. In: Davis AM (ed.) *Meteorites, Comets and Planets*. *Treatise on Geochemistry*, Vol. 1, pp. 325–345. Elsevier-Pergamon.
Haack H, Scott ERD, Love SG, Brearley AJ, and McCoy TJ (1996) Thermal histories of IVA stony-iron and iron meteorites: Evidence for asteroid fragmentation and reaccretion. *Geochimica et Cosmochimica Acta* 60: 3103–3113.
Haba MK, Wotzlaw JF, Lai YJ, Yamaguchi A, and Schönbächler M (2019) Mesosiderite formation on asteroid 4 Vesta by a hit-and-run collision. *Nature Geoscience* 12: 510–515. Halliday AN and Canup RM (2022) The accretion of planet Earth. *Nature Reviews Earth and Environment* 4: 18–35.
Hammouda T, Boyet M, Frossard P, and Cartier C (2022) The message of oldhamites from enstatite chondrites. *Progress in Earth and Planetary Science* 9: 1–19.
Hammouda T, Frossard P, Boyet M, Bouvier A, Newville M, and Lanzirotti A (2024) Mapping the redox state of the young Solar System using ytterbium valence state. *Geochimica et Cosmochimica Acta* 372: 124–133.
Harkins WD (1917) The evolution of the elements and the stability of complex atoms. I. A new periodic system which shows a relation between the abundance of the elements and the structure of the nuclei of atoms. *Journal of the American Chemical Society* 39: 856–879.
Hartmann WK and Davis DR (1975) Satellite-sized planetesimals and lunar origin. *Icarus* 24(4): 504–515.
He H, Ji J, Zhang Y, Hu S, Lin Y, Hui H, Hao J, Li R, Yang W, Tian H, Zhang C, Anand M, Tartèse R, Gu L, Li J, Zhang D, Mao Q, Jia L, Li X, Chen Y, Zhang L, Ni H, Wu S, Wang H, Li Q, He H, Li X, and Wu F (2023) A solar wind-derived water reservoir on the Moon hosted by impact glass beads. *Nature Geoscience* 16: 294–300.
Heber VS, Wieler R, Baur H, Olinger C, Friedmann TA, and Burnett DS (2009) Noble gas composition of the solar wind as collected by the Genesis mission. *Geochimica et Cosmochimica Acta* 73: 7414–7432.
Heber VS, Baur H, Bochsler P, McKeegan KD, Neugebauer M, Reisenfeld DB, Wieler R, and Wiens RC (2012) Isotopic mass fractionation of solar wind: Evidence from fast and slow solar wind collected by the genesis mission. *APJ* 759: 121.
Heck PR, Greer J, Kööp L, Trappitsch R, Gyngard F, Busemann H, Maden C, Ávila JN, Davis AM, and Wieler R (2020) Lifetimes of interstellar dust from cosmic ray exposure ages of presolar silicon carbide. *Proceedings of the National Academy of Sciences of the United States of America* 117(4): 1884–1889.
Herwartz D, Pack A, Friedrichs B, and Bischoff A (2014) Identification of the giant impactor Theia in lunar rocks. *Science* 344(6188): 1146–1150.
Herzog GF (2003) Cosmic-ray exposure ages of meteorites. In: Davis AM, Holland HD, and Turekian KK (eds.). *Treatise on Geochemistry*, Vol. 1, pp. 347–380. Elsevier.
Hezel DC and Palme H (2010) The chemical relationship between chondrules and matrix and the chondrule matrix complementarity. *Earth and Planetary Science Letters* 294: 85–93.
Hidaka H, Ebihara M, and Yoneda S (2000) Isotopic study of neutron capture effects on Sm and Gd in chondrites. *Earth and Planetary Science Letters* 180(1–2): 29–37.
Hiesinger H, van der Bogert CH, Pasckert JH, Funcke L, Giacomini L, Ostrach LR, and Robinson MS (2012) How old are young lunar craters? *Journal of Geophysical Research: Planets* 117(E12): E00H10.
Hilton CD and Walker RJ (2020) New implications for the origin of the IAB main group iron meteorites and the isotopic evolution of the noncarbonaceous (NC) reservoir. *Earth and Planetary Science Letters* 540: 116248.
Hilton CD, Bermingham KR, Walker RJ, and McCoy TJ (2019) Genetics, crystallization sequence, and age of the South Byron Trio iron meteorites: New insights to carbonaceous chondrite (CC) type parent bodies. *Geochimica et Cosmochimica Acta* 251: 217–228.
Hilton CD, Ash RD, Piccoli PM, Kring DA, McCoy TJ, and Walker RJ (2020a) Origin and age of metal veins in Canyon Diablo graphite nodules. *Meteoritics & Planetary Science* 55: 771–780.
Hilton CD, Ash RD, and Walker RJ (2020b) Crystallization histories of the group IIF iron meteorites and Eagle Station pallasites. *Meteoritics & Planetary Science* 55: 2579–2586.
Hilton CD, Ash RD, and Walker RJ (2022) Chemical characteristics of iron meteorite parent bodies. *Geochimica et Cosmochimica Acta* 318: 112–125.
Hin RC, Coath CD, Carter PJ, Nimmo F, Lai Y-J, Pogge von Strandmann PAE, Willbold M, Leinhardt ZM, Walter MJ, and Elliott T (2017) Magnesium isotope evidence that accretional vapour loss shapes planetary compositions. *Nature* 549: 511–515.
Hirschmann MM, Bergin EA, Blake GA, Ciesla FJ, and Li J (2021) Early volatile depletion on planetesimals inferred from C–S systematics of iron meteorite parent bodies. *Proceedings of the National Academy of Sciences of the United States of America* 118: e2026779118.
Hogmalm KJ, Zack T, Karlsson AK-O, Sjöqvist AS, and Garbe-Schönberg D (2017) In situ Rb–Sr and K–Ca dating by LA-ICP-MS/MS: An evaluation of N 2 O and SF 6 as reaction gases. *Journal of Analytical Atomic Spectrometry* 32: 305–313.
Hoppe P, Leitner J, Kodolányi J, Borrmann S, and Jones AP (2022) Dust from supernovae and their progenitors in the solar nebula. *Nature Astronomy* 6: 1027–1034. Hoyle F (1946) The synthesis of the elements from hydrogen. *Monthly Notices of the Royal Astronomical Society* 106: 342–383.
Hoyle F (1954) On nuclear reactions occuring in very hot stars. I. the synthesis of elements from carbon to nickel. *Astrophysical Journal Supplement* 1: 121.
Huang J, Andrews SM, et al. (2018) The disk substructures at high angular resolution project (DSHARP). III. Spiral structures in the millimeter continuum of the Elias 27, IM Lup, and WaOph 6 disks. *The Astrophysical Journal Letters* 869: L43.

Hulston JR and Thode HG (1965) Variations in the S^{33}, S^{34}, and S^{36} contents of meteorites and their relation to chemical and nuclear effects. *Journal of Geophysical Research* 70(14): 3475–3484.
Hunt AC, Ek M, and Schönbächler M (2017) Platinum isotopes in iron meteorites: Galactic cosmic ray effects and nucleosynthetic homogeneity in the p-process isotope ^{190}Pt and the other platinum isotopes. *Geochimica et Cosmochimica Acta* 216: 82–95.
Hunt AC, Cook DL, Lichtenberg T, Reger PM, Ek M, Golabek GJ, and Schönbächler M (2018) Late metal–silicate separation on the IAB parent asteroid: Constraints from combined W and Pt isotopes and thermal modelling. *Earth and Planetary Science Letters* 482: 490–500.
Hunt AC, Theis KJ, Rehkämper M, Benedix GK, Andreasen R, and Schönbächler M (2022) The dissipation of the solar nebula constrained by impacts and core cooling in planetesimals. *Nature Astronomy* 6: 812–818.
Hutchison R (2004) *Meteorites: A Petrologic, Chemical and Isotopic Synthesis. Cambridge Planetary Science Series*. Cambridge, New York, Melbourne: Cambridge University Press. 506 p.
Ireland TR (1990) Presolar isotopic and chemical signatures in hibonite-bearing refractory inclusions from the Murchison carbonaceous chondrite. *Geochimica et Cosmochimica Acta* 54: 3219–3237.
Ireland TR, Avila J, Greenwood RC, Hicks LJ, and Bridges JC (2020) Oxygen isotopes and sampling of the Solar System. *Space Science Reviews* 216: 25.
Isella A, Guidi G, et al. (2016) Ringed structures of the HD 163296 protoplanetary disk revealed by ALMA. *Physical Review Letters* 117: 251101.
Israel C, Boyet M, Doucelance R, Bonnand P, Frossard P, Auclair D, and Bouvier A (2020) Formation of the Ce-Nd mantle array: Crustal extraction vs. recycling by subduction. *Earth and Planetary Science Letters* 530: 115941.
Ivanova MA (2023) Principal studies of the first solid material formed in the early Solar System: A review. *Geochemistry International* 61: 781–909.
Izidoro A, Dasgupta R, Raymond SN, Deienno R, Bitsch B, and Isella A (2021) Planetesimal rings as the cause of the Solar System's planetary architecture. *Nature Astronomy* 6: 357–366.
Jacobsen B, Yin Q-Z, Moynier F, Amelin Y, Krot AN, Nagashima K, Hutcheon ID, and Palme H (2008) ^{26}Al–^{26}Mg and ^{207}Pb–^{206}Pb systematics of Allende CAIs: Canonical solar initial ^{26}Al/^{27}Al ratio reinstated. *Earth and Planetary Science Letters* 272: 353–364.
Jacquet E (2022) *Meteorite Petrology Versus Genetics: Toward a Unified Binominal Classification*. Wiley Online Library.
Jaffey A, Flynn K, Glendenin L, Bentley W, and t., Essling, A. (1971) Precision measurement of half-lives and specific activities of U-235 and U-238. *Physical Review C* 4: 1889.
Johnson CM, Breard BL, and Albarède F (2004) *Geochemistry of Non-Traditional Isotopes, Reviews in Mineralogy and Geochemistry*, Vol. 55. De Gruyter, Berlin/Boston: Mineralogical Society of America.
Kallemeyn GW and Wasson JT (1981) The compositional classification of chondrites—I. The carbonaceous chondrite groups. *Geochimica et Cosmochimica Acta* 45: 1217–1230.
Jurewicz AJG, Rieck KD, Hervig R, Burnett DS, Wadhwa M, et al. (2020) Magnesium isotopes of the bulk solar wind from Genesis diamond-like carbon films. *Meteoritics and Planetary Science* 55: 352–375.
Kallemeyn GW, Rubin AE, and Wasson JT (1996) The compositional classification of chondrites: VII. The R chondrite group. *Geochimica et Cosmochimica Acta* 60: 2243–2256. Kawasaki N, et al. (2022) Oxygen isotopes of anhydrous primary minerals show kinship between asteroid Ryugu and comet 81P/Wild2. *Science Advances* 8: eade2067.
Keil K (2010) Enstatite achondrite meteorites (aubrites) and the histories of their asteroidal parent bodies. *Geochemistry* 70: 295–317.
Keil K (2012) Angrites, a small but diverse suite of ancient, silica-undersaturated volcanic-plutonic mafic meteorites, and the history of their parent asteroid. *Geochemistry* 72: 191–218.
Keil K (2014) Brachinite meteorites: Partial melt residues from an FeO-rich asteroid. *Geochemistry* 74: 311–329.
Keil K and McCoy TJ (2018) Acapulcoite-lodranite meteorites: Ultramafic asteroidal partial melt residues. *Geochemistry* 78: 153–203.
Kimura K, Lewis RS, and Anders E (1974) Distribution of gold and rhenium between nickel-iron and silicate melts: Implications for the abundance of siderophile elements on the Earth and Moon. *Geochimica et Cosmochimica Acta* 38: 683–701.
Kimura M, Tsuchiyama A, Fukuoka T, and Iimura Y (1992) Antarctic primitive achondrites Yamato-74025, -75300, and -75305: Their mineralogy, thermal history and the relevance to winonaite. *Proceedings of the NIPR Symposium on Antarctic Meteorites* 5: 165–190.
Kimura M, Grossman J, and Weisberg M (2008) Fe-Ni metal in primitive chondrites: Indicators of classification and metamorphic conditions for ordinary and CO chondrites. *Meteoritics & Planetary Science* 43: 1161–1177.
King AJ, Bates HC, Krietsch D, Busemann H, Clay PL, Schofield PF, and Russell SS (2019) The Yamato-type (CY) carbonaceous chondrite group: Analogues for the surface of asteroid Ryugu? *Geochemistry* 79: 125531.
Kita NT, Yin Q-Z, MacPherson GJ, Ushikubo T, Jacobsen B, Nagashima K, Kurahashi E, Krot AN, and Jacobsen SB (2013) ^{26}Al-^{26}Mg isotope systematics of the first solids in the early solar system. *Meteoritics & Planetary Science* 48: 1383–1400.
Kleiber IA (1885) *Zh. Russ. Fiziko-Khim. Obshch. (St. Petersburg)*, Vol.17, pp. 147–171.
Kleine T, Budde G, Burkhardt C, Kruijer T, Worsham E, Morbidelli A, and Nimmo F (2020) The non-carbonaceous–carbonaceous meteorite dichotomy. *Space Science Reviews* 216: 1–27.
Kobayashi S, Imai H, and Yurimoto H (2003) New extreme ^{16}O-rich reservoir in the early solar system. *Geochemical Journal* 37: 663–669.
Kokubo E and Ida S (1998) Oligarchic growth of protoplanets. *Icarus* 131: 171–178.
Kondev F, Wang M, Huang W, Naimi S, and Audi G (2021) The NUBASE2020 evaluation of nuclear physics properties. *Chinese Physics C* 45: 030001.
Kööp L, Davis AM, Nakashima D, Park C, Krot AN, Nagashima K, Tenner TJ, Heck PR, and Kita NT (2016) A link between oxygen, calcium and titanium isotopes in ^{26}Al-poor hibonite-rich CAIs from Murchison and implications for the heterogeneity of dust reservoirs in the solar nebula. *Geochimica et Cosmochimica Acta* 189: 70–95.
Kööp L, Nagashima K, Davis AM, and Krot AN (2020) A refractory inclusion with solar oxygen isotopes and the rarity of such objects in the meteorite record. *Meteoritics and Planetary Science* 55: 524–534.
Kracher A, Willis J, and Wasson JT (1980) Chemical classification of iron meteorites—IX. A new group (IIF), revision of IAB and IIICD, and data on 57 additional irons. *Geochimica et Cosmochimica Acta* 44: 773–787.
Krestianinov E, Amelin Y, Yin Q-Z, Cary P, Huyskens MH, Miller A, Dey S, Hibiya Y, Tang H, and Young ED (2023) Igneous meteorites suggest Aluminium-26 heterogeneity in the early Solar Nebula. *Nature Communications* 14: 4940.
Krot AN, Amelin Y, Cassen P, and Meibom A (2005a) Young chondrules in CB chondrites from a giant impact in the early Solar System. *Nature* 436: 989–992.
Krot A, Keil K, Goodrich C, Scott ERD, and Weisberg MK (2005b) Classification of meteorites. In: Davis AM (ed.) *Meteorites, Comets, and Planets: Treatise on Geochemistry*, Vol. 1, pp. 84–128. Oxford: Elsevier-Pergamon.

Krot AN, Keil K, Scott ERD, Goodrich CA, and Weisberg MK (2014) Classification of meteorites and their genetic relationships. In: Davis AM (ed.) *Treatise on Geochemistry*, 2nd edn, Vol. 1, pp. 1–63. Amsterdam: Elsevier.
Kruijer TS and Kleine T (2019) Age and origin of IIE iron meteorites inferred from Hf-W chronology. *Geochimica et Cosmochimica Acta* 262: 92–103.
Kruijer TS, Sprung P, Kleine T, Leya I, Burkhardt C, and Wieler R (2012) Hf–W chronometry of core formation in planetesimals inferred from weakly irradiated iron meteorites. *Geochimica et Cosmochimica Acta* 99: 287–304.
Kruijer TS, Fischer-Gödde M, Kleine T, Sprung P, Leya I, and Wieler R (2013) Neutron capture on Pt isotopes in iron meteorites and the Hf–W chronology of core formation in planetesimals. *Earth and Planetary Science Letters* 361: 162–172.
Kruijer TS, Kleine T, Fischer-Gödde M, Burkhardt C, and Wieler R (2014a) Nucleosynthetic W isotope anomalies and the Hf–W chronometry of Ca–Al-rich inclusions. *Earth and Planetary Science Letters* 403: 317–327.
Kruijer TS, Touboul M, Fischer-Gödde M, Bermingham KR, Walker RJ, and Kleine T (2014b) Protracted core formation and rapid accretion of protoplanets. *Science* 344: 1150–1154.
Kruijer TS, Burkhardt C, Budde G, and Kleine T (2017) Age of Jupiter inferred from the distinct genetics and formation times of meteorites. *Proceedings of the National Academy of Sciences of the United States of America* 114: 6712–6716.
Kruijer TS, Burkhardt C, Borg LE, and Kleine T (2022) Tungsten and molybdenum isotopic evidence for an impact origin of pallasites. *Earth and Planetary Science Letters* 584: 117440.
Kubik E, Sossi PA, Siebert J, Inglis E, Roskosz M, Siciliano Rego E, Wehr N, and Moynier F (2022) The absence of an effect of nickel on iron isotope fractionation during core formation. *Geochimica et Cosmochimica Acta* 327: 186–199.
Labidi J, Farquhar J, Alexander CMO'D, Eldridge DL, and Odura H (2017) Mass independent sulfur isotope signatures in CMs: implications for sulfur chemistry in the early solar system. *Geochimica et Cosmochimica Acta* 196: 326–350.
Lambrechts M and Johansen A (2012) Rapid growth of gas-giant cores by pebble accretion. *Astronomy & Astrophysics* 544: A32.
Lammer H, Brasser R, Johansen A, Scherf M, and Leitzinger M (2020) Formation of Venus, Earth and Mars: Constrained by isotopes. *Space Science Reviews* 217: 7.
Leitner J, Metzler K, Vollmer C, Floss C, Haenecour P, Kodolányi J, Harries D, and Hoppe P (2020) The presolar grain inventory of fine-grained chondrule rims in the Mighei-type (CM) chondrites. *Meteoritics & Planetary Science* 55: 1176–1206.
Levison HF, Kretke KA, Walsh KJ, and Bottke WF (2015) Growing the terrestrial planets from the gradual accumulation of submeter-sized objects. *Proceedings of the National Academy of Sciences of the United States of America* 112: 14180–14185.
Lichtenberg T, Dra˛z˙kowska J, Schönbächler M, Golabek GJ, and Hands TO (2021) Bifurcation of planetary building blocks during Solar System formation. *Science* 371: 365–370.
Lin Y (2022) Enstatite chondrites: condensation and metamorphism under extremely reducing conditions and contributions to the Earth. *Progress in Earth and Planetary Science* 9: 1–16.
Lin JF, Struzhin VV, Jacobsen SD, Hu MY, Chow P, et al. (2005) Spin transition of iron in magnesiowüstite in the Earth's lower mantle. *Nature* 436: 377–380.
Liu Y, Dipierro G, et al. (2019) Ring structure in the MWC 480 disk revealed by ALMA. *Astronomy & Astrophysics* 622: A75.
Lockyer N (1890) *The Meteoritic Hypothesis: A Statement of the Results of a Spectroscopic Inquiry Into the Origin of Cosmical Systems*. Macmillan.
Lodders K (2003) Solar System abundances and condensation temperatures of the elements. *The Astrophysical Journal* 591: 1220–1247.
Lodders K (2021) Relative atomic solar system abundances, mass fractions, and atomic masses of the elements and their isotopes, composition of the solar photosphere, and compositions of the major chondritic meteorite groups. *Space Science Reviews* 217: 44.
Lodders K and Fegley B (2015) *Chemistry of the Solar System*. Royal Society of Chemistry. 494 p.
Lodders K and Fegley B Jr (2023) Solar system abundances and condensation temperatures of the halogens fluorine, chlorine, bromine, and iodine. *Geochemistry* 83: 125957.
Lovering JF, Nichiporuk W, Chodos A, and Brown H (1957) The distribution of gallium, germanium, cobalt, chromium, and copper in iron and stony-iron meteorites in relation to nickel content and structure. *Geochimica et Cosmochimica Acta* 11: 263–278.
Lyons JR, Gharib-Nezhad E, and Ayres TR (2018) A light carbon isotope composition for the Sun. *Nature Communications* 9: 908.
Ma M, Neumann W, Néri A, Schwarz WH, Ludwig T, Trieloff M, Klahr H, and Bouvier A (2022) Early formation of primitive achondrites in an outer region of the protoplanetary disc. *Geochemical Perspectives Letters* 23: 33–37.
MacPherson G, Bullock E, Janney P, Kita N, Ushikubo T, Davis A, Wadhwa M, and Krot A (2010) Early solar nebula condensates with canonical, not supracanonical, initial $^{26}Al/^{27}Al$ ratios. *The Astrophysical Journal Letters* 711: L117.
MacPherson GJ, Bullock ES, Tenner TJ, Nakashima D, Kita NT, Ivanova MA, Krot AN, Petaev MI, and Jacobsen SB (2017) High precision Al–Mg systematics of forsterite-bearing Type B CAIs from CV3 chondrites. *Geochimica et Cosmochimica Acta* 201: 65–82.
Mah J, Brasser R, Bouvier A, and Mojzsis SJ (2021) Effects of pebble accretion on the growth and composition of planetesimals in the inner Solar system. *Monthly Notices of the Royal Astronomical Society* 511: 158–175.
Mahaffy PR, Donahue TM, Atreya SK, Owen TC, and Niemann HB (1998) Galileo probe measurements of D/H and 3He/4He in Jupiter's atmosphere. *Space Science Reviews* 84: 251–263.
Malvin DJ, Wang D, and Wasson JT (1984) Chemical classification of iron meteorites—X. Multielement studies of 43 irons, resolution of group IIIE from IIIAB, and evaluation of Cu as a taxonomic parameter. *Geochimica et Cosmochimica Acta* 48: 785–804.
Mane P, Hervig R, Bose M, and Wadhwa M (2015) Trace element abundances in Wark-lovering rims of CAIs from a CV3 meteorite: Implications for their chronology. In:, Vol. 5327, *78th Annual Meeting of the Meteoritical Society*.
Marin-Carbonne J, Kiss A, Bouvier A-S, Meibom A, Baumgartner L, Bovay T, Plane F, Escrig S, and Rubatto D (2022) Surface analysis by secondary ion mass spectrometry (SIMS): Principles and applications from Swiss laboratories. *Chimia* 76: 26.
Marks NE, Borg LE, Hutcheon ID, Jacobsen B, and Clayton RN (2014) Samarium–neodymium chronology and rubidium–strontium systematics of an Allende calcium–aluminum-rich inclusion with implications for ^{146}Sm half-life. *Earth and Planetary Science Letters* 405: 15–24.
Marrocchi Y, Villeneuve J, Batanova V, Piani L, and Jacquet E (2018) Oxygen isotopic diversity of chondrule precursors and the nebular origin of chondrules. *Earth and Planetary Science Letters* 496: 132–141.
Martinet S, Meynet G, Nandal D, Ekström S, Georgy C, Haemmerlé L, Hirschi R, Yusof N, Gounelle M, and Dwarkadas V (2022) Very massive star winds as sources of the short-lived radioactive isotope ^{26}Al. *Astronomy & Astrophysics* 664: A181.
Martins R, Kuthning S, Coles BJ, Kreissig K, and Rehkämper M (2023) Nucleosynthetic isotope anomalies of zinc in meteorites constrain the origin of Earth's volatiles. *Science* 379: 369–372.
Marty B, Chaussidon M, Wiens RC, Jurewicz AJG, and Burnett DS (2011) A ^{15}N-poor isotopic composition for the solar system as shown by Genesis solar wind samples. *Science* 332: 1533–1536.

Mason B (1979) Data of geochemistry, 6th edition, Chapter B cosmochemistry, Part 1 meteorites. In: *Geological Survey Professional Paper 440-B-1*. Washington, USA: United States Government Printing Office.
Matsuhisa Y, Goldsmith JR, and Clayton RN (1978) Mechanisms of hydrothermal crystallization of quartz at 250°C and 15 kbar. *Geochimica et Cosmochimica Acta* 42: 173–182.
McCain KA, Matsuda N, Liu M-C, McKeegan KD, Yamaguchi A, Kimura M, Tomioka N, Ito M, Imae N, and Uesugi M (2023) Early fluid activity on Ryugu inferred by isotopic analyses of carbonates and magnetite. *Nature Astronomy* 7: 309–317.
McCord TB, Adams JB, and Johnson TV (1970) Asteroid Vesta: Spectral reflectivity and compositional implications. *Science* 168: 1445–1447.
McCoy TJ, Keil K, Muenow DW, and Wilson L (1997) Partial melting and melt migration in the acapulcoite-lodranite parent body. *Geochimica et Cosmochimica Acta* 61: 639–650.
McKay G, Le L, Wagstaff J, and Crozaz G (1994) Experimental partitioning of rare earth elements and strontium: Constraints on petrogenesis and redox conditions during crystallization of Antarctic angrite Lewis Cliff 86010. *Geochimica et Cosmochimica Acta* 58: 2911–2919.
McKeegan KD, Kallio APA, Heber VS, Jarzebinski G, Mao PH, Coath CD, Kunihiro T, Wiens RC, Nordholt JE, Moses RW Jr, Reisenfeld DB, Jurewicz AJG, and Burnett DS (2011) The oxygen isotopic composition of the Sun inferred from captured solar wind. *Science* 332: 1528–1532.
McSween HY Jr (1977) Petrographic variations among carbonaceous chondrites of the Vigarano type. *Geochimica et Cosmochimica Acta* 41: 1777–1790. McSween HY Jr and Huss GR (2022) In: *Cosmochemistry*, 2nd ed. Cambridge: Cambridge University Press.
McSween HY Jr (1994) What we have learned about Mars from SNC meteorites. *Meteoritics* 29: 757–779.
McSween HY, Mittlefehldt DW, Beck AW, Mayne RG, and McCoy TJ (2011) HED meteorites and their relationship to the geology of Vesta and the Dawn mission. *Space Science Reviews* 163: 141–174.
Meshik A, Mabry J, Hohenberg C, Marrocchi Y, Pravdivtseva O, Burnett D, Olinger C, Wiens R, Reisenfeld D, Allton J, McNamara K, Stansbery E, and Jurewicz AJG (2007) Constraints on neon and argon isotopic fractionation in solar wind. *Science* 318: 433–435.
Metzler K, Hezel DC, Barosch J, Wölfer E, Schneider JM, Hellmann JL, Berndt J, Stracke A, Gattacceca J, and Greenwood RC (2021) The Loongana (CL) group of carbonaceous chondrites. *Geochimica et Cosmochimica Acta* 304: 1–31.
Mezger K, Schönbächler M, and Bouvier A (2020) Accretion of the Earth—Missing components? *Space Science Reviews* 216: 27.
Mikhail S and Füri E (2019) On the origin(s) and evolution of Earth's carbon. *Elements* 15: 307–312. https://doi.org/10.2138/gselements.15.5.307
Min K, Farah AE, Lee SR, and Lee JI (2017) (U-Th)/He ages of phosphates from Zagami and ALHA77005 Martian meteorites: Implications to shock temperatures. *Geochimica et Cosmochimica Acta* 196: 160–178.
Mittlefehldt DW (2005) Ibitira: A basaltic achondrite from a distinct parent asteroid and implications for the Dawn mission. *Meteoritics and Planetary Science* 40: 665–677.
Mittlefehldt DW (2014) 1.6—Achondrites. In: Holland HD and Turekian KK (eds.) *Treatise on Geochemistry*, 2nd edn., pp. 235–266. Amsterdam: Elsevier.
Mittlefehldt DW (2015) Asteroid (4) Vesta: I. The howardite-eucrite-diogenite (HED) clan of meteorites. *Geochemistry* 75: 155–183.
Mittlefehldt DW and McCoy TJ (2014) Achondrites and irons. In: Righter K, Corrigan CM, McCoy TJ, and Harvey RP (eds.) *35 Seasons of U.S. Antarctic Meteorites (1976–2010)*, pp. 79–99. American Geophysical Union (AGU).
Mittlefehldt DW, McCoy TJ, Goodrich CA, and Kracher A (1998) Non-chondritic meteorites from asteroidal bodies. In: Papike JJ (ed.) *Planetary Materials, Reviews in Mineralogy*, Vol. 36, pp. 4.1–4.195. Mineralogical Society of America.
Morris MA, Boley AC, Desch SJ, and Athanassiadou T (2012) Chondrule formation in bow shocks around eccentric planetary embryos. *The Astrophysical Journal* 752: 27.
Nagao K, Okazaki R, Nakamura T, Miura YN, Osawa T, Bajo K, Matsuda S, Ebihara M, Ireland TR, Kitajima F, Naraoka H, Noguchi T, Tsuchiyama A, Yurimoto H, Zolensky ME, Uesugi M, Shirai K, Abe M, Yada T, Ishibashi Y, Fujimura A, Mukai T, Ueno M, Okada T, Yoshikawa M, and Kawaguchi J (2011) Irradiation history of Itokawa Regolith material deduced from noble gases in the hayabusa samples. *Science* 333: 1128–1131.
Nakamura T, Noguchi T, Tanaka M, Zolensky ME, Kimura M, Tsuchiyama A, Nakato A, Ogami T, Ishida H, Uesugi M, Yada T, Shirai K, Fujimura A, Okazaki R, Sandford SA, Ishibashi Y, Abe M, Okada T, Ueno M, Mukai T, Yoshikawa M, and Kawaguchi J (2011) Itokawa dust particles: A direct link between S-type asteroids and ordinary chondrites. *Science* 333: 1113–1116.
Nakamura T, et al. (2022) Formation and evolution of carbonaceous asteroid Ryugu: Direct evidence from returned samples. *Science* 379: eabn8671.
Nanne JAM, Nimmo F, Cuzzi JN, and Kleine T (2019) Origin of the non-carbonaceous–carbonaceous meteorite dichotomy. *Earth and Planetary Science Letters* 511: 44–54.
Neukum G, Ivanov BA, and Hartmann WK (2001) Cratering records in the inner Solar System in relation to the lunar reference system. *Space Science Reviews* 96: 55–86.
Neumann W, Kruijer T, Breuer D, and Kleine T (2018) Multistage core formation in planetesimals revealed by numerical modeling and Hf-W chronometry of iron meteorites. *Journal of Geophysical Research: Planets* 123: 421–444.
Neumann W, Luther R, Trieloff M, Reger PM, and Bouvier A (2023) Fitting thermal evolution models to the chronological record of Erg Chech 002 and modeling the ejection conditions of the meteorite. 4, 196. *The Planetary Science Journal* 4: 196.
Nguyen AN, et al. (2023) Abundant presolar grains and primordial organics preserved in carbon-rich exogenous clasts in asteroid Ryugu. *Science Advances* 9: eadh1003.
Ni P, Shahar A, Badro J, Yang J, Bi W, Zhao J, Hu MY, and Alp EE (2022) Planet size controls Fe isotope fractionation between mantle and core. *Geophysical Research Letters* 49(20): e2022GL098451.
Nittler LR (2003) Presolar stardust in meteorites: recent advances and scienti¢c frontiers. *Earth and Planetary Science Letters* 209: 259–273.
Nittler LR, Stroud RM, Trigo-Rodríguez JM, De Gregorio BT, Alexander CMOD, Davidson J, Moyano-Cambero CE, and Tanbakouei S (2019) A cometary building block in a primitive asteroidal meteorite. *Nature Astronomy* 3: 659–666.
O'Neill C, O'Neill HSC, and Jellinek AM (2020) On the distribution and variation of radioactive heat producing elements within meteorites, the Earth, and Planets. *Space Science Reviews* 216: 37.
Oddo G (1914) Die Molekularstruktur der radioaktiven Atome. *Zeitschrift für Anorganische Chemie* 87: 253–268.
Okazaki R, Miura YN, Takano Y, Sawada H, Sakamoto K, Yada T, Yamada K, et al. (2022) Noble gases and nitrogen in samples of asteroid Ryugu record its volatile sources and recent surface evolution. *Science* 379: eabo0431. https://doi.org/10.1126/science.abo0431
Olsen E and Jarosewich E (1971) Chondrules: First occurrence in an iron meteorite. *Science* 174: 583–585.
Owen T, Mahaffy PR, Niemann HB, Atreya S, and Wong M (2001) Protosolar nitrogen. *The Astrophysical Journal* 552: L77–L79.
Palme H, Hezel DC, and Ebel DS (2015) The origin of chondrules: Constraints from matrix composition and matrix-chondrule complementarity. *Earth and Planetary Science Letters* 411: 11–19.

Palme H, Lodders K, and Jones A (2014) Solar system abundances of the elements. In: Davis AM (ed.) *Treatise on Geochemistry (Second Edition)*, pp. 15–36. Elsevier.
Patterson CC (1956) Age of meteorites and the Earth. *Geochimica et Cosmochimica Acta* 10: 230–237.
Pearson VK, Sephton MA, Franchi IA, Gibson JM, and Gilmour I (2006) Carbon and nitrogen in carbonaceous chondrites: Elemental abundances and stable isotopic compositions. *Meteoritics and Planetary Science* 41: 1899–1918.
Péron S, Moreira M, and Agranier A (2018) Origin of light noble gases (He, Ne, and Ar) on Earth: A review. *Geochemistry, Geophysics, Geosystems* 19: 979–996.
Peterson LD, Newcombe ME, Alexander CMO, Wang J, Klein F, Bekaert DV, and Nielsen SG (2023) The H content of aubrites: An evaluation of bulk versus in situ methods for quantifying water in meteorites. *Earth and Planetary Science Letters* 620: 118341.
Piani L, Marrocchi Y, Rigaudier T, Vacher LG, Thomassin D, and Marty B (2020) Earth's water may have been inherited from material similar to enstatite chondrite meteorites. *Science* 369: 1110–1113.
Piralla M, Villeneuve J, Schnuriger N, Bekaert DV, and Marrocchi Y (2023) A unified chronology of dust formation in the early solar system. *Icarus* 394: 115427.
Poitrasson F, Halliday AN, Lee D-C, Levasseur S, and Teutsch N (2004) Iron isotope differences between Earth, Moon, Mars and Vesta as possible records of contrasted accretion mechanisms. *Earth and Planetary Science Letters* 223: 253–266.
Poitrasson F, Levasseur S, and Teutsch N (2005) Significance of iron isotope mineral fractionation in pallasites and iron meteorites for the core–mantle differentiation of terrestrial planets. *Earth and Planetary Science Letters* 234: 151–164.
Poole GM, Rehkämper M, Coles BJ, Goldberg T, and Smith CL (2017) Nucleosynthetic molybdenum isotope anomalies in iron meteorites—New evidence for thermal processing of solar nebula material. *Earth and Planetary Science Letters* 473: 215–226.
Qin L, Nittler LR, Alexander CMO, Wang J, Stadermann FJ, and Carlson RW (2011) Extreme ^{54}Cr-rich nano-oxides in the CI chondrite Orgueil – Implication for a late supernova injection into the solar system. *Geochimica et Cosmochimica Acta* 75: 629–644.
Ramsley KR and Head JW (2013) Mars impact ejecta in the regolith of phobos: Bulk concentration and distribution. *Planetary and Space Science* 87: 115–129.
Raymond SN and Morbidelli A (2022) Planet formation: Key mechanisms and global models. In: *Demographics of exoplanetary systems: Lecture notes of the 3rd Advanced School on Exoplanetary Science*, pp. 3–82.
Regelous M, Elliott T, and Coath CD (2008) Nickel isotope heterogeneity in the early Solar System. *Earth and Planetary Science Letters* 272: 330–338.
Reger PM, Roebbert Y, Neumann W, Gannoun A, Regelous M, Schwarz WH, Ludwig T, Trieloff M, Weyer S, and Bouvier A (2023) Al-Mg and U-Pb chronological records of Erg Chech 002 ungrouped achondrite meteorite. *Geochimica et Cosmochimica Acta* 343: 33–48.
Reiners PW, Carlson RW, Renne PR, Cooper KM, Granger DE, McLean NM, and Schoene B (2017) *Geochronology and Thermochronology*. John Wiley & Sons. Renne PR, Balco G, Ludwig KR, Mundil R, and Min K (2011) Response to the comment by WH Schwarz et al. on "Joint determination of ^{40}K decay constants and ^{40}Ar*/^{40}K for the Fish Canyon sanidine standard, and improved accuracy for ^{40}Ar/^{39}Ar geochronology" by PR Renne et al.(2010). *Geochimica et Cosmochimica Acta* 75: 5097–5100.
Righter K and Drake MJ (1996) Core formation in Earth's Moon, Mars, and Vesta. *Icarus* 124: 513–529. Righter K, Drake MJ, and Scott ERD (2006) Compositional relationships between meteorites and terrestrial planets. In: Lauretta DS and McSween HY Jr (eds.) *Meteorites and the Early Solar System II*, p. 943. Houston: University of Arizona Press, Tucson in collaboration with Lunar and Planetary Institute.
Righter K and Neff KE (2007) Temperature and oxygen fugacity constraints on CK and R chondrites and implications for water and oxidation in the early solar system. *Polar Science* 1: 25–44.
Righter K, Sutton SR, Danielson L, Pando K, and Newville M (2016) Redox variations in the inner solar system with new constraints from vanadium XANES in spinels. *American Mineralogist* 101: 1928–1942.
Robert F, Tartèse R, Lombardi G, Reinhardt P, Roskosz M, Doisneau B, Deng Z, and Chaussidon M (2020) Mass-independent fractionation of titanium isotopes and its cosmochemical implications. *Nature Astronomy* 4: 762–768.
Robert F, Chaussidon M, Gonzalez-Cano A, and Mostefaoui S (2021) Oxygen and magnesium mass-independent isotopic fractionation induced by chemical reactions in plasma. *Proceedings of the National Academy of Sciences of the United States of America* 118(52): e2114221118.
Rubin AE (1997) Mineralogy of meteorite groups. *Meteoritics & Planetary Science* 32: 231–247.
Rubin AE (2000) Petrologic, geochemical and experimental constraints on models of chondrule formation. *Earth-Science Reviews* 50: 3–27. Rubin AE (2007) Petrogenesis of acapulcoites and lodranites: A shock-melting model. *Geochimica et Cosmochimica Acta* 71(9): 2383–2401.
Rubin AE (2018) Carbonaceous and noncarbonaceous iron meteorites: Differences in chemical, physical, and collective properties. *Meteoritics and Planetary Science* 53: 2357–2371.
Rubin AE (2023) *Asteroids, Moons, Planets, and Meteorites. Surface/volume: How Geometry Explains Why Grain Elevators Explode, Hummingbirds Hover, and Asteroids are Colder than Ice*. Springer.
Rubin AE and Grossman JN (2010) *Meteorite and Meteoroid: New Comprehensive Definitions*. Meteoritics and Planetary Science. Rubin AE and Huber H (2005) A weathering index for CK and R chondrites. *Meteoritics and Planetary Science* 40: 1123–1130.
Rubin AE, Fegley B, and Brett R (1988) Oxidation state in chondrites. In: Kerridge JF and Matthews MS (eds.) *Meteorites and the Early Solar System*, p. 488. Tucson, AZ: Univ. Arizona Press.
Rubin AE, Scott ERD, and Keil K (1997) Shock metamorphism of enstatite chondrites. *Geochimica et Cosmochimica Acta* 61: 847–858.
Rüfenacht M, Morino P, Lai Y-J, Fehr MA, Haba MK, and Schönbächler M (2023) Genetic relationships of solar system bodies based on their nucleosynthetic Ti isotope compositions and sub-structures of the solar protoplanetary disk. *Geochimica et Cosmochimica Acta* 355: 110–125.
Russell HN (1929) On the composition of the Sun's atmosphere. *Astrophysical Journal* 70: 11.
Russell SS, Connolly HC Jr, and Krot AN (2018) *Chondrules: Records of Protoplanetary Disk Processes*. Cambridge University Press.
Ruzicka A (2014) Silicate-bearing iron meteorites and their implications for the evolution of asteroidal parent bodies. *Geochemistry* 74: 3–48. Ruzicka A, Grossman J, Bouvier A, Herd CD, and Agee CB (2015) *The Meteoritical Bulletin, No. 101*. Wiley Online Library.
Sakamoto N, Seto Y, Itoh S, Kuramoto K, Fujino K, Nagashima K, Krot AN, and Yurimoto H (2007) Remnants of the early Solar System water enriched in heavy oxygen isotopes. *Science* 317: 231–233.
Sandford SA, Brownlee DE, and Zolensky ME (2021) Chapter 4—The Stardust sample return mission. In: Longobardo A (ed.) *Sample Return Missions: The Last Frontier of Solar System Exploration*, pp. 79–104. Amsterdam: Elsevier.
Savage PS, Moynier F, and Boyet M (2022) Zinc isotope anomalies in primitive meteorites identify the outer solar system as an important source of Earth's volatile inventory. *Icarus* 386: 115172.
Schaefer L and Elkins-Tanton LT (2018) Magma oceans as a critical stage in the tectonic development of rocky planets. *Philosophical Transactions of the Royal Society A* 376: 20180109.

Schauble EA (2004) Applying stable isotope fractionation theory to new systems. In: Johnson CM, Beard BL, and Albarède F (eds.) *Geochemistry of Non-Traditional Isotopes, Reviews in Mineralogy and Geochemistry 55*, pp. 65–111. Berlin/Boston: Mineralogical Society of America, De Gruyter.
Schaudy R, Watson JT, and Buchwald VF (1972) The chemical classification of iron meteorites. VI. A reinvestigation of irons with Ge concentration lower than 1 ppm. *Icarus* 17: 174–192.
Scherer E, Münker C, and Mezger K (2001) Calibration of the Lutetium-Hafnium clock. *Science* 293: 683–687.
Schiller M, Connelly JN, Glad AC, Mikouchi T, and Bizzarro M (2015) Early accretion of protoplanets inferred from a reduced inner solar system 26Al inventory. *Earth and Planetary Science Letters* 420: 45–54.
Schiller M, Bizzarro M, and Fernandes VA (2018) Isotopic evolution of the protoplanetary disk and the building blocks of Earth and the Moon. *Nature* 555: 507.
Schrader DL, McCoy TJ, and Gardner-Vandy K (2017) Relict chondrules in primitive achondrites: Remnants from their precursor parent bodies. *Geochimica et Cosmochimica Acta* 205: 295–312.
Scott ERD (1972) Chemical fractionation in iron meteorites and its interpretation. *Geochimica et Cosmochimica Acta* 36: 1205–1236.
Scott ERD (1977a) Formation of olivine-metal textures in pallasite meteorites. *Geochimica et Cosmochimica Acta* 41: 693–710.
Scott ERD (1977b) Geochemical relationships between some pallasites and iron meteorites. *Mineralogical Magazine* 41: 265–272.
Scott ERD (1979) Origin of anomalous iron meteorites. *Mineralogical Magazine* 43: 415–421.
Scott ERD (2020) *Iron Meteorites: Composition, Age, and Origin*. Oxford Research Encyclopedia of Planetary Science, Oxford University Press.
Scott ERD and Krot AN (2005) Chondritic meteorites and the high-temperature nebular origins of their components. In: *Chondrites and the protoplanetary disk*, 341, p. 15. ASP Conference Series.
Scott ERD and Wasson JT (1975) Classification and properties of iron meteorites. *Reviews of Geophysics* 13: 527–546.
Scott ERD and Wasson JT (1976) Chemical classification of iron meteorites—VIII. Groups IC. IIE, IIIF and 97 other irons. *Geochimica et Cosmochimica Acta* 40: 103–115.
Scott ERD, Wasson JT, and Buchwald VF (1973) The chemical classification of iron meteorites—VII. A reinvestigation of irons with Ge concentrations between 25 and 80 ppm. *Geochimica et Cosmochimica Acta* 37: 1957–1983.
Scott ERD, Haack H, and Love SG (2001) Formation of mesosiderites by fragmentation and reaccretion of a large differentiated asteroid. *Meteoritics & Planetary Science* 36: 869–881.
Scott ERD, Keil K, and Stöffler D (1992) Shock metamorphism of carbonaceous chondrites. *Geochimica et Cosmochimica Acta* 56: 4281–4293.
Shu FH, Shang H, Gounelle M, Glassgold AE, and Lee T (2001) The origin of chondrules and refractory inclusions in chondritic meteorites. *The Astrophysical Journal* 548: 1029–1050.
Simon S, Davis A, and Grossman L (2001) Formation of orange hibonite, as inferred from some Allende inclusions. *Meteoritics & Planetary Science* 36: 331–350.
Simon S, Sutton S, and Grossman L (2007) Valence of titanium and vanadium in pyroxene in refractory inclusion interiors and rims. *Geochimica et Cosmochimica Acta* 71: 3098–3118.
Siron G, Fukuda K, Kimura M, and Kita NT (2022) High precision ^{26}Al-^{26}Mg chronology of chondrules in unequilibrated ordinary chondrites: Evidence for restricted formation ages. *Geochimica et Cosmochimica Acta* 324: 312–345.
Söderlund U, Patchett PJ, Vervoort JD, and Isachsen CE (2004) The ^{176}Lu decay constant determined by Lu-Hf and U-Pb isotope systematics of Precambrian mafic intrusions. *Earth and Planetary Science Letters* 219: 311–324.
Sossi PA, Nebel O, O'Neill HSC, and Moynier F (2018) Zinc isotope composition of the Earth and its behaviour during planetary accretion. *Chemical Geology* 477: 73–84.
Spitzer F, Burkhardt C, Budde G, Kruijer TS, Morbidelli A, and Kleine T (2020) Isotopic evolution of the inner Solar System inferred from molybdenum isotopes in meteorites. *The Astrophysical Journal* 898: L2.
Spitzer F, Burkhardt C, Nimmo F, and Kleine T (2021a) Nucleosynthetic Pt isotope anomalies and the Hf-W chronology of core formation in inner and outer solar system planetesimals. *Earth and Planetary Science Letters* 576: 117211.
Spitzer F, Burkhardt C, Pape J, and Kleine T (2021b) Collisional mixing between inner and outer solar system planetesimals inferred from the Nedagolla iron meteorite. *Meteoritics & Planetary Science* 57: 261–276.
Spivak-Birndorf LJ, Wadhwa M, and Janney PE (2009) 26Al–26Mg systematics in D'Orbigny and Sahara 99555 angrites: Implications for high-resolution chronology using extinct chronometers. *Geochimica et Cosmochimica Acta* 73: 5202–5211.
Sprung P, Scherer EE, Upadhyay D, Leya I, and Mezger K (2010) Non-nucleosynthetic heterogeneity in non-radiogenic stable Hf isotopes: Implications for early solar system chronology. *Earth and Planetary Science Letters* 295: 1–11.
Srinivasan P, Dunlap DR, Agee CB, Wadhwa M, Coleff D, Ziegler K, Zeigler R, and McCubbin FM (2018) Silica-rich volcanism in the early solar system dated at 4.565 Ga. Nature. *Communications* 9: 3036.
Stacey JS and Kramers JD (1975) Approximation of terrestrial lead isotope evolution by a two-stage model. *Earth and Planetary Science Letters:* 207–221.
Steller T, Burkhardt C, Yang C, and Kleine T (2022) Nucleosynthetic zinc isotope anomalies reveal a dual origin of terrestrial volatiles. *Icarus* 386: 115171.
Stephan T and Davis AM (2021) Molybdenum isotope dichotomy in meteorites caused by s-process variability. *The Astrophysical Journal* 909: 8.
Stephan T, Trappitsch R, Davis AM, Pellin MJ, Rost D, Savina MR, Yokochi R, and Liu N (2016) CHILI–the Chicago Instrument for Laser Ionization–a new tool for isotope measurements in cosmochemistry. *International Journal of Mass Spectrometry* 407: 1–15.
Stephant A, Garvie LAJ, Mane P, Hervig R, and Wadhwa M (2018) Terrestrial exposure of a fresh Martian meteorite causes rapid changes in hydrogen isotopes and water concentrations. *Scientific Reports* 8: 12385.
Stephant A, Carli C, Anand M, Néri A, Davidson J, Pratesi G, Cuppone T, Greenwood RC, and Franchi IA (2023) Tissemouminites: A new group of primitive achondrites spanning the transition between acapulcoites and winonaites. *Meteoritics and Planetary Science* 58: 111–134.
Stern JC and Wiemann ST (2021) Traditional stable isotope geochemistry. In: Alderton D and Alias SA (eds.) *Encyclopedia of Geology*, 2nd edn., pp. 100–113. Academic Press.
Stirling CH, Halliday AN, and Porcelli D (2005) In search of live ^{247}Cm in the early solar system. *Geochimica et Cosmochimica Acta* 69: 1059–1071.
Stirling CH, Andersen MB, Potter E-K, and Halliday AN (2007) Low-temperature isotopic fractionation of uranium. *Earth and Planetary Science Letters* 264: 208–225.
Stöffler D, Keil K, and Scott ERD (1991) Shock metamorphism of ordinary chondrites. *Geochimica et Cosmochimica Acta* 55: 3845–3867.
Suess HE and Urey HC (1956) Abundances of the elements. *Reviews of Modern Physics* 28: 53–74.

Sugiura N and Fujiya W (2014) Correlated accretion ages and ε^{54}Cr of meteorite parent bodies and the evolution of the solar nebula. *Meteoritics and Planetary Science* 49: 772–787.
Suttle M, Greshake A, King A, Schofield P, Tomkins A, and Russell S (2021) The alteration history of the CY chondrites, investigated through analysis of a new member: Dhofar 1988. *Geochimica et Cosmochimica Acta* 295: 286–309.
Tachibana S, et al. (2022) Pebbles and sand on asteroid (162173) Ryugu: In situ observation and particles returned to Earth. *Science* 375: 1011–1016.
Tagawa S, Sakamoto N, Hirose K, Yokoo S, Hernlund J, Ohishi Y, and Yurimoto H (2021) Experimental evidence for hydrogen incorporation into Earth's core. *Nature Communications* 12: 2588.
Tait AW, Tomkins AG, Godel BM, Wilson S, and Hasalova P (2014) Investigation of the H7 ordinary chondrite, Watson 012: Implications for recognition and classification of Type 7 meteorites. *Geochimica et Cosmochimica Acta* 134: 175–196.
Tarduno JA, Cottrell RD, Nimmo F, Hopkins J, Voronov J, Erickson A, Blackman E, Scott ERD, and McKinley R (2012) Evidence for a dynamo in the main group pallasite parent body. *Science* 338: 939–942.
Tatsumoto M, Knight RJ, and Allègre CJ (1973) Time differences in the formation of meteorites as determinated from the ratio of lead 207 to lead 206. *Science* 180: 1279–1283.
Teng F-Z, Dauphas N, and Watkins JM (2017) Non-traditional stable isotopes: Retrospective and prospective. In: Teng F-Z, Watkins JM, and Dauphas N (eds.) *Non-Traditional Stable Isotopes, Reviews in Mineralogy and Geochemistry 82*, pp. 1–26. Berlin/Boston: Mineralogical Society of America, De Gruyter.
Tera F and Wasserburg GJ (1972) U-Th-Pb systematics in lunar highland samples from the Luna 20 and Apollo 16 missions. *Earth and Planetary Science Letters* 17: 36–51.
Thiemens MH and Heidenreich JE (1983) The mass-independent fractionation of oxygen: A novel isotope effect and its possible cosmochemical implications. *Science* 219: 1073–1075.
Thiemens MH and Lin M (2021) Discoveries of mass independent isotope effects in the solar system: Past, present and future. In: Bindeman IN and Pack A (eds.). *Triple Oxygen Isotope Geochemistry, Reviews in Mineralogy and Geochemistry*, Vol. 86, pp. 35–95. Mineralogical Society of America.
Tissot FLH, Dauphas N, and Grossman L (2016) Origin of uranium isotope variations in early solar nebula condensates. *Science Advances* 2: e1501400.
Tissot FL, Dauphas N, and Grove TL (2017) Distinct ^{238}U/^{235}U ratios and REE patterns in plutonic and volcanic angrites: Geochronologic implications and evidence for U isotope fractionation during magmatic processes. *Geochimica et Cosmochimica Acta* 213: 593–617.
Tissot FLH, Collinet M, Namur O, and Grove TL (2022) The case for the angrite parent body as the archetypal first-generation planetesimal: Large, reduced and Mg-enriched. *Geochimica et Cosmochimica Acta* 338: 278–301.
Tomkins AG, Johnson TE, and Mitchell JT (2020) A review of the chondrite–achondrite transition, and a metamorphic facies series for equilibrated primitive stony meteorites. *Meteoritics & Planetary Science* 55: 857–885.
Tornabene HA, Ash RD, Walker RJ, and Bermingham KR (2023) Genetics, age, and crystallization history of group IC iron meteorites. *Geochimica et Cosmochimica Acta* 340: 108–119.
Touboul M, Sprung P, Aciego SM, Bourdon B, and Kleine T (2015) Hf-W chronology of the eucrite parent body. *Geochimica et Cosmochimica Acta* 156: 106–121.
Trieloff M, Jessberger EK, Herrwerth I, Hopp J, Fiéni C, Ghélis M, Bourot-Denise M, and Pellas P (2003) Structure and thermal history of the H-chondrite parent asteroid revealed by thermochronometry. *Nature* 422: 502–506.
Trinquier A, Birck J, and Allegre CJ (2007) Widespread ^{54}Cr heterogeneity in the inner Solar System. *The Astrophysical Journal* 655: 1179–1185.
Trinquier A, Elliott T, Ulfbeck D, Coath C, Krot AN, and Bizzarro M (2009) Origin of nucleosynthetic isotope heterogeneity in the solar protoplanetary disk. *Science* 324: 374–376.
Tschauner O, Ma C, Beckett JR, Prescher C, Prakapenka VB, and Rossman GR (2014) Discovery of bridgmanite, the most abundant mineral in Earth, in a shocked meteorite. *Science* 346: 1100–1102.
Tsuchiyama A, Uesugi M, Matsushima T, Michikami T, Kadono T, Nakamura T, Uesugi K, Nakano T, Sandford SA, Noguchi R, Matsumoto T, Matsuno J, Nagano T, Imai Y, Takeuchi A, Suzuki Y, Ogami T, Katagiri J, Ebihara M, Ireland TR, Kitajima F, Nagao K, Naraoka H, Noguchi T, Okazaki R, Yurimoto H, Zolensky ME, Mukai T, Abe M, Yada T, Fujimura A, Yoshikawa M, and Kawaguchi J (2011) Three-dimensional structure of Hayabusa samples: Origin and evolution of Itokawa regolith. *Science* 333: 1125–1128. https://doi.org/ 10.1126/science.1207807.
Tyburczy JA, Krishnamurthy RV, Epstein S, and Ahrens TJ (1990) Impact-induced devolatilization and hydrogen isotopic fractionation of serpentine: Implications for planetary accretion. *Earth and Planetary Science Letters* 98: 245–261.
Udry A, Howarth GH, Herd CDK, Day JMD, Lapen TJ, and Filiberto J (2020) What Martian meteorites reveal about the interior and surface of Mars. *Journal of Geophysical Research: Planets* 125: e2020JE006523.
Urey HC (1947) The thermodynamic properties of isotopic substances. *Journal of the Chemical Society*: 562–581.
Urey HC and Craig H (1953) The composition of the stone meteorites and the origin of the meteorites. *Geochimica et Cosmochimica Acta* 4: 36–82.
Ushikubo T, Kimura M, Kita NT, and Valley JW (2012) Primordial oxygen isotope reservoirs of the solar nebula recorded in chondrules in Acfer 094 carbonaceous chondrite. *Geochimica et Cosmochimica Acta* 90: 242–264.
Vacher LG and Fujiya W (2022) Recent advances in our understanding of water and aqueous activity in chondrites. *Elements* 18: 175–180.
Vacher LG, Piani L, Rigaudier T, Thomassin D, Florin G, Piralla M, and Marrocchi Y (2020) Hydrogen in chondrites: Influence of parent body alteration and atmospheric contamination on primordial components. *Geochimica et Cosmochimica Acta* 281: 53–66.
Vacher L, Ogliore R, Jones C, Liu N, and Fike D (2021) Cosmic symplectite recorded irradiation by nearby massive stars in the solar system's parent molecular cloud. *Geochimica et Cosmochimica Acta* 309: 135–150.
Valdes MC, Bermingham KR, Huang S, and Simon JI (2021) Calcium isotope cosmochemistry. *Chemical Geology* 581: 120396.
Van Roosbroek N, Debaille V, Pittarello L, Goderis S, Humayun M, Hecht L, Jourdan F, Spicuzza MJ, Vanhaecke F, and Claeys P (2015) The formation of IIE iron meteorites investigated by the chondrule-bearing Mont Dieu meteorite. *Meteoritics & Planetary Science* 50: 1173–1196.
Van Schmus WRV and Wood JA (1967) A chemical-petrologic classification for the chondritic meteorites. *Geochimica et Cosmochimica Acta* 31: 747–765.
Villa IM, Holden NE, Possolo A, Ickert RB, Hibbert DB, Renne PR, Bonardi ML, and Bièvre PD (2022) IUGS–IUPAC recommendations and status reports on the half-lives of ^{87}Rb, ^{146}Sm, ^{147}Sm, ^{234}U, ^{235}U, and ^{238}U (IUPAC Technical Report). *Pure and Applied Chemistry* 94: 1085–1092.

Villeneuve J, Chaussidon M, and Libourel G (2009) Homogeneous distribution of ^{26}Al in the Solar System from the Mg isotopic composition of chondrules. *Science* 325: 985–988.
Villeneuve J, Chaussidon M, and Libourel G (2011) Magnesium isotopes constraints on the origin of Mg-rich olivines from the Allende chondrite: Nebular versus planetary? *Earth and Planetary Science Letters* 301: 107–116.
Voelkel O, Deienno R, Kretke K, and Klahr H (2021) Linking planetary embryo formation to planetesimal formation. *Astronomy and Astrophysics* 645: A132.
Wadhwa M (2001) Redox state of Mars' upper mantle and crust from Eu anomalies in shergottite pyroxenes. *Science* 291: 1527–1530.
Wadhwa M, Kita N, Nakashima D, Bullock E, MacPherson G, and Bouvier A (2014) High precision ^{26}Al-^{26}Mg systematics for an almost pristine refractory inclusion: Implications for the absolute age of the solar system. In: *Lunar and Planetary Science Conference*, p. 2698.
Wai CM and Wasson JT (1979) Nebular condensation of Ga, Ge and Sb and the chemical classification of iron meteorites. *Nature* 282: 790–793.
Walker RJ (2009) Highly siderophile elements in the Earth, Moon and Mars: Update and implications for planetary accretion and differentiation. *Geochemistry* 69: 101–125.
Walker RJ (2012) Evidence for homogeneous distribution of osmium in the protosolar nebula. *Earth and Planetary Science Letters* 351–352: 36–44.
Walsh KJ, Morbidelli A, Raymond SN, O'brien DP, and Mandell AM (2011) A low mass for Mars from Jupiter's early gas-driven migration. *Nature* 475: 206.
Walte NP, Solferino GFD, Golabek GJ, Souza DS, and Bouvier A (2020) Two-stage formation of pallasites and the evolution of their parent bodies revealed by deformation experiments. *Earth and Planetary Science Letters* 546: 116419.
Walton CR, Jeon H, C̆ernok A, Rae ASP, Baziotis I, Tang F, Kuppili VSC, Ferrière L, Darling J, Hu S, Whitehouse MJ, Anand M, and Shorttle O (2023) In-situ phosphate U-Pb ages of the L chondrites. *Geochimica et Cosmochimica Acta* 359: 191–204.
Wang H, Weiss BP, Bai X-N, Downey BG, Wang J, Wang J, Suavet C, Fu RR, and Zucolotto ME (2017) Lifetime of the solar nebula constrained by meteorite paleomagnetism. *Science* 355: 623–627.
Wark D and Lovering J (1977) Marker events in the early evolution of the solar system-Evidence from rims on Ca-Al-rich inclusions in carbonaceous chondrites. In: *Lunar Science Conference 8th, Houston, Tex., March 14-18, 1977, Proceedings*, pp. 95–112.
Warren PH (1985) The magma ocean concept and lunar evolution. *Annual Review of Earth and Planetary Sciences* 13: 201–240.
Warren PH (2011) Stable-isotopic anomalies and the accretionary assemblage of the Earth and Mars: A subordinate role for carbonaceous chondrites. *Earth and Planetary Science Letters* 311: 93–100.
Wasserburg GJ, Lee T, and Papanastassiou DA (1977) Correlated O and Mg isotopic anomalies in Allende inclusions: II. Magnesium. *Geophysical Research Letters* 4: 299–302.
Wasson JT (1967) The chemical classification of iron meteorites: I. A study of iron meteorites with low concentrations of gallium and germanium. *Geochimica et Cosmochimica Acta* 31: 161–180.
Wasson JT (1969) The chemical classification of iron meteorites—III. Hexahedrites and other irons with germanium concentrations between 80 and 200 ppm. *Geochimica et Cosmochimica Acta* 33: 859–876.
Wasson JT (1970) The chemical classification of iron meteorites: IV. Irons with Ge concentrations greater than 190 ppm and other meteorites associated with group I. *Icarus* 12: 407–423.
Wasson JT (1985) *Meteorites: Their Record of Early Solar-System History*. Freeman. 267 p.
Wasson JT (2017) Formation of non-magmatic iron-meteorite group IIE. *Geochimica et Cosmochimica Acta* 197: 396–416.
Wasson JT and Choi B-G (2003) Main-group pallasites: Chemical composition, relationship to IIIAB irons, and origin. *Geochimica et Cosmochimica Acta* 67: 3079–3096.
Wasson JT and Kallemeyn GW (2002) The IAB iron-meteorite complex: A group, five subgroups, numerous grouplets, closely related, mainly formed by crystal segregation in rapidly cooling melts. *Geochimica et Cosmochimica Acta* 66: 2445–2473.
Wasson JT and Kimbeblin J (1967) The chemical classification of iron meteorites—II. Irons and pallasites with germanium concentrations between 8 and 100 ppm. *Geochimica et Cosmochimica Acta* 31: 2065–2093.
Wasson JT and Schaudy R (1971) The chemical classification of iron meteorites—V groups IIIC and IIID and other irons with germanium concentrations between 1 and 25 ppm. *Icarus* 14: 59–70.
Wasson JT and Wai C-M (1976) Explanation for the very low Ga and Ge concentrations in some iron meteorite groups. *Nature* 261: 114–116.
Wasson JT, Matsunami Y, and Rubin AE (2006) Silica and pyroxene in IVA irons; possible formation of the IVA magma by impact melting and reduction of L-LL-chondrite materials followed by crystallization and cooling. *Geochimica et Cosmochimica Acta* 70: 3149–3172.
Wasson JT, Ouyang X, Wang J, and Eric J (1989) Chemical classification of iron meteorites: XI. Multi-element studies of 38 new irons and the high abundance of ungrouped irons from Antarctica. *Geochimica et Cosmochimica Acta* 53: 735–744.
Wasson JT, Choi B-G, Jerde EA, and Ulff-Møller F (1998) Chemical classification of iron meteorites: XII. New members of the magmatic groups. *Geochimica et Cosmochimica Acta* 62: 715–724.
Weisberg MK, Prinz M, Clayton RN, Mayeda TK, Grady MM, and Pillinger CT (1995) The CR chondrite clan. *Antarctic Meteorite Research* 8: 11.
Weisberg MK, McCoy TJ, and Krot AN (2006) Systematics and evaluation of meteorite classification. In: Lauretta DS and Sween HY Jr (eds.) *Meteorites and the Early Solar System II*, pp. 19–52. Univ. of Arizona Press.
Wetherill GW (1956) Discordant uranium-lead ages. *Transactions - American Geophysical Union* 37: 320–326. White WM (2020) *Geochemistry*. Wiley.
Wiechert U, Halliday AN, Lee D-C, Snyder GA, Taylor LA, and Rumble D (2001) Oxygen isotopes and the Moon-forming giant impact. *Science* 294: 345–348.
Wiens RC, Burnett DS, Hohenberg CM, Meshik A, Heber V, Grimberg A, Wieler R, and Reisenfeld DB (2007) Solar and Solar-wind composition results from the genesis mission. *Space Science Reviews* 130: 161–171.
Williams CD, Ushikubo T, Bullock ES, Janney PE, Hines RR, Kita NT, Hervig RL, MacPherson GJ, Mendybaev RA, Richter FM, and Wadhwa M (2017) Thermal and chemical evolution in the early solar system as recorded by FUN CAIs: Part I—Petrology, mineral chemistry, and isotopic composition of Allende FUN CAI CMS-1. *Geochimica et Cosmochimica Acta* 201: 25–48.
Williams CD, Sanborn ME, Defouilloy C, Yin Q-Z, Kita NT, Ebel DS, Yamakawa A, and Yamashita K (2020) Chondrules reveal large-scale outward transport of inner Solar System materials in the protoplanetary disk. *Proceedings of the National Academy of Sciences of the United States of America* 117: 23426–23435.
Willis J and Wasson JT (1978a) Cooling rates of group IVA iron meteorites. *Earth and Planetary Science Letters* 40: 141–150.

Willis J and Wasson JT (1978b) A core origin for group IVA iron meteorites: A reply to Moren and Goldstein. *Earth and Planetary Science Letters* 40: 162–167.
Windmill RJ, Franchi IA, Hellmann JL, Schneider JM, Spitzer F, Kleine T, Greenwood RC, and Anand M (2022) Isotopic evidence for pallasite formation by impact mixing of olivine and metal during the first 10 million years of the Solar System. *PNAS Nexus* 1: pgac015.
Wlotzka F (1993) A weathering scale for the ordinary chondrites. *Meteoritics* 28: 460.
Woo JMY, Brasser R, Matsumura S, Mojzsis SJ, and Ida S (2018) The curious case of Mars' formation. *Astronomy & Astrophysics* 617: A17.
Wood JA (2005) The chondrite types and their origins. In: Krot AN, Scott ERD, and Reipurth B (eds.) *Chondrites and the Protoplanetary Disk*. *Astronomical Society of the Pacific Conference Series*, Vol. 341, pp. 953–971.
Worsham EA, Bermingham KR, and Walker RJ (2016) Siderophile element systematics of IAB complex iron meteorites: New insights into the formation of an enigmatic group. *Geochimica et Cosmochimica Acta* 188: 261–283.
Worsham EA, Bermingham KR, and Walker RJ (2017) Characterizing cosmochemical materials with genetic affinities to the Earth: Genetic and chronological diversity within the IAB iron meteorite complex. *Earth and Planetary Science Letters* 467: 157–166.
Worsham EA, Burkhardt C, Budde G, Fischer-Gödde M, Kruijer TS, and Kleine T (2019) Distinct evolution of the carbonaceous and non-carbonaceous reservoirs: Insights from Ru, Mo, and W isotopes. *Earth and Planetary Science Letters* 521: 103–112.
Wu J, Desch SJ, Schaefer L, Elkins-Tanton LT, Pahlevan K, and Buseck PR (2018) Origin of Earth's water: Chondritic inheritance plus nebular ingassing and storage of hydrogen in the core. *Journal of Geophysical Research* 123: 2691–2712.
Wu S, Wang H, Yang Y, Niu J, Lan Z, Zhang L, Huang C, Xie L, Xu L, and Yang J (2023) In situ Lu–Hf geochronology with LA-ICP-MS/MS analysis. *Journal of Analytical Atomic Spectrometry* 38: 1285–1300.
Yada T, et al. (2021) Preliminary analysis of the Hayabusa2 samples returned from C-type asteroid Ryugu. *Nature Astronomy* 6: 214–220.
Yanai K and Kojima H (1995) Yamato-841: A newly identified pyroxene-bearing pallasite. In: *Nineteenth Symposium on Antarctic Meteorites. Proceedings of the NIPR Symposium, No. 8, held May 30-June 1, 1994, at the National Institute of Polar Research, Tokyo. Editor in Chief, Keizo Yanai. Published by the National Institute of Polar Research, 1995*, p. 1.
Yang L and Ciesla FJ (2012) The effects of disk building on the distributions of refractory materials in the solar nebula. *Meteoritics & Planetary Science* 47: 99–119.
Yang J and Goldstein JI (2005) The formation of the Widmanstätten structure in meteorites. *Meteoritics & Planetary Science* 40: 239–253.
Yang J, Goldstein JI, and Scott ERD (2010) Main-group pallasites: Thermal history, relationship to IIIAB irons, and origin. *Geochimica et Cosmochimica Acta* 74: 4471–4492.
Yang J, Lin Y, Changela H, Xie L, Chen B, and Yang J (2020) Early sulfur-rich magmatism on the ungrouped achondrite Northwest Africa 7325 differentiated parent body. *Meteoritics & Planetary Science* 55: 1951–1978.
Yano H, Kubota T, Miyamoto H, Okada T, Scheeres D, Takagi Y, Yoshida K, Abe M, Abe S, Barnouin-Jha O, Fujiwara A, Hasegawa S, Hashimoto T, Ishiguro M, Kato M, Kawaguchi J, Mukai T, Saito J, Sasaki S, and Yoshikawa M (2006) Touchdown of the Hayabusa spacecraft at the muses sea on Itokawa. *Science* 312: 1350–1353.
Yokoyama T, Alexander CMO, and Walker RJ (2011) Assessment of nebular versus parent body processes on presolar components present in chondrites: Evidence from osmium isotopes. *Earth and Planetary Science Letters* 305: 115–123.
Yokoyama T, Nagashima K, Nakai I, Young ED, Abe Y, et al. (2022) Samples returned from the asteroid Ryugu are similar to Ivuna-type carbonaceous meteorites. *Science* 379: eabn7850.
Yoshizaki T, Ash RD, Lipella MD, Yokoyama T, and McDonough WF (2021) Variable refractory lithophile element compositions of planetary building blocks: Insights from components of enstatite chondrites. *Geochimica et Cosmochimica Acta* 308: 173–187.
Young ED and Russell SS (1998) Oxygen reservoirs in the early Solar Nebula inferred from an Allende CAI. *Science* 282: 452–455.
Young ED, Galy A, and Nagahara H (2002) Kinetic and equilibrium mass-dependent isotope fractionation laws in nature and their geochemical and cosmochemical significance. *Geochimica et Cosmochimica Acta* 66: 1095–1104.
Young ED, Kohl IE, Warren PH, Rubie DC, Jacobson SA, and Morbidelli A (2016) Oxygen isotopic evidence for vigorous mixing during the Moon-forming giant impact. *Science* 351(6272): 493–496.
Yurimoto H, Abe K-i, Abe M, Ebihara M, Fujimura A, Hashiguchi M, Hashizume K, Ireland TR, Itoh S, Katayama J, Kato C, Kawaguchi J, Kawasaki N, Kitajima F, Kobayashi S, Meike T, Mukai T, Nagao K, Nakamura T, Naraoka H, Noguchi T, Okazaki R, Park C, Sakamoto N, Seto Y, Takei M, Tsuchiyama A, Uesugi M, Wakaki S, Yada T, Yamamoto K, Yoshikawa M, and Zolensky ME (2011) Oxygen isotopic compositions of asteroidal materials returned from Itokawa by the Hayabusa mission. *Science* 333: 1116–1119. https://doi.org/10.1126/science.1207776.
Zanda B, Lewin E, Humayun M, and Connolly HC Jr (2018) The chondritic assemblage: Complementarity is not a required hypothesis. In: Krot AN and Russell SS (eds.) *Chondrules: Records of Protoplanetary Disk Processes*. Cambridge: Cambridge University Press.
Zhang H, Hirschmann M, Cottrell E, and Withers A (2017) Effect of pressure on Fe3+/SFe ratio in a mafic magma and consequences for magma ocean redox gradients. *Geochimica et Cosmochimica Acta* 204: 83–103.
Zheng Y-F (2011) On the theoretical calculations of oxygen isotope fractionation factors for carbonate-water systems. *Geochemical Journal* 45: 341–354.
Zhu K, Becker H, Li S-J, Fan Y, Liu X-N, and Elliott T (2022) Radiogenic chromium isotope evidence for the earliest planetary volcanism and crust formation in the Solar System. *Monthly Notices of the Royal Astronomical Society: Letters* 515: L39–L44.
Zinner E (1998) Stellar nucleosynthesis and the isotopic composition of presolar grains from primitive meteorites. *Annual Review of Earth and Planetary Sciences* 26: 147–188.

Relevant websites

https://gfo.rocks/ The Global Fireball Observatory is a multi-institutional collaboration, with partner networks around the world. Its observatories take pictures of fireballs so meteorites that might have landed on the ground can be recovered.
https://www.lpi.usra.edu/meteor/about.php The Meteoritic Bulletin Database which provides authoritative information about meteorite names.